THE LEBER CONGENITAL AMAUROSIS *CEP290* CAT MODEL:
WORKING TOWARDS A CURE

By

Andrea Louise Minella

A DISSERTATION

Submitted to
Michigan State University
in partial fulfillment of the requirements
for the degree of

Comparative Medicine and Integrative Biology — Doctor of Philosophy

2017

ABSTRACT

THE LEBER CONGENITAL AMAUROSIS *CEP290* CAT MODEL: WORKING TOWARDS A CURE

By

Andrea Louise Minella

Leber Congenital Amaurosis (LCA) is an early-onset and severe inherited retinal dystrophy. The most commonly implicated gene is the centrosomal 290kDa (*CEP290*) gene. There are currently no treatments for LCA^{CEP290}. Animal models are integral for treatment safety and efficacy testing, with a feline model for *CEP290* retinopathies showing promise for this purpose. This model has a spontaneous mutation in *CEP290* resulting in a progressive retinal degeneration and vision loss. This mutation alters splicing and is predicted to result in a truncated protein. CEP290 is integrally involved in the transport within photoreceptor cells, localizing to the interconnecting cilium.

The *CEP290* mutant cat ("*rdAc*") has a milder phenotype than the phenotype most commonly associated with *CEP290* mutations in people. Understanding the reason for this milder phenotype was an important aim of this dissertation. We analyzed the wild-type and truncated mutant transcript levels and total CEP290 protein levels in cat retinal tissue across genotypes (wild-type, heterozygous, homozygous mutant). Our findings show that the milder phenotype in mutant cats is likely the result of low-level production of wild-type transcript and protein combined with production of truncated protein that we suspect retains some function. These measures can also serve as objective markers of disease progression or treatment success in future studies.

Further objective markers were investigated utilizing spectral-domain optical coherence tomography. By analyzing photoreceptor layer thickness (receptor plus/REC

+) and the ellipsoid zone (EZ), a zone noted to change with disease in people, we showed that REC+ thickness and EZ integrity can be used as markers of disease progression. These findings support the cat as a *CEP290* model, and show the affected cats have a degeneration with central retinal sparing as described in human patients.

We also developed an *in vitro* tool by developing primary fibroblast cell cultures from skin samples of *CEP290* cats. We showed that cilia formation, which involves CEP290, can be induced, opening the door for future cilia studies. We assessed cilia length as an objective marker of disease, however, no difference was found in cilia length across genotypes. Utilizing this new tool, we tested a CRISPR/Cas-9 genome editing treatment in an attempt to replace the mutated region with a sequence that would direct splicing to the correct location. We achieved high efficiency transduction of CRISPR components, however, we failed to detect insertion of our chosen sequence.

As we work towards a treatment, it is imperative to develop an optimized method to deliver the treatment to feline photoreceptors. To achieve this aim we tested hybrid adeno-associated viral (AAV) vectors, the retinal viral vector of choice, in the wild-type feline retina. We showed that all serotypes studied, AAV2/2, 2/5, 2/8, and 2/9, transduce photoreceptor cells with AAV2/8 and 2/9 showing higher transduction and faster onset. Interestingly, we found more efficient transduction of cones than rods, an unusual finding that speaks to the need to use caution when extrapolating across species.

It is our hope that these data will help the scientific community move closer to treatments for *CEP290* retinopathies. We have added to the understanding of the *rdAc* cat model and determined objective markers, supported the cat as a model, and have made progress towards a treatment.

I dedicate this dissertation to my cousin Mikey- my first and forever best friend, my family, my motivation in the fight against genetic diseases. To my inspiration- may you always remember to smell the roses and 'just breathe'.

ACKNOWLEDGMENTS

I would first and foremost like to thank my mentor, Dr. Simon Petersen-Jones for his never-ending guidance and patience. From the day I asked to be a summer research student in his lab while he was on vacation (and he answered his email anyway) to the day he had enough belief in me to let me stay as a PhD student, his commitment to my success and growth as a budding scientist will forever be appreciated.

I would like to thank my committee members, Drs. Bartoe, Komaromy, Kruger, and Langohr, I am so appreciative of your guidance and inspired by you. You are amazing scientists who have taught me not just through mentorship but also through example.

To the many people involved in my PhD experience, I am forever grateful:

- To Dr. Yuzbasiyan-Gurkan for being the ultimate student advocate, enthusiastic scientist, and a woman I truly look up to
- To Dr. Vicki Hoelzer-Maddox and Dimity Palazzola for their tireless efforts to answer my many (probably annoying) emails and make sure that the many little details of being a PhD student run smoothly
- To our many collaborators especially Dr. Steve Suhr and Dr. Marie-Claude Senut for their enthusiastic contribution to our studies and undying patience for my questions
- To Kimberly Williamson and the Campus Animal Resources for their animal care
- To Janice Querubin, Kristin Koehl, Christine Harman for their assistance, hard work, and friendly encouragement

- To my parents- people I know I can always count on to have my back and keep me on my feet, to love me even in my crankiest hours, to believe in me when I don't believe in myself, and to show me what strength, resiliency, and love look like

- To my 'little' sister who is wise beyond her years and has always offered words of wisdom, a sense of humor, a ray of positivity, and a strength for conquering life with a smile that I will always admire

- To the rest of my family who have been behind me cheering me on since the day I was barely old enough to hold the toy stethoscope they gave me that set the stage for my career path

- To my friends who kept me laughing through even the most stressful of times

- To the many animals who have touched my life and my heart especially my "fur kids" Millie, Gemma, Apollo, and Fred for being my saving grace during my darkest hours

- And last but never least, to all of the cats involved in these studies for making a contribution to science that will help us reach a cure someday- their sacrifice was not taken lightly and will never be forgotten

TABLE OF CONTENTS

LIST OF TABLES

LIST OF FIGURES

KEY TO ABBREVIATIONS

RP — Retinitis Pigmentosa

LCA — Leber Congenital Amaurosis

PRA — Progressive Retinal Atrophy

OLM — outer limiting membrane

ONL — outer nuclear layer

INL — inner limiting membrane

IPL — inner plexiform layer

GCL — ganglion cell layer

ILM — inner limiting membrane

RPE — retinal pigment epithelium

PDE — phosphodiesterase

CNG — cyclic nucleotide gated channel

CEP290 — centrosomal protein 290kDa

KAP3 — kinesis-associated protein 3

KIF3A — kinesin family member 3A

RPGR — retinitis pigmentosa GTP-ase regulator

RPGRIP1 — RPGR-interacting protein

ATF4 — activation transcription factor 4

rd16 — retinal degeneration 16 (mouse)

rdAc — retinal degeneration in the Abyssinian cat

MGS — Meckel-Grüber Syndrome

BBS — Bardet-Biedl Syndrome

SLS — Senor-Løken Syndrome

JS — Joubert Syndrome

CORS — cerebella-ocular-renal syndrome

rds — retinal degeneration slow (mouse)

ERG — electroretinogram

SD-OCT — spectral-domain optical coherence tomography

CRISPR — clustered regularly interspersed short palindromic repeats

Cas — CRISPR-associated (protein)

iPSC — induced pluripotent stem cell

AAV — adeno-associated viral (vector)

RPE65 — retinal pigment epithelium specific protein 65

MERTK — MER receptor tyrosine kinase

EIAV — equine infectious anemia virus

ITR — inverted terminal repeat

Rep — replication

Cap — capsid

CMV — cytomegalovirus

CBA — chicken beta actin

mOP — mouse opsin

GRK — G-protein coupled receptor protein kinase

EZ — ellipsoid zone

GFP — green fluorescent protein

CHAPTER 1

INTRODUCTION

1.1 The eye and ocular disease

1.1.1 Vision and its importance

What we see and how we visually process the world around us influences how we live. It is a sense that we rely on heavily in our daily lives for most tasks and need for many, allowing us to process light to perceive shapes, colors, movements, and our world around us. Losing the sense of sight can therefore be devastating and have a significantly negative impact on one's quality of life.

Ocular diseases are widespread and varied, ranging from traumatic injuries, to infectious diseases, to inherited conditions, all of which can affect any part of the eye. When these diseases affect the eye in a manner that impairs its ability to take in or process light, visual loss can occur, taking away a crucial component of one's sensory system and jeopardizing quality of life.

1.1.2 Ocular disease

Ocular diseases make up a common category of conditions that range from mild to vision threatening, with millions of people afflicted by diseases that significantly impair vision (https://nei.nih.gov/eyedata/vision_impaired/tables). These diseases can affect any part of the eye and can impair vision through a variety of mechanisms, such as by opacifying the cornea or lens such that light cannot traverse them or by affecting the health of the retina such that the light that reaches it cannot be processed to be sent to the brain. While there are treatments for many conditions- surgeries to remove cataracts, replacing them with an artificial lens, and medications or surgical procedures

to decrease corneal edema, as examples, many other conditions have no treatments or have proven difficult to develop effective therapies.

Retinal diseases are particularly difficult to treat as many involve the photoreceptor cells, or rods and cones, which are a type of terminally differentiated neuron. A common type of inherited retinal disease that poses a particularly devastating impact on both the individual and society are inherited retinal degenerations. These retinal dystrophies encompass an entire subcategory of eye disease that has a significant worldly impact to both people and animals and as such, is an active area of research.

1.1.3 Retinal disease

Inherited retinal dystrophies make up a leading cause of blindness in both humans and companion animals. Characterized by progressive retinal degeneration causing decreasing vision that ultimately leads to blindness, they are devastating diseases that significantly affect quality of life.

Inherited retinopathies are a group of genetically heterogenous diseases that have been associated with mutations in many different genes. These mutations affect the production of a variety of important retinal proteins, including those involved in metabolism, trafficking, transcription and other integral retinal functions.

In humans, inherited retinal diseases include a wide variety of conditions such as Retinitis Pigmentosa (RP) in adults, which has an estimated prevalence as high as 1 in 2,500 people, and Leber Congenital Amaurosis (LCA) in children, which has an estimated prevalence of 1 in every 81,000 and makes up the most common inherited

cause of blindness in children.(1-3) In companion animals, this group of retinopathies is denoted as Progressive Retinal Atrophy (PRA). These diseases occur naturally within the pet and lab animal populations and can also be genetically created in some species. With striking similarities to the conditions in people, including homologous genes mutated and comparable phenotypes, these animals provide an assortment of useful animal models. Interest in retinal disease and treatment development to combat these diseases is therefore of interest to both scientists and physicians invested in treating the human conditions as well as scientists and veterinarians concerned about the ocular health of companion animals. Understanding the retina, its functioning, and how to treat diseases within it are therefore important and active areas of research.

1.2 The Retina

1.2.1 Retinal anatomy and physiology

The retina is a highly organized tissue that lies at the posterior pole of the eye. Through a process known as phototransduction, it is responsible for taking the light that enters the eye and transforming that light into chemical and electrical signals that can then be sent to the brain for final processing and visual perception. To do this, the retina is organized into multiple layers each comprised of different cell types. The cells of the various layers work in a cooperative and complementary manner to create a cascade of events for this first stage of processing to occur.(4)

After traversing the anterior components of the eye including the cornea and lens, light that enters the eye hits the retina, first striking the inner limiting membrane, the boundary between the vitreous and the retina, and then nerve fiber layer which is compromised of the axons of the ganglion cells. These axons gather at the center of the fundus to form the optic nerve head, which then continues as the optic nerve towards the brain, carrying the electrical signal created by phototransduction for visual processing. Following the ganglion cells are amacrine cells, which are laterally functioning regulatory cells that interact with the ganglion cells or bipolar cells. Bipolar cells interact between photoreceptor cells or horizontal cells and ganglion cells, deriving their name from the two poles of dendrites extending from their central cell body to do so. Bipolar cells interact with rod and cone photoreceptors allowing for extensive regulatory capacity. Downstream from bipolar cells, horizontal cells, as the name suggests, act laterally much like amacrine cells to infer additional regulatory capacity,

integrating information between multiple photoreceptor cells. Spanning the entire

thickness of the retina are Müller cells, a specialized glial cell that provides support to

the retina via functions such as electrical insulation, uptake of neurotransmitters and

waste debris, regulation of electrolytes, and storage of energy. At the far end of the

retina, past the photoreceptor cells, is the retinal pigment epithelium, a layer of further

retinal support. The cells of this layer nourish and support the photoreceptor cells which

interdigitate with their processes. The photoreceptor cells, or rods and cones, are a

specialized type of neuron that respond to light of different wavelengths based on

subtype. These integral cells are those in which phototransduction occurs, allowing for

the processing of light stimuli into chemical and electrical impulses that can ultimately

lead to visually perception by the brain.(4, 5) (Figure 1.1)
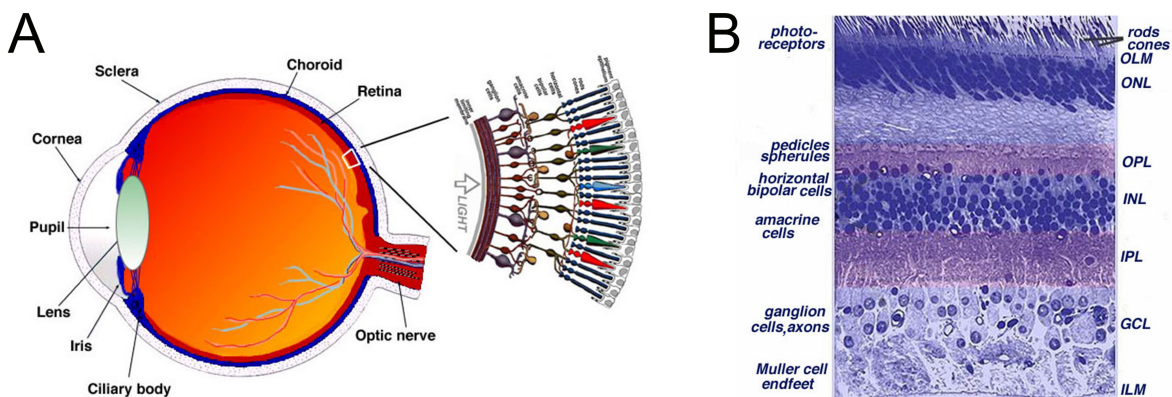
Figure 1.1: The eye and the retina. A. Cross-sectional schematic showing the major ocular structures and the location of the retina. B. Histological cross section of the human retina, illustrating the layers. From top to bottom, the photoreceptor cells (rods and cones) are the outer layer of the retina. The outer limiting membrane (OLM) is positioned between the photoreceptor inner/outer segments and the nuclear region. The outer nuclear layer (ONL) contains the nuclei of the photoreceptors and is followed by the outer plexiform layer, which consists of the synapses between photoreceptors and bipolar and horizontal cells. The inner nuclear layer (INL) is composed of the nuclei of the inner retinal cells including bipolar, horizontal, and amacrine cells. The inner plexiform layer (IPL) consists of the synapses between bipolar cells and ganglion cells, and the ganglion cell layer (GCL) consists of the ganglion cells. Lastly, the inner limiting membrane (ILM) makes up the barrier between the retina and the vitreous and is composed of the end plates of Müller cells. Adapted from (4)

1.2.2 Photoreceptor cells and phototransduction

Photoreceptor cells are a specialized neuron in which the process of phototransduction occurs. Photoreceptors contain multiple domains, namely inner and outer segments, an interconnecting region that connects those regions known as the ciliary zone, and nuclear and synaptic regions. The outer segment is the region responsible for phototransduction which occurs entirely within this segment. This segment contains layers of membranous "discs", which function to increase the membrane surface area available to accommodate the proteins needed for phototransduction. However, the outer segment does not contain any cell machinery for the production of proteins and energy or for the processing and disposal of waste. These functions occur in the inner segment and retinal pigment epithelium (RPE). The inner segment is integral for production of proteins and energy needed by the outer segment, necessitating transport between the inner and outer segments for delivery of inner segment produced products. This transport occurs in the interconnecting region, which contains a connecting cilium that extends between the two segments. The RPE is a monolayer of cells external to photoreceptor cells, with processes that interdigitate between the photoreceptor outer segments. This layer is integral for providing substances to the outer segments, absorbing scattered light to offset the photo-oxidative stress on the retina, and for the processing of outer segment discs. Additionally, photo-oxidative stress on photoreceptors as a given consequence of their role in processing light causes a continual process of shedding of the outer segment discs and renewal of the discs at the proximal end of the outer segment. The RPE serves a crucial role by phagocytosing the spent outer segment discs.(4, 6) (Figure 1.2)
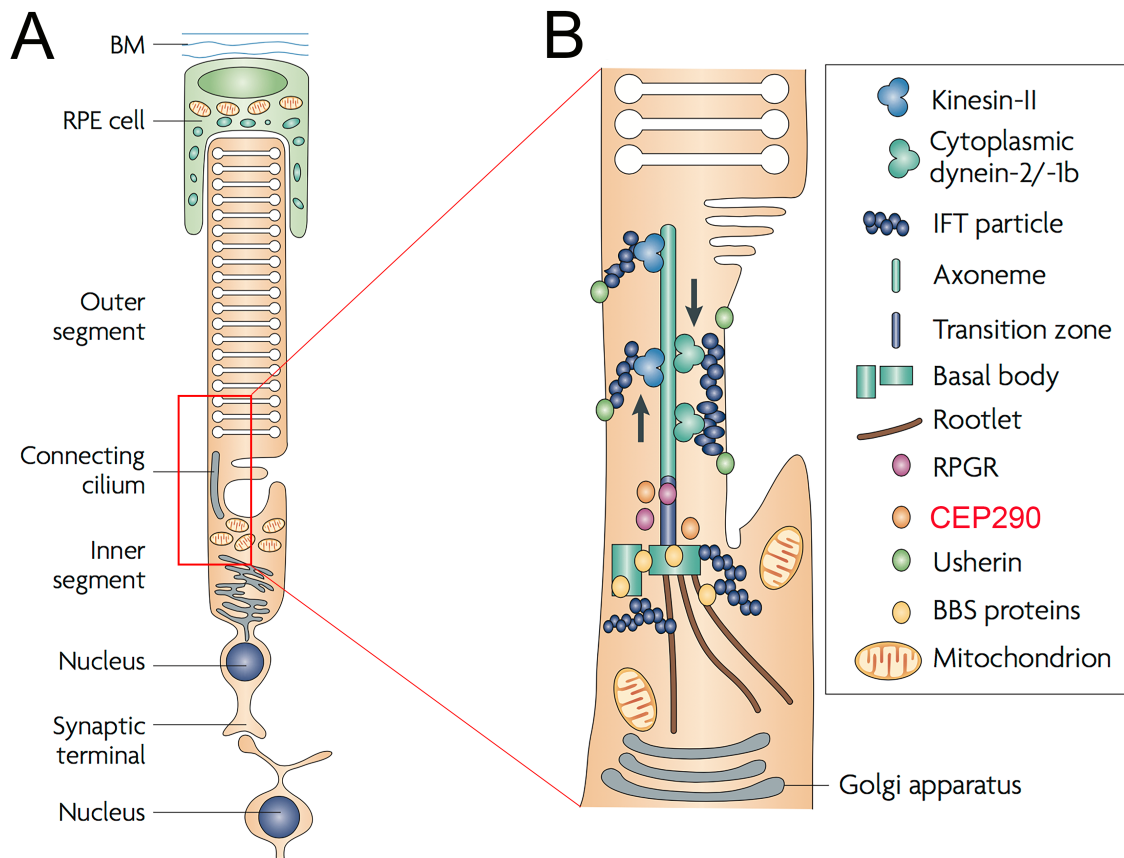
Figure 1.2: The photoreceptor cell and connecting cilium. A. Schematic of a rod photoreceptor cell illustrating the membrane disks and different regions of the cell. B. Magnified view of the interconnecting region illustrating the location of CEP290 protein in relation to the major machinery in this region. Adapted from (7)

Phototransduction is the process by which photoreceptor cells process light that enters the eye into signals that can be transmitted to downstream cells for eventual transmission to the brain for final visual processing and perception. It is a complex process characterized by a series of sequential changes within the cell. It begins when photons of light enter the eye, traverse the retina, and reach the outer segments of photoreceptor cells. These photons are absorbed by a protein known as rhodopsin in rod cells or opsin in cone cells, which are G-protein coupled receptors that contain the light-absorbing chromophore "11-*cis* retinal".(8)

This photon absorption causes a conformational change in the retinal chromophore. In the example of a rod photoreceptor cell, it changes 11-*cis* retinal to an all-*trans* configuration. This in turn leads to activation of a G-protein called transducin, which in turn activates a cGMP phosphodiesterase (PDE). The PDE molecule then hydrolyzes cGMP. The hydrolysis of cGMP lowers the concentration of this molecule in the outer segment, resulting in fewer of these molecules available to the membrane's cGMP-gated cation channels. The result is closure of the cyclic nucleotide-gated (CNG) channels and hyperpolarization of the cell.(8) (Figure 1.3)
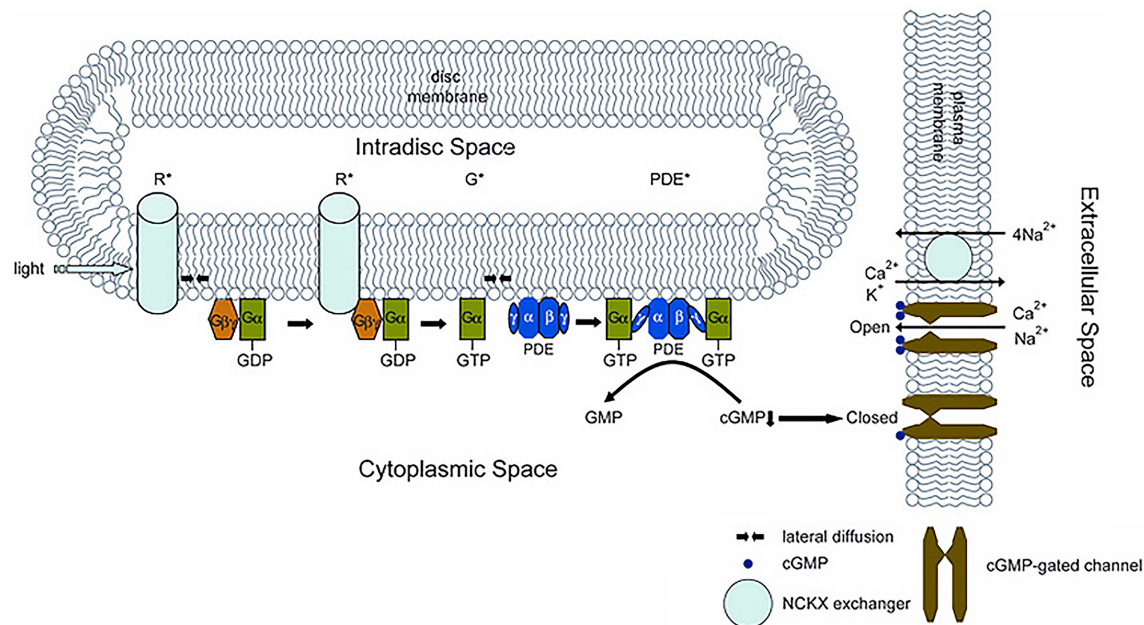
Figure 1.3: The phototransduction cascade. Photons of light activate rhodopsin (R*), which in turn activates the G-protein. The activated G-protein binds to the inhibitory subunits of phosphodiesterase (PDE), catalyzing the hydrolysis of cGMP causing a decrease of cGMP concentration in the cell. The lack of cGMP results in the closure of cGMP-gated channels in the surface membrane of the cell, causing hyperpolarization of the cell. Adapted from (8)

Though phototransduction occurs in the outer segments of photoreceptor cells, the rest of the cell supports this function by maintaining overall cell health and providing

the necessary support for the outer segments. The inner segments contain the cell machinery that conduct cell functions such as the production of energy and proteins. As stated earlier, the outer segments are not capable of these functions and as such rely on the inner segments to supply the products necessary for phototransduction. To allow for this, photoreceptors have a ciliary zone between the inner and outer segments that is responsible for the transportation of proteins to and from the outer segment. Within this zone is a primary cilium that extends between the inner and outer segments known as a connecting cilium, along which products are transported. This transport is facilitated by a kinesin motor system that moves products toward the outer segment and a dynein motor system that moves products towards the inner segment. In addition to the transportation machinery, support proteins are integral for regulating the movement of products and waste along this cilium. 'Gate-keeper' proteins, for example, bridge the gap between the cilium and the wall of the photoreceptor, maintaining an appropriate distance between components and regulating what products pass through. These proteins interact with other proteins within the ciliary zone and together these complexes are imperative for proper cell function, health, and phototransduction.

1.2.3 Inherited retinal dystrophies

Inherited retinal dystrophies are a leading cause of blindness that affect approximately 1 in every 2,000 people worldwide.(9) They are debilitating and devastating diseases that significantly impair or destroy vision and adversely affect quality of life. The inherited nature of these diseases and the cell types they affect, often the terminally differentiated photoreceptor cells, make them difficult to treat. As such,

effective treatments are currently limited and primarily consist of clinical trials. However, there are treatments that show promise in the laboratory, making these conditions both imperative and exciting to study.

Two types of retinal dystrophy, Retinitis Pigmentosa (RP) and Leber Congenital Amaurosis (LCA) make up a large portion of retinal dystrophies. The study of these conditions are active areas of research and of specific interest to this dissertation, as will be detailed in upcoming sections.

1.2.3.1 Retinitis Pigmentosa (RP)

Retinitis Pigmentosa, or RP, is a human retinal dystrophy that affects about 1 in every 3,700 people (10). It is characterized by progressive loss of vision that begins in the peripheral retina and spares central vision leading to tunnel vision. Most forms affect rod photoreceptor cells prior to cones and are hence considered rod-cone dystrophies, which results in diminished dim light vision first with bright light visual deterioration occurring in later stages of disease. Visual acuity is preserved in early to mid stages of disease and later is lost with patients experiencing increasing photophobia throughout the course of the disease. (11)

Funduscopically, patients typically show characteristic changes to the retina. Signs include pigmentary deposits that begin in the peripheral retina and extend centrally, blood vessel attenuation, optic nerve head pallor, and visible retinal atrophy. Electroretinographically, patients show progressively decreased a- and b-wave amplitudes. (11)

1.2.3.2 Leber Congenital Amaurosis (LCA)

Leber Congenital Amaurosis, or LCA, is the most severe inherited retinal disease leading to blindness. It is characterized and diagnosed based on four features; severe loss of vision that occurs early in life, nystagmus, amaurotic pupils and a nonrecordable electroretinogram.(12) It is considerably more rare than Retinitis Pigmentosa with an estimated prevalence of 1 in every 81,000, however, it is a particularly devastating form of retinal dystrophy owing to its early-onset and often severe phenotype.(2)

Children affected with LCA typically begin showing clinical features of disease within the first few weeks of life.(13) The speed with which the disease progresses as well as the changes in fundic appearance depend upon the gene mutated and the subsequent effect on the protein product.(14) This varies considerably as LCA has been associated with over 400 mutations that occur in seventeen genes to date. These genes account for roughly 70% of all LCA cases, suggesting mutations in other yet-to-be identified genes as well.(14)

1.2.3.2.a *CEP290* associated disease and LCA

Of the identified mutations association with LCA, over 100 involve the centrosomal ciliary 290kDa (*CEP290*) gene, accounting for approximately twenty percent of LCA cases.(15) Understanding this gene, the function of the protein it encodes, and the effects mutations within this gene have on phenotype are therefore important areas of research. (Figure 1.4)

In humans *CEP290*, also known as nephrocystin 6, or NPHP6, is 93.2kb long

and is located on human chromosome 12, at q21.13. It contains a total of 54 exons and

encodes an 8kb transcript.(16)

Figure 1.4: Disease-causing mutations in the *CEP290* gene in people. The
schematic illustrates the protein with known domains. Each mutation is marked based
on where it affects the protein.(17)

The protein produced by this gene is a large 290 kDa protein that has multiple

domains, many of which are highly evolutionarily conserved. There are thirteen coiled-

coil domains, three tropomyosin homology domains, a hook domain, six RepA/Rep

protein kinase inducible domain motifs, a bipartite nuclear localization signal, an ATP/

GTP-binding site motif A (P-loop), a region with homology to structural maintenance of

chromosomes chromosome segregation ATPases, and a region with homology to a

myosin-tail domain. It is mostly unknown what roles these domains play in this particular

protein.(16) However, it has been suggested that the BPNLS domain likely functions in

the nuclear localization of the CEP290 protein (18), and that the myosin-tail-like domain

13

may be important in the movement of the protein to centrosomes along microtubules by providing a backbone for the myosin motor.(18, 19)

The protein is localized within the centrosomes of mitotic cells, nuclei, and in certain cell types including photoreceptors, within the basal bodies at the base of ciliary apparatuses. It has most notably been found to be expressed in rod and cone photoreceptor cells, kidney cells, olfactory sensory neurons, and the brain.(18-22) The protein is integral for the proper function of centrosomes and cilia, as it acts as part of a protein complex that facilitates transport along microtubules. This protein complex includes centrin, dynactin subunit P150, gamma-tubulin, kinesin-associated protein 3 (KAP3), kinesin family member 3A (KIF3A), ninein, p-50 dynamitin, pericentrin, retinitis pigmentosa GTP-ase regulator (RPGR), and RPGR-interacting protein 1 (RPGRIP1), all of which make up the important dynein-dynactin molecular motor. In the rd16 mouse, a model of *CEP290* mutation-associated retinal disease, it has been shown that the CEP290 protein is integral for the proper trafficking of important phototransduction molecules including rhodopsin and arrestin.(19)

Moreover, CEP290 seems to play a role in the assembly of primary cilia, through its interactions with the proteins PCM-1 and Rab8a. PCM-1 is required for the proper organization of microtubule networks, and it has been shown that CEP290 is recruited to centrioles by PCM-1 and that disrupted CEP290 concentrations lead to the mislocalization of PCM-1. Rab8a is recruited by CEP290, and is a GTPase required for the proper elongation of ciliary membranes.(23)

CEP290 has been shown to interact with other important proteins as well. The protein segment encoded by exons 2-21 of the CEP290 N-terminus interact with

Activation Transcription Factor 4 (ATF4) and can lead to the activation of transcription mediated by this factor.(18) Furthermore, CEP290 interacts with two important G-proteins within olfactory epithelial cells, suggesting an important role in G-protein trafficking during olfaction.(22)

The CEP290 protein is important during the development of photoreceptor cells due to its involvement in the transport of the proteins and lipids necessary for this process. It accomplishes this by facilitating transport along the primary cilium that eventually gives rise to the interconnecting cilium of photoreceptor cells, where it remains localized following maturation of these cells. It is also essential for the maintenance of photoreceptor cells, as rod photoreceptor discs have a high turnover rate and therefore require a functional transport system to sustain their regenerative processes.(24)

Due to the fairly widespread expression of CEP290 and the many important roles it plays both alone and through its interactions with other proteins, several diseases including syndromic and non-syndromic disorders have been associated with mutations in the gene encoding this protein. These diseases have mostly been identified in humans; however, non-syndromic retinal diseases have been identified in other species, including the retinal degeneration 16 (rd16) mouse and the retinal degeneration in the Abyssinian (*rdAC)* cat, two *CEP290* mutant models to be discussed later in this chapter.

Owing to the ciliary location of the CEP290 protein, mutations in this gene have been associated with a variety of "ciliopathies," a class of diseases characterized by dysfunction of cilia. These diseases range greatly in phenotype given the widespread

presence of cilia throughout many cells types within the body and include diseases of organs such as the kidneys, liver, brain, and retina.(25)

Due to the ubiquitous nature of the CEP290 protein and the existence of several known mutations in the gene in humans, multiple ciliopathies and ciliopathy syndromes have been associated specifically with *CEP290* mutations in people, including four different syndromic disorders; Meckel-Grüber Syndrome, Bardet-Biedl Syndrome, Senor-Løken Syndrome, and Joubert Syndrome, as well as non-syndromic Leber Congenital Amaurosis.

Meckel-Grüber Syndrome (MGS) is an autosomal recessively inherited disease that has been associated with *CEP290* mutations in eight families, and an additional four families show Meckle-like Syndromes, with incomplete MGS phenotypes, due to mutations in this gene (26, 27). MGS is a severe and devastating disease that is fatal in the neonatal stage. The syndrome includes severe central nervous system malformations such as occipital meningo encephalocele, renal abnormalities typically including bilateral cyctic kidney dysplasia, hepatic abnormalities including portal ductal proliferation, as well as postaxial polydactyly. The syndrome may also present with additional abnormalities in the cardiac system as well as additional developmental abnormalities including cleft palate, *situs inversus* or malformations of the genitalia.(28)

Bardet-Biedl Syndrome (BBS) is a severe syndromic ciliopathy that ranges considerably in phenotype and genotype. Fourteen genes have been implicated as causes of BBS, including *CEP290*, and in most cases the disease is inherited in an autosomal recessive manner. It has been reported that many patients have multiple mutations in different genes with resulting effects on expressivity and penetrance

16

(Zaghloul, 2009). The syndrome most commonly consists of retinal degeneration, obesity, renal dysfunction, polydactyl, and hypogonadism, but may also include neurological, cardiovascular, hepatic, and metabolic impairments as well as speech deficits, hearing loss, diabetes mellitis, and Hirschsprung disease.(29)

Senor-Løken Syndrome (SLS) has been associated with mutations in *CEP290* in several families. The syndrome is characterized by nephronophthisis-like renal impairment and retinal degeneration. An autosomal recessively inherited syndrome, SLS causes severe renal impairment including tubulointerstitial fibrosis, tubular atrophy, tubular dilatation and the formation of renal cysts, which together lead to end-stage renal disease typically within the first thirty years of life.(30) The retinal degeneration that occurs in patients with SLS also tends to be severe.(18, 31, 32) While certain *CEP290* mutations are recognized as causative of SLS, they are considered an infrequent cause of the disease, as determined by mutation screenings in those affected.(32, 33)

Mutations in several genes have thus far been associated with Joubert Syndrome, or JS, a severe syndromic disorder characterized by psychomotor delay, hypotonia and ataxia, and sometimes also associated with neonatal respiratory dysfunction and oculomotor apraxia.(18, 34) A hallmark of JS is the "Molar Tooth Sign", a cerebellar abnormality apparent on magnetic resonance imaging.(35) The *CEP290* mutations that cause this phenotype are almost entirely frameshift or nonsense mutations that lead to severe loss of function of the CEP290 protein in multiple body systems.(36) While mutations in *CEP290* only account for approximately twenty percent of JS cases, *CEP290* mutations have been associated with a significant proportion of

Joubert Syndrome Related Disorders, or JSRDs, which include not only the above-mentioned clinical features, but others including retinopathy, renal abnormalities, cerebello-ocular-renal syndrome (CORS), orofacialdigital syndrome type VI, or COACH syndrome.(37) Of these disorders, mutations in *CEP290* are a major cause of CORS syndrome, of which they are estimated to cause about half of all cases (37).

Lastly, mutations in *CEP290* have been associated with approximately twenty percent of all non-syndromic LCA cases warranting a considerable amount of research involving the *CEP290* gene to develop treatments for this devastating disease.(15) As described previously, LCA is a form of childhood blindness due to retinal degeneration.

The retinal phenotype most commonly caused by *CEP290* mutations is an LCA (LCA*CEP290*) characterized by severe visual impairment.(38) Fundic changes include white dots on the fundus and progression to pigmentation in the midperipheral fundus. (15, 17, 38, 39) Microscopically, retinas show significant thickening of inner retinal layers in the rod-rich periphery with good preservation of the outer nuclear layer in the region of the fovea, even when the inner retina is significantly affected.(21, 40) Interestingly, some LCA*CEP290* patients exhibit significant olfactory dysfunction and as many as thirty-three percent show neurologic dysfunction however, while these cases are often classified as LCA they more closely resemble syndromic diseases caused by *CEP290* mutations and are therefore probably misclassified.(17, 22, 38, 41)

The correlation between genotypes and phenotypes in cases of LCA*CEP290* is not always clear. However, studies suggest that the phenotype may be determined by which domains are adversely affected by the respective mutation. The rd16 mouse, for example, displays a strictly retinal degeneration phenotype, which is caused by a

mutation that cleaves only the myosin-tail homology domain leaving the downstream domains intact. This suggests that this domain performs a retina-specific function in the mouse, and likely in other species. Similarly, *CEP290* mutant cats also display only retinal degeneration, as detailed below. In these cats, though the myosin-tail homology domain is intact, two other C-terminal domains, KIDV and VI, are cleaved. These data all point to retina-specific functions of the C-terminal domains of the CEP290 protein. (19)

Despite the many diseases associated with mutations in *CEP290* and the severity of these conditions, there are currently no treatments specifically aimed at CEP290 diseases. Research to better understand disease mechanisms and develop treatments are therefore of great importance. For the development of treatments and testing of both the safety and efficacy needed to reach human clinical trials, animal models are imperative. In the case of inherited retinopathies, including LCA[CEP290] there are several species available for this purpose.

1.3 Animal models for inherited retinopathies

Establishing animal models for human diseases is integral for establishing the data necessary to begin human clinical trials. Rodent models, including transgenic models as well as spontaneously occurring models, provide a strong backbone from which to better understand disease mechanisms and take steps towards treatment development. However, these models have certain limitations which can be overcome by the use of large animal models such as cats and dogs.

With the discoveries of naturally occurring PRA-causing mutations in dogs and cats, companion animals have become important large animal models for human retinal dystrophies that can provide more information and more comparable information than rodent models.

All of these animal models provide important information for human retinal dystrophy studies. For instance, candidate genes may be found in animals that can then be more efficiently tested in humans. Furthermore, once mutated genes are identified in animals, the nature of that gene and its protein product and their effect on phenotype can be more easily studied in the animal model and data can then be extrapolated to humans. Importantly, treatment testing must first begin in animal models to provide the proof-of-principle, safety, and efficacy data necessary to reach human clinical trials.(42)

1.3.1 Rodent models

Rodent models of retinal degenerations are numerous and have been described since the 1920's, with the *rodless* mouse marking the first animal model of a human

retinal degeneration.(43) This naturally-occurring mouse model is now known as the rd1 mouse and is still a commonly used model for autosomal recessive retinal dystrophies Shortly thereafter, a naturally-occurring rat model, the RCS rat, was identified.(44-46) The retinal degeneration slow mouse model, or rds mouse, is another early-described naturally-occurring model that was later described and characterized and remains in use today.(47)

A variety of transgenic rodent models have since been created, which allows for a specific gene to be genetically modified as a means of creating a desired model. These techniques have proven particularly useful for creating models for the more rare forms of human retinal dystrophy, including those inherited in autosomal dominant or X-linked fashions. For instance, a murine model with an opsin knock-out has been created that mimics human autosomal dominant Retinitis Pigmentosa, as well as an X-linked model created by the knock-out of the *Retinitis Pigmentosa GTPase Regulator (RPGR)* gene.(48, 49)

Rodent models make excellent tools for studying retinal degenerations. They are inexpensive and can easily be housed in large numbers, making them efficient models that can allow studies of high power due to higher animal numbers. They are relatively easy to handle and in general pose fewer ethical and welfare concerns than higher order models. However, there are differences in the anatomy and physiology of the rodent eye, relative to the human eye, that pose significant limitations to their usefulness as models of human retinal disease. The first most obvious difference is the size of the eye; the strikingly smaller size of the rodent eye makes extrapolating conclusions concerning surgical techniques from the rodent to the human more difficult.

Similarly, the proportions of the structures within the eye are different, with a proportionally larger lens, for example. Furthermore, most rodent models have a rod-dominant retina that lacks a macula and fovea. People rely heavily on the macula and fovea for visual acuity and as such, studying treatment effects on these regions is imperative. Furthermore, diseases of the macula make up a leading cause of visual impairment, necessitating models with a homologous central retinal region and disease for studying these diseases and developing treatments against them.(50) Therefore, while rodents make useful animal models for retinal dystrophies, they have some significant limitations that warrant the use of other species whose eyes bear greater resemblance to the human eye.

1.3.2 Large animal models

Dogs and cats are moderately priced and relatively easy to house while affording the benefits of eyes that are similar to humans, in size as well as anatomy. Companion animal models of human retinal dystrophies have therefore become important models used in research today. In particular, the dog, with retinal dystrophy occurring in a large number of breeds, has established itself as a top spontaneously occurring model. With the characterization of multiple forms of PRA in cats and the identification of the mutations causing these forms, however, the cat has also become a useful animal model for retinal dystrophies.(51-54)

Progressive Retinal Atrophy (PRA) is a group of genetically heterogenous retinal diseases that cause blindness in companion animals. PRA makes up the leading inherited cause of blindness in purebred dogs and has been identified in over 100

breeds.(55) It is a naturally-occurring disease, and that characteristic, along with the desirable characteristics of the canine eye, make canine forms of PRA excellent models of RP and LCA in humans.

Though the canine eye is still smaller than the human eye it is more similar in size to the human eye than rodent models, and in addition, has similar proportions.(56, 57) These characteristics make surgical techniques more comparable to the human.(55) Moreover, though the canine does not have a macula or fovea it does have an *area centralis*, a region of significantly increased cone density that may play a role in visual acuity, much like the human macula.(58-60)

PRA in dogs makes an excellent model for RP or LCA in humans, as it is a group of heterogeneous diseases that mimic RP and LCA both genetically and phenotypically. Genes that are associated with PRA in dogs are the same genes associated with RP and LCA in humans, and the phenotypes caused by these mutations are often similar between the species.

Several mutations have been identified in dogs that cause PRA, including several that contribute significantly to human retinal dystrophies such as *CNGB1*, and *PDE6* both alpha and beta.(61-64) Most of these mutations cause autosomal recessively inherited forms of PRA, though autosomal dominant and X-linked forms have been described.(55, 65-67)

In addition to elucidating information concerning the defective genes and their products, canine models have provided a platform in which to test prospective treatments for retinal dystrophies. Such treatments have shown success in dog models and have been important in the development of human clinical trials.(68-70)

The discoveries of naturally-occurring disease-causing mutations in the dog, the fact that these are in the same genes as disease-causing mutations in people, and the similarities of their eye with the human eye, have made the species a leading large animal model for human retinal dystrophies. As more mutations are identified in the species, the dog will provide further opportunities for studying inherited retinal dystrophies and will continue to be a popular large animal model for these diseases.

Two forms of PRA were identified in the cat in the 1980's.(71, 72) With the discoveries of the disease-causing mutations for these two forms of feline PRA, mutations in the *CEP290* and the *CRX* genes, the cat has presented itself as another important large animal model for human retinal dystrophies.(53, 73) These feline forms of PRA have allowed the establishment of two important and much needed LCA models; a model for autosomal dominant LCA and for LCA caused by the commonly mutated *CEP290* gene.(72, 74)

Like the dog, the cat makes an excellent animal for use as a model of retinal dystrophy. The feline eye shares great similarity in both size and anatomy to humans, and has proportions conducive to practicing surgical techniques and treatments. Cats also possess a photoreceptor and cone dense *area centralis* region, allowing for extrapolation to the human macula. (Figure 1.5)

These two cat models are new valuable tools as the scientific community moves towards the development of treatments for LCA. However, before these models can be fully utilized, it is important that baseline information regarding these therapies and their effects in cats be established.
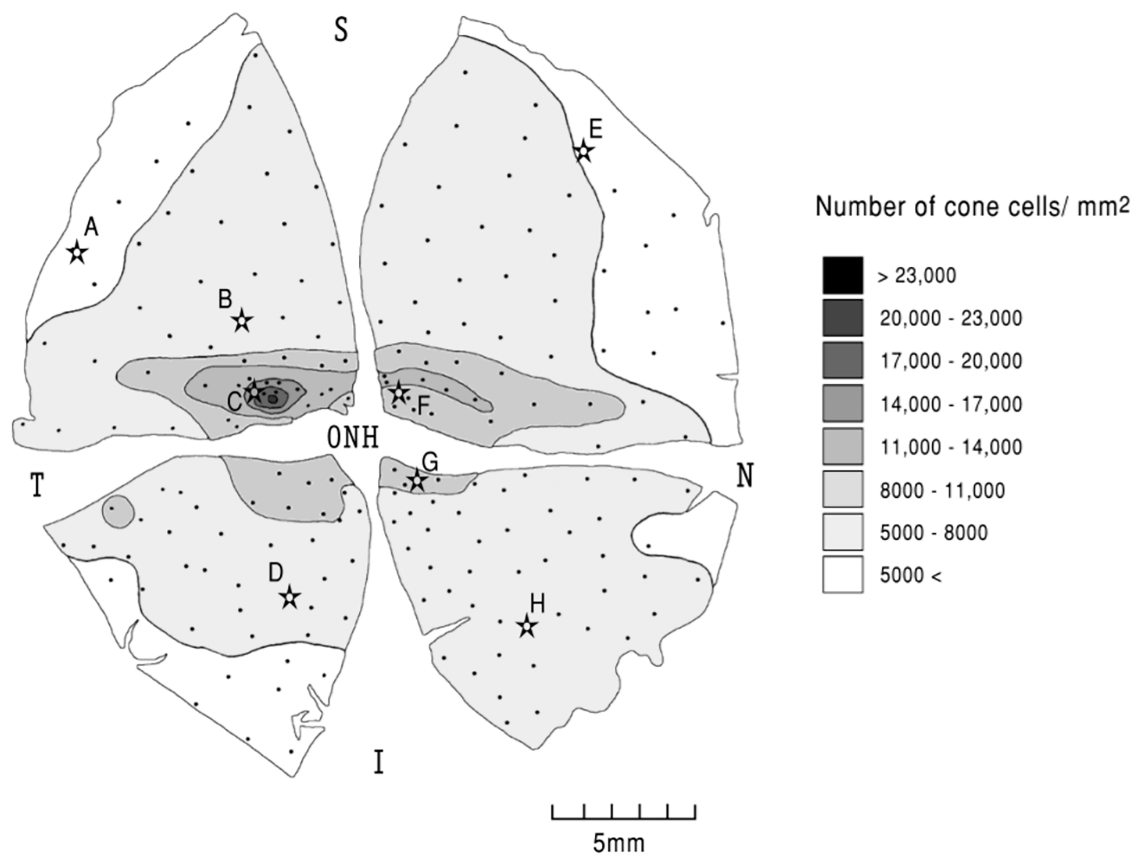
Figure 1.5: Distribution of cones in the feline retina. The schematic depicts a heat map derived from the cone density of the retina with darker colors indicating higher cone density. Cone density is higher along the visual streak than the peripheral retina and is highest at the area centralis. S = superior, N = nasal, I = inferior, and T = temporal. Letters A-H indicate regions the investigators characterized further. Adapted from (75)

1.3.2.1 The feline *CEP290* model

A form of spontaneously inherited PRA was discovered in Abyssinian cats in

Sweden in the 1980's.(71) It was determined through breeding that this form is inherited

in an autosomal recessive fashion and it was determined that it is caused by a mutation

in the centrosomal ciliary 290kDa, or *CEP290*, gene.(73, 74) This intronic one base-pair

substitution allows for the usage of a GT sequence four base pairs upstream of the

mutation to be utilized as a splice donor site. This results in a four base-pair insertion in

the transcript during splicing and a predicted truncation of the protein that would

25

eliminate 159 out of the total 2,479 amino acids.(52) *CEP290* is the most commonly mutated gene implicated in LCA cases, making the *CEP290* PRA (PRA^*CEP290*) cat a new and important LCA model.(15) (Figure 1.6)
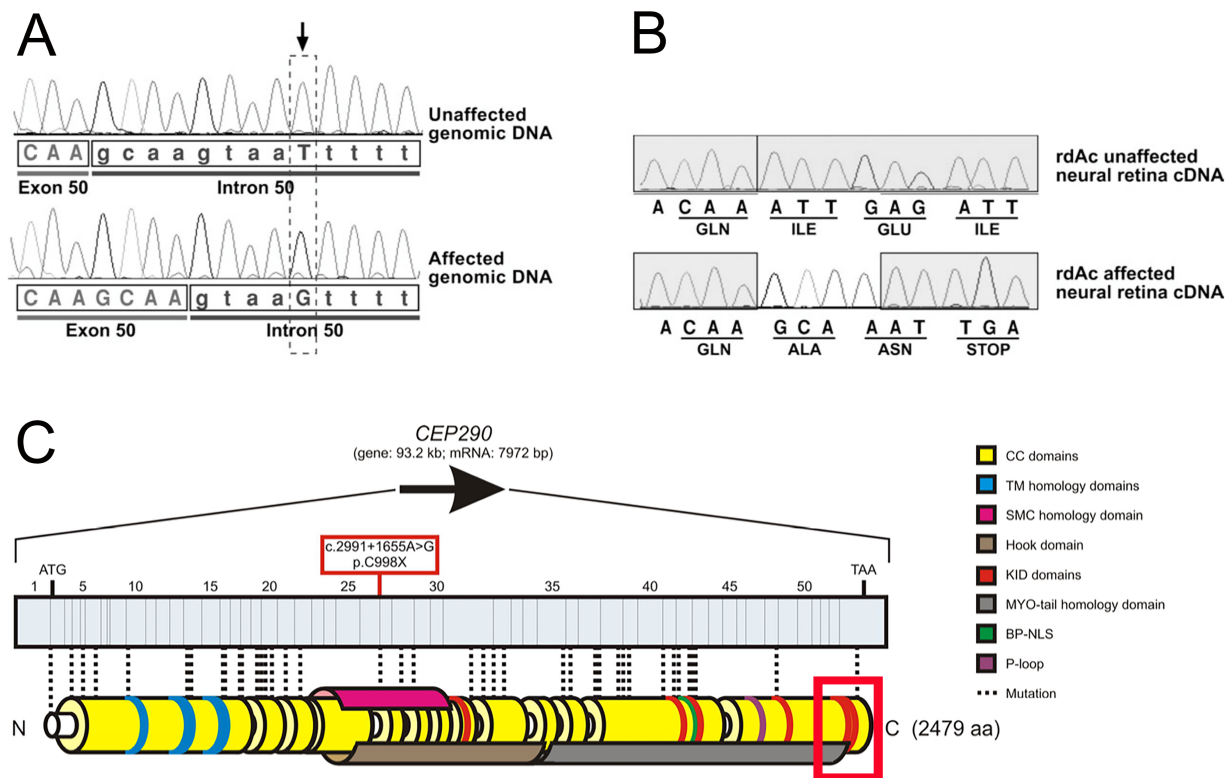
Figure 1.6: The feline *CEP290* mutation and resultant truncated protein. A. Electropherogram of the feline genomic sequence in the region of the *CEP290* mutation. The top row shows the wild-type T nucleotide, which is substituted with a G in the mutant allele. This change allows for the GT upstream of the mutation to be used as a splice donor site (spicing depicted by boxes). B. Electropherogram of the corresponding cDNA shows the four base-pair insertion in the transcript. C. Schematic representing the human gene and protein. Dotted lines indicate disease-causing mutations in people, with the most common mutation highlighted in the red box at the top of the image. The red box on the protein image represents the region of the protein truncated by the *CEP290* mutation in cats. Adapted from (16, 52)

The phenotype caused by the above-mentioned *CEP290* mutation in the feline is exclusively retinal and is considered a form of PRA.(71) This phenotype is most similar to that seen in humans with non-syndromic Leber Congenital Amaurosis (LCA) caused

by mutations in *CEP290*. However, the phenotype in cats is less severe than seen in typical cases of *CEP290* retinopathies in people, with a later onset and slower progression, an interesting difference worth investigating that could help guide treatment development. This question was addressed by our laboratory and the results are detailed in Chapter 2 of this dissertation.

In homozygous animals, clinical signs include features characteristic of PRA. Signs of progressive blindness are first apparent in early adulthood. Funduscopic abnormalities are first observed at 1.5-2 years of age and include blood vessel attenuation and changes in tapetal reflectivity that correspond to morphological changes in retinal thickness. Initially, the fundus typically shows patchy regions of hyporeflectivity, a sign that is different from other forms of PRA, but later becomes hyperreflective, as is typical with PRA as the retina thins on top of the tapetum lucidum. This hyperreflectivity is initially most obvious in the peripheral fundus and is not apparent in the central fundus until late stages of disease. Cats are functionally blind by 3-5 years of age.(76)

Electroretinographically, the waveform of affected ERGs has a normal shape, however, amplitudes progressively decrease. Beginning early in the disease, affected cats show decreased b-wave amplitudes, an elevation in b-wave threshold, and may begin showing a decrease in a-wave amplitude.(77, 78) At a more advanced stage of disease, thresholds are significantly elevated, the amplitudes of both a- and b-waves are markedly reduced, and flicker responses are non-recordable.(77, 79-81) At this stage, oscillatory potentials are also non-recordable.(82) Eventually, all ERG responses become non-recordable.(83) Implicit time changes are less severe throughout disease,

with an increased implicit time noticed only for b-waves at high light intensities in later stages of disease.(83)

Use of multifocal ERG can be used to study the distribution of electrical responses across the retina. In one study using this technique, it was reported that regional differences in ERG responses were not evident until a moderately advanced stage of disease. At that stage they saw a slightly higher response from the area centralis region, which is consistent with the morphological findings described below and taken together suggest that the central retina may be spared until late stages of disease.(84) This characteristic would be consistent with LCA^{CEP290} in which central retina sparing is seen and would support the cat as a model for this retinal dystrophy. (21) However, studies to determine regional rates of degeneration were not conducted to confirm this. We therefore aimed to study this change utilizing spectral-domain optical coherence tomography (SD-OCT), a useful tool for *in vivo* monitoring of retinal architecture and layer thicknesses, as detailed in Chapter 3 of this dissertation.

These changes correspond to the morphological changes noted histologically by many studies. Though this form of feline PRA typically does not become evident clinically until cats are adults, ultrastructural changes are evident early on. By about four weeks of age rod outer segment discs show disorientation.(85) The same study noted that these initial changes were later followed by rod degeneration, with individual rods or small patches of rods beginning to degenerate before clinical signs become evident. This patchy degeneration was reported to start in the peripheral and mid-peripheral fundus, with significant shortening of the photoreceptor inner and outer segments and slight reduction of the outer nuclear layer occurring in early stages in those patches.

(86). Based on these findings, the authors divided the phenotype into two phases. The first phase occurs before complete maturation of the retina and is characterized by disorientation and disorganization of rod outer segment disc membranes. The second phase occurs later on and is characterized by progressive degeneration of photoreceptor cells culminating in photoreceptor cell death. Furthermore, vesicle formation is evident in photoreceptor cells as degeneration progresses.(87)

Changes in the inner retina are also apparent, with changes most notable in horizontal cells. These cells show significant extension and thickening of the lateral processes beginning in the first stage of the disease. The apical dendrites then degenerate as the disease progresses. Rod bipolar cells also show changes, but only in the later stage of disease. They show loss of their fine dendritic processes and disorganized axons, and decrease in number over time.(88) Furthermore, the axon terminal boutons in the innermost section of the inner plexiform layer of the retina were decreased in number and smaller in size in affected animals. However, it has also been noted that the innermost region of the retina appears to be preserved throughout the course of the disease.(89)

The feline *CEP290* form of Progressive Retinal Atrophy is characterized by progressive degeneration and thinning of the retina ultimately leading to blindness. The phenotype is similar to LCA[CEP290] in people with likely central retinal sparing but with a later onset and slower progression, warranting investigation of these differences.

1.4 Treatments for retinal dystrophies

There are currently no treatments available for *CEP290* associated retinal dystrophies. With the cat now established as a useful model for LCA*CEP290*, great opportunity exists for treatment development and testing. Though *CEP290* retinopathies pose unique challenges for treatment development, stem cell transplantation, gene therapy, and genome editing, all present promising treatment possibilities.

Stem cell therapy is appealing because it may allow for the replacement of photoreceptor cells, a type of terminally differentiated cell, even after they have been lost. This is something that gene therapy or genome editing cannot achieve, as they must be administered prior to the loss of photoreceptor cells and therefore would need to be administered earlier than stem cell therapy. However, while some reasonable success has been demonstrated, this treatment has produced very limited success in the feline *CEP290* model.(90-99) One study was only able to achieve successful transplantation in two out of the four cats studied, and in those two, host blood vessels did not extend into the transplants and no improvement in vision could be recorded electroretinographically.(100) Another study found some promising results, suggesting that allografts can survive without rejection in the mutant feline retina; however, the allografts caused significant photoreceptor detachment from the retinal pigment epithelium and subsequent photoreceptor degeneration, and they found no improvement in the rate of photoreceptor degeneration.(101)

Therefore, while stem cell transplantation holds promise in theory, it is important to study alternative treatment methods. Gene therapy would allow the wild-type gene to

be introduced into the host to promote the creation of the unaffected gene product. With genome editing, the mutation may be edited out either *in vivo* or be combined with similar methods presented above to edit the mutation out of a patient's own cells for re-transplantation.

Gene therapy based treatments show great promise for the treatment of inherited retinal dystrophies. Leber Congenital Amaurosis cases caused by *CEP290* mutations are no exception, and felines affected with PRA caused by the *CEP290* mutation provide an invaluable tool to test this therapy before proceeding to human clinical trials.

As discussed, the phenotype in the feline progresses fairly slowly and has an age of onset that would allow administration of a gene therapy treatment prior to the loss of the photoreceptor cells. Following introduction of the therapeutic gene into the feline retina, cats could be examined for visual improvement and monitored for signs of adverse reactions.

There is a significant obstacle to *CEP290* gene therapy, however. With a transcript size of approximately 8kb it may be impossible to fit the transcript into the vector of choice for the retina, the adeno-associated viral vector.(16) Though ambitious and still in the beginning stages of exploration, there are a few methods that may overcome this obstacle, including heavily packing the AAV vectors, co-transduction, inclusion of a partial transcript in the vector, or utilizing a different vector system altogether.(102-108)

Alternatively, these obstacles can be avoided using a different treatment type, genome editing. Genome editing is a method by which changes can be made to the genome to achieve aims such as making insertions or deletions or even replacing a

segment of the genome. Two previously common systems used to accomplish this were TALENS (transcription activator-like effector-based nucleases) and zinc-finger nucleases, both classes of enzymes known as nucleases that makes cuts in DNA and through bioengineering can be directed to cut specific sequences. More recently, the CRISPR-Cas nuclease (clustered regularly interspaced short palindromic repeats) has gained favor as a more easily engineered, affordable, and scalable method of genome editing.(109)

The CRISPR-Cas system is a bacterial immune system that infers an acquired immunity against foreign nucleases such as the sequences contained within viruses and plasmids. The DNA of this system, the basis of the name, consists of short palindromic repeats next to which short "spacer" sequences are added through recognition and copying of invading nucleases. Next to the CRISPR sequences are sequences encoding the Cas (CRISPR-associated system) nuclease. Together this system recognizes, remembers, and then in subsequence infections destroys invading nucleases.(110)

This system has been harvested and bioengineered for use as a genome engineering tool. Typically utilizing Cas type 9 (Cas 9), the CRISPR/Cas 9 system can be introduced into cells along with a "guide" RNA, or gRNA, designed by the investigator with a specific sequence to guide the system to cut at a designated location within the genome.(111) (Figure 1.7)
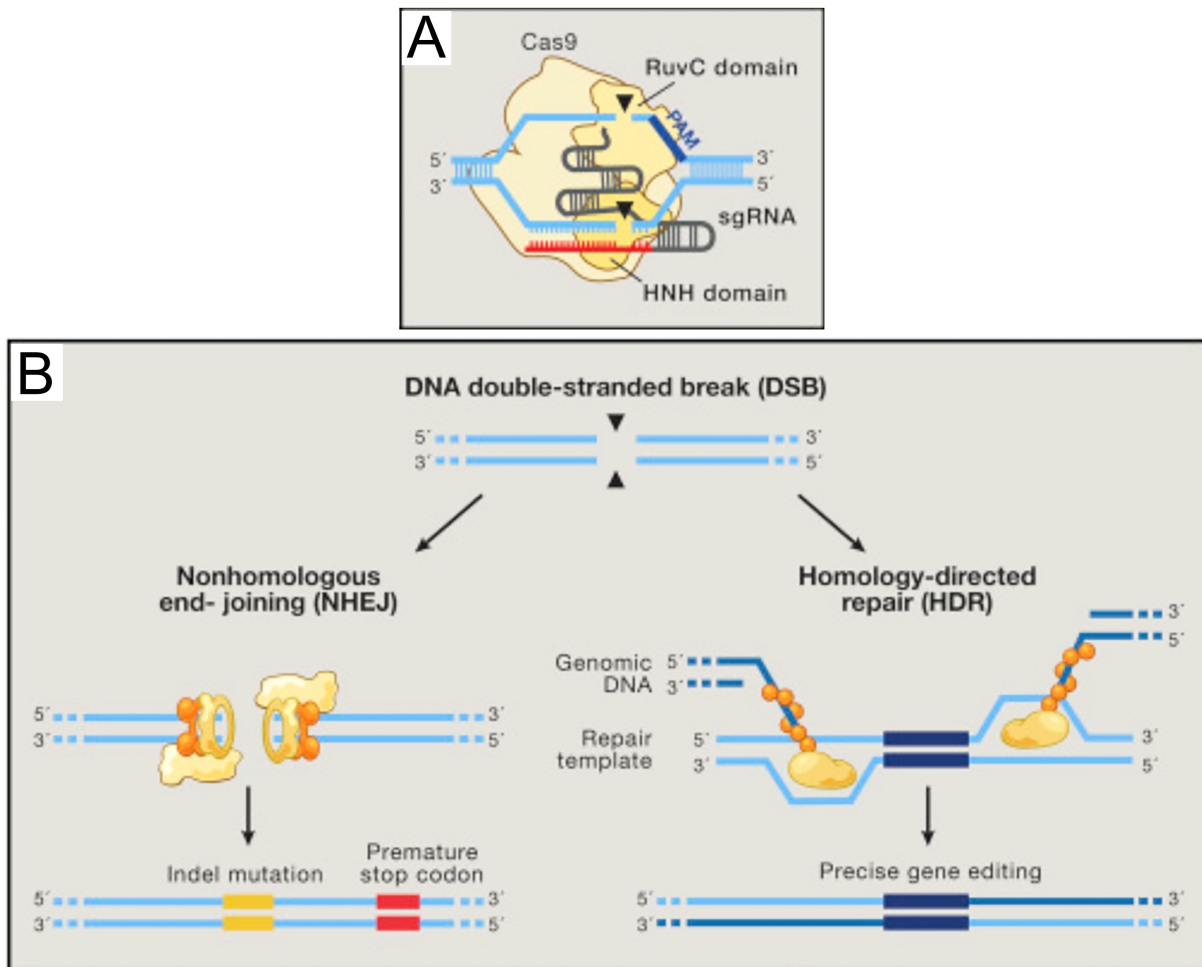
Figure 1.7: CRISPR/Cas9 Genome Engineering. A. Schematic representation of the Cas9 nuclease. The enzyme is directed to a specific DNA sequence by the guide RNAs (sgRNA) via a guide sequence (red). This sequence base-pairs with the target sequence (light blue). The PAM (protospacer-adjacent motif) binds downstream of the target and directs the double-stranded DNA breaks. The RuvC domain cleaves the sequence that is not complementary to the guide sequence while the HNH domain cleaves the sequence that is complementary to the guide sequence. B. The breaks are then repaired by cell machinery via either nonhomologous end-joining or homology-directed repair. Adapted from (112)

This system can be utilized to genome edit for a variety of different purposes including the creation of new models as well as the development of treatments against inherited diseases. It therefore provides a useful tool in the fight against inherited

retinopathies and is of particular interest in the development of treatments against those retinopathies that pose challenges to methods such as gene therapy, as is the case with LCA^{CEP290}.

Use of this system for therapies could be achieved in a variety of ways. Against LCA^{CEP290} the most likely method designs include the editing of patient-derived induced pluripotent stem cells (iPSCs) or photoreceptor precursor cells for re-transplantation into the retina (allowing for avoidance of immune responses to foreign cell transplantation), or, direct *in vivo* delivery of the CRISPR system to the photoreceptor cells. For *in vivo* delivery of this system, a delivery vehicle would be necessary to carry the system into photoreceptor cells. The same vectors utilized in gene therapy could be utilized for this purpose, amplifying the importance of developing, testing, and optimizing delivery vehicles for retinal treatments.

1.4.1 Vehicles for treatment delivery

An integral component of many retinal dystrophy attempts is a vehicle to deliver the transgene or machinery needed for repair to the appropriate cells. Gene therapy and *in vivo* CRISPR genome editing based treatments would both require a vehicle, as examples. Delivery vector testing has been extensively studied in the retina with ideal vector systems determined in several species. However, minimal vector testing has been conducted in some species including the feline. Only one study prior to our investigation had analyzed AAV vector transduction in the feline and only studied a basic AAV2 construct. This study showed effective transduction of photoreceptor cells,

suggesting AAV vectors could be used in the feline retina, and highlighting the need to study additional serotypes, the basis for Chapter 5 of this dissertation.(113)

There are several types of vectors available for delivery of treatment components to the retina, encompassing both non-viral and viral forms. Many types have been tested in the eye; however, most have shown limited success.

Many vector types being studied today are based on viral systems, however, non-viral vector systems have also been investigated. One such vector utilizes plasmid DNA. This vector may be useful for delivering therapeutic genes, however limited success has been found in the retina unless used in conjunction with electroporation (114). Though when combined with this technique plasmid DNA was shown to lead to reporter gene expression in rodent photoreceptor, bipolar, and Müller cells, this technique has fallen out of favor for more effective viral systems.(115) Similar results have been found using other non-viral vector systems such as liposomes and nanoparticles, though these systems show more promise and continue to be investigated today.(116-120)

Viral vectors may stem from several different families of viruses, each with its own advantages and disadvantages. Several virus systems have been tested specifically for therapies to the retina, with varied success.

Adenovirus vectors have overall proven inefficient for retinal gene therapy. This is especially true when using them to target photoreceptor cells.(121, 122) They have shown inconsistent and overall poor photoreceptor transduction, with preferential transduction of the RPE, though a recent study showed some transduction of photoreceptors.(123, 124) Given the RPE targeting of these vectors, they are more

useful for RPE related retinal dystrophies and have shown promise for treatments against retinopathies caused by mutations in *RPE65* and *MERTK*.(125, 126)

Slightly more success has been reported using lentivirus based vectors. Lentiviral vectors are appealing because they are capable of transducing terminally differentiated cells, a class of cells that includes photoreceptor cells, and because they have a large carrying capacity capable of holding longer transcripts.(114) Despite that however, lentivirus vectors favor transduction of the retinal pigment epithelium and have shown unpredictable transduction of photoreceptors.(127) However, studies investigating alterations to lentiviral vectors such as the use of bicistronic or dual-promotor vectors has resulted in successful delivery to the retina in some studies and are currently in clinical trials against Stargardt's Disease.(128-132)

A concern with lentiviral vectors is the possibility of insertional mutagenesis due to their integration into the host genome, though more recent studies have suggested this risk is low.(133, 134) They also carry a higher risk of immune reactions against them, which has demonstrated in our laboratory when an equine infectious anemia virus (EIAV) vector was tested in a pilot study in a wild-type feline (unpublished results). In this study the EIAV vector induced a severe acute immune response necessitating the early sacrifice of the animal for humane purposes.

The greatest promise for a safe and effective retinal vector system has come from the adeno-associated viral (AAV) vector. This vector type has repeatedly been shown to effectively target retinal cells with minimal adverse side effects and has many characteristics that make it ideally suited for use in the eye, resulting in its wide use in retinal gene therapy studies and clinical trials.

1.4.1.1 Adeno-associated viruses and adeno-associated viral vectors

The adeno-associated viruses (AAVs) are small, non-enveloped, single-stranded DNA viruses of the parvovirus family.(135, 136) They exist endogenously in primates, including humans, but are not associated with any pathological states and result solely in latent infections.(135, 137) Their genome consists of two inverted terminal repeat (ITR) regions that flank replication (Rep) and capsid (Cap) protein encoding regions that are contained in two open reading frames.(138) These components are removed to make room for the packaging cassette when creating AAV vectors.

AAVs gained their name from the discovery that they require a helper virus to replicate, which is typically an adenovirus but may also be a herpes virus.(136) Wild-type AAVs integrate into the host genome in a specific location. In humans, they integrate into chromosome 19, and 60-70% of the time, specifically at the location 19q13.3-qter.(139) However, AAV vectors do not integrate but instead exist in episomal form, decreasing the risk of insertional mutagenesis.(140)

Vectors created from these viruses, denoted adeno-associated viral vectors, show the greatest promise as vectors for retinal gene therapy, owing largely to the inherent properties of this type of virus. Their endogenous and non-pathological nature in primates infers a level of safety not offered by other virus type vectors, although recent studies raise concerns that they can activate proto-oncogenes in both murine and human hepatocellular carcinoma, a serious concern that warrants further investigation.(135, 141, 142) AAV vectors have also been associated with more minimal immune reactions than other vector types.(139) Lastly, AAV vectors induce long-term expression at a stable level.(143)

AAV vectors are particularly well suited for the retina. They have been shown to transduce a variety of retinal cell types, are capable of transducing nondividing cells, including photoreceptor cells, and are up to two-thousand times more efficient at transducing said cells than adenovirus vectors.(139, 143-145). This characteristic is essential for the treatment of most retinal dystrophies, which are predominantly diseases of the photoreceptors.

The characteristics of AAV vectors make them a promising and exciting option for treatment delivery. However, it is important to recognize a significant drawback of this vector type. As they are derived from smaller viruses, AAV vectors have a small packing capacity of only 4.7 kilobases.(146, 147) This may present a significant limiting factor that may preclude AAV vector use for the delivery of larger products, such as gene therapy treatments involving larger genes that would exceed this capacity.

An example of a gene of this type is the *CEP290* gene. With a size of approximately 8 kilobases the *CEP290* transcript would not fit inside the compact AAV vector.(16) However, there are ways in which this limitation may be overcome, notably, over-packing of the AAV vector, the use of co-transduction, or the use of a partial transcript.

It has been suggested that the capacity of AAV vectors can be stretched by manipulating the vector.(104) One study showed the successful packaging of up to 8.9kb of transcript into an AAV2/5 hybrid vector, using genes including *CEP290*.(106) They illustrated that the AAV5 capsid is capable of holding more transcript than six other serotypes, and were able to demonstrate successful transgene expression of the large

human ABCA4 gene using this over-packing construct. A method such as this may therefore hold promise for gene therapy treatments involving large genes.(106)

An alternative method to increasing the capacity of the vector is to utilize more than one vector to deliver the therapeutic gene. This method of co-transduction, or "dual-vector" allows the transcript to be split into two parts, with each part inserted into different AAV vectors. The gene is then pieced back together in the host *in vivo*. This can be accomplished by either using different vectors with non-overlapping sequences through concatamerization and trans-splicing, or using different vectors with overlapping sequences using homologous recombination.(103)

Some studies have shown promise. One such study utilizing *in vitro* and murine models to investigate this method's use as a treatment for hemophilia A showed strong transduction and improved phenotypes in both models.(148) However, another study showed that the large *ABCA4* gene can be packed into two AAV vectors and result in in vitro transcript levels, however, no protein could be detected.(149) While this method therefore shows promise, it is clear that further studies are necessary to fine-tune this methodology.

For some genes the entire gene is not necessary for proper function within a given tissue. In these cases, it may be possible to compensate for the small AAV packing capacity by only inserting the necessary segment of the gene of interest into the vector. Using the *CEP290* gene for example, one study reported that replacing only the N-terminus rescued vision in a zebrafish model of retinal dystrophy.(108)

Another significant drawback of the AAV vector is the presence of a lag-phase that precedes transgene expression. This lag-phase is related to the single-stranded

nature of AAVs, as a single-stranded genome requires a conversion to a double-stranded genome in the host nucleus before expression can occur (150-152). This drawback could preclude the use of the AAV vector for the treatment of early-onset or rapidly-progressing forms of retinal dystrophy. To compensate for this drawback, self-complementary vectors can be created in which the DNA synthesis step is averted using a construct that is capable of folding over on itself to create a double-strand.(153)

AAVs posses many different serotypes, each of which carries different properties including capsid surface proteins, the receptors utilized to enter cells, and therefore, the cellular tropism. Over 100 adeno-associated virus serotypes have been identified, several of which have been studied in a variety of species to determine cellular tropism in different tissues.(154-160)

The main steps involved in the process that leads to transgene expression includes the binding of the vector to the host cell's surface, the subsequent entry of the vector into the host cell, and the intracellular trafficking and processing of the virus.

Adeno-associated virus vector binding to the cell-surface receptors of the host cell are dependent on the surface proteins on the virus's capsid. The receptors to which AAV vectors bind is therefore variable and depends upon the serotype used to create the capsid. AAV2 serotype vectors have been shown to bind primarily to heparin sulfate proteoglycans, however there is also evidence for binding to alphaV beta 5 integrin, or fibroblast or hepatocyte growth factor receptors.(161-164) AAV3 is similar to AAV2 and has been shown to also bind to heparin sulfate proteoglycans.(144, 165) Similarly, AAV6 also binds heparin sulfate, while is has been shown that AAV1 lacks the necessary amino acid sequence to do so and AAV12 enters cells in a sialic acid and heparan

sulfate proteoglycan independent manner.(144, 166, 167) AAV4 and AAV5 both bind to sialic acid, with AAV4 binding the alpha2-3 O-linked form and AAV5 binding the alpha 2-3 N-linked form.(168, 169)

Once bound to the host cell-surface receptor, the vector is taken up into the cell. How this occurs is still largely unknown for most serotypes, however, it has been moderately well characterized for AAV2. AAV2 particles are taken up into the cell through clathrin-coated pits through the process of endocytosis.(170) This is initiated by the binding of the capsid to the host cell receptors, which stimulates Rac1 activation, a GTP-binding protein necessary for AAV2 endocytosis.(171) The energy necessary for this to occur is provided by the GTP-ase dynamin, which is located in the cytosol of the cell and is commonly associated with clathrin-mediated endocytosis.(172) It has also been demonstrated that alpha V beta integrin is important in this process.(163) Evidence suggests that AAV5 also enters cells through clathrin-mediated endocytosis. (173)

Once endocytosed into the cell, intracellular trafficking and processing moves the particles to the nucleus and prepares their genomes for integration into the host genome. Processing begins while the virus particles are still within the endosome.(174) It appears that acidification of the endosome and protease inhibitors are integrally involved in this process.(175, 176) Studies suggest that the proteasome inhibitors are involved in the ubiquitination of virus particles while in the endosome, and further hypotheses have been made suggesting that this functions to prime the capsid for disassembly and hence virus uncoating.(177, 178)

Trafficking of the virus particles to the nucleus involves a pathway that utilizes Rab proteins, a class of GTP-ases that regulate endosome functions such as budding, movement, and fusion to a cell membrane.(179) The early endosome contains Rab5, and for AAV2, has been shown to traffic either to late endosomes containing Rab7, or to perinuclear recycling endosomes containing Rab11.(180, 181) New Rab proteins, Rab7 and Rab9, then direct the late endosome to either a lysosome or the trans golgi, respectively.(181, 182)

Following the trafficking of the virus particles through the endosomal pathways, it is necessary for the virions to escape the endosome. This process is not well understood but seems to involve the acidification of the endosome as well as phospholipase A2 activity.(183) Once the virions have exited the endosome and entered the cytoplasm, they must enter the nucleus to gain access to the host's genome.

There is strong evidence that the nuclear transport of AAV2 occurs via tubular networks facilitated by ATP-powered molecular motors.(184) Once at the nucleus, it has been suggested that AAV2 enters passively through diffusion, since their small size would permit passage through nuclear pores.(185) It is thought that this occurs while the particles are still coated.(170)

Once the particles have entered the nucleus, uncoating occurs. This is followed by the conversion of the single-stranded genome into a double stranded genome, a necessary rate-limiting step.(151) It is then that the genetic material of the virus can be integrated into the host genome, in the case of wild-type virus, or maintained in an episomal state, in the case of vectors.(140) (Figure 1.8)

The main components of an AAV vector are the genetic backbone of the adeno-associated virus, the capsid of that virus or that of another serotype, the gene of interest, and a promoter and poly-adenylation signal of the experimenter's choice. They are therefore created by removing the virus's genome, leaving only the inverted terminal repeat (ITR) regions, combining this "backbone" with the transgene of interest and a promoter of interest, and by adding the genetics for the capsid of choice.(186) (Figure 1.8)
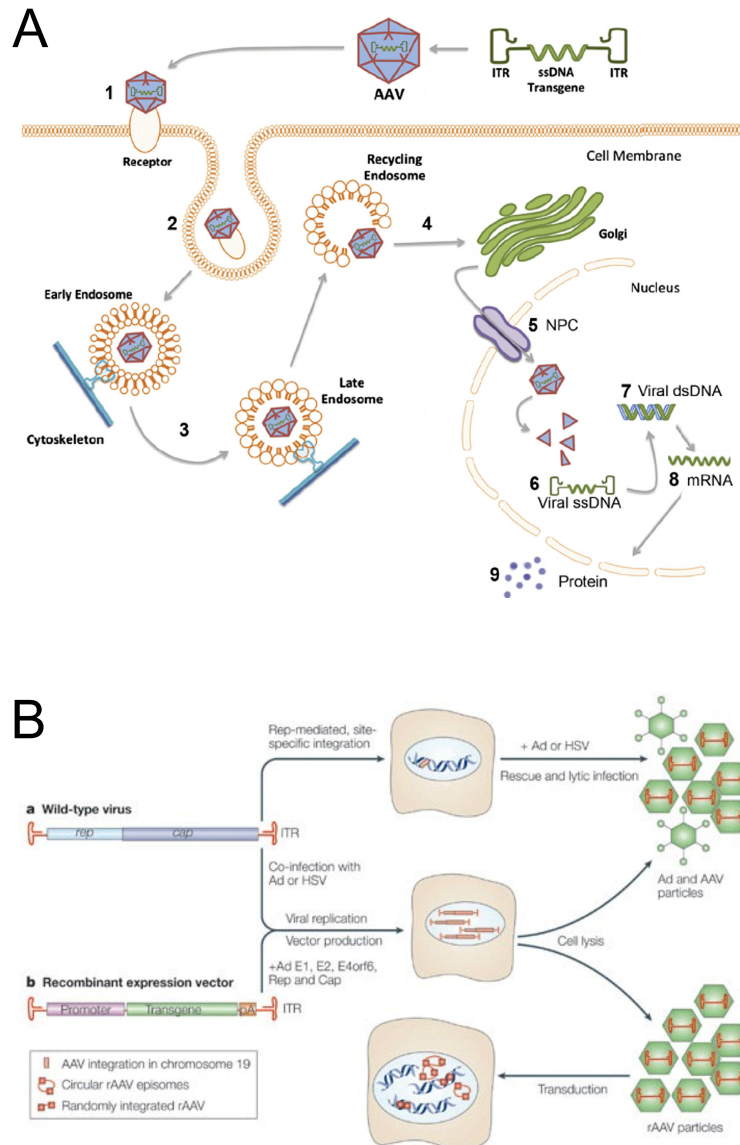
Figure 1.8 Adeno-associated viral vector transduction and creation. A. Schematic representation of the process by which AAV vectors enter the cell. 1- The rAAV capsid binds to the cell surface receptors. 2- The viral particle enters the cell through endocytosis. 3- The endosome is trafficked through the cytoplasm. 4- The particle is released by the endosome and processed by the golgi apparatus. 5- The particle enters the nucleus. 6- The capsid breaks down and ssDNA sequence is released. 7- ssDNA is converted to dsDNA. 8- dsDNA is converted to mRNA. 9- Protein is translated. B. Schematic representation of wild-type AAV and AAV vector creation. a- The wild-type virus contains rep (replication) and cap (capsid) genes. Co-infection with a helper virus results in viral replication and integration into the host genome. b- The rep and cap sequences are removed and replaced by a poly-A tail (pA) and a promoter and transgene sequence of the investigator's design. Vector production utilizing adenovirus or herpes virus helper components (Ad E1, E2, E4orf6) results in the production of rAAV vector particles only that remain as episomes in the host cell.

A common method used to accomplish this is a protocol that utilizes plasmids. (187) Two different plasmid lines are created, one containing the AAV backbone that includes only the long terminal repeat regions with the transgene, and the other containing the coding sequences from the virus.(188, 189) These plasmids are then transfected into an adenovirus or herpesvirus infected cell line, which in turn provides the helper functions necessary for AAV production.(190, 191) Alternatively, a single plasmid that contains the adenovirus genes can be used, thereby eliminating the need for actual adenovirus.(192, 193)

Other methods have been developed to allow higher yield production. Mainly, it has been demonstrated that higher titers of vector can be produced by introducing adenovirus that contains the vector genome into cell lines that express the Rep and Cap proteins required for vector production.(194-196) A more recent method illustrated the feasibility of using an insect cell line. It appears that AAVs do not require helper virus in insect cells, simplifying the protocol.(197)

To create the commonly used hybrid vectors, a cross-packaging method is utilized. With the discovery that expression of AAV2 Rep proteins, when combined with expression of another serotype's Cap proteins, leads to the packaging of the AAV2 genome inside the other's capsid, a method was derived in which the Cap expression cassettes of the desired capsid is simply placed downstream of an otherwise unaltered AAV Rep expression cassette.(144, 198)

The last step of vector production is purification to assure removal of all adenovirus helper virus and safety. This is most often accomplished using a cesium

chloride density gradient centrifugation method, though a multitude of other methods have been developed. These include non-specific methods utilizing ion-exchange chromatography, and serotype specific methods including the purification of AAV5 using mucin columns that take advantage of the serotype's ability to bind sialic acid in mucin. (199-201)

There are several factors that have significant effects on the cellular tropism and the transgene expression of vector constructs, and these factors can have a significant impact on treatment success and which cell types particular serotypes are ideal for targeting. Factors may be related to characteristics of the virus(s) from which the vector is created, or from elements added to the genome. In particular, the virus capsid and its associated proteins and the promoter added to the genome, can alter the tropism and expression of vectors. Moreover, the route of vector administration can have significant effects on the which cells are transduced due to the differential cell exposure between different routes.

The varying properties of different capsids can be utilized to increase the efficacy of vector constructs. The cellular tropism is largely determined by the proteins located on the capsid. As discussed in more detail in a previous section, the capsid proteins determine the receptors to which the serotype binds, thereby determining the cellular tropism of the serotype. Furthermore, the capsid proteins affect how efficiently the virus can bind and lead to uptake into the host cell, and thus also plays a role in the speed of transgene expression.

Another way in which AAV vectors can be altered to affect cellular tropism is through the use of different promoters. The use of ubiquitous promoters, such as the

cytomegalovirus (CMV) promoter, drives transgene expression in the photoreceptor cells, retinal pigment epithelium, and some inner retinal cells in dog models of retinal dystrophy.(113) Similarly, the use of the constituitive chicken beta-actin (CBA) enhancer, typically used with the CMV promotor, has been shown to drive expression in both rod and cone photoreceptor cells as well as inner retinal cells including Müller, ganglion, and horizontal cells.(202) With the use of more specific promoters, transgene expression can be targeted to particular cells of interest. The use of the mouse opsin (mOP) promoter or the human G-protein coupled receptor protein kinase 1 (hGRK1) promoter in a dog model for retinal dystrophy, for example, directed expression specifically to rod photoreceptor cells.(202) Similar findings were found in the pig retina utilizing this promotor.(203) It is important to note the significance of species differences in cellular tropism, however. Different studies have found that the same mOP promoter drives both rod and cone transduction in a mouse model and that the GRK promotor can drive cone transduction in mice.(204, 205)

There are two main administration routes that have been investigated for potential use in gene therapy treatments; subretinal and intravitreous. Both routes require surgery, however, subretinal injections require a more precise surgery that involves carefully injecting the gene therapy vector beneath the layers of the retina. This causes a "bleb," or retinal detachment in the region of injection, but allows more efficient transduction of the photoreceptor cell layer, which lies at the back of the retina adjacent to the retinal pigment epithelium.(139) This is crucial for the treatment of many retinal dystrophies as the photoreceptors are a commonly affected cell type. The intravitreal approach has the benefit of a more widespread administration of the vector, allowing the

entire retinal surface to be exposed to the treatment, rather than a smaller region as in the subretinal approach. However, it has been demonstrated that intravitreal injections favor transduction of the inner retina, and does not effectively lead to outer retina transduction.(139, 206-208) Combination of this approach with vector modifications however, such as the tyrosine mutations discussed below, has resulted in more promising transduction of the outer retina via an intravitreal approach.

Adeno-associated viruses can be combined or altered to create superior vectors with increased efficacy, or more specific cell targeting. The three most common engineered vector types in use for retinal gene therapy are hybrid vectors, mutant capsid vectors, and self-complementary vectors.(209)

The proteins on the capsid surface of the virus infer the cellular tropism and have a significant effect on the speed and strength of transgene expression. The efficacy of a vector can therefore be enhanced by creating pseudotypes of vectors in which the genome of one AAV serotype is packaged within the capsid of another serotype.(144, 157) These "hybrid" vectors are widely used in retinal gene therapy research. Traditionally, the genome from the AAV2 serotype is used and packaged into the capsids of other vectors to make AAV2/x vectors. The capsid from another serotype can then be used to infer greater efficacy through increased speed and strength of transgene expression, as well as a specific desired cellular tropism.

Another method that can be used to improve the efficiency of AAV vectors involves creating mutations in the capsid proteins to bypass the ubiquitination rate-limiting step described earlier.(175) It has been shown that phosphorylation of tyrosine residues within capsid proteins mark the proteins for ubiquitination, and thereby make

the virus particle more likely to be degraded in the cytosol before reaching the nucleus. (210, 211) Taking advantage of this, vectors can now be created with mutations in the tyrosine residues, protecting them from phosphorylation and hence preventing ubiquitination of the virus particle.(212) These "mutant capsid vectors" provide a promising alternative to other vector types that may infer significantly increased efficiency.

As discussed briefly previously, a significant drawback of the AAV vector is the lag-phase created by the conversion of the single-stranded genome into a double stranded genome. This drawback can be overcome through the creation of self-complementary vectors. This type of vector is most commonly designed such that the genome contains a single-stranded inverted-repeat genome, which contains a mutated terminal resolution site in-between the repeats. This design allows the DNA to fold over onto itself, thereby creating a double-stranded transgene without a DNA synthesis step. (153) Using these self-complementary constructs, studies have shown that they infer faster and stronger transgene expression. In mouse models, it has been illustrated that self-complementary AAV2/8 (scAAV2/8) was shown to lead to faster and stronger transgene expression than its single-stranded counterpart, and that scAAV2/5 led to a stronger transgene expression with similar speed of onset.(213, 214) In a dog model, it was shown that scAAV2/5 leads to a faster time of onset and a stronger expression than ssAAV2/5.(215)

1.4.1.1.a The need for AAV testing in the feline retina

The work that has been done thus far testing adeno-associated virus vectors in the retina has been extensive in rodents, dogs and primates. In these species, a multitude of serotypes have been tested and in some cases, proof-of principle has been established for the ability of AAV vector based gene therapy to restore vision.

The most notable example of this is in the naturally-occurring dog model of Leber Congenital Amaurosis caused by a mutation in the retinal pigment epithelium (*RPE*) gene. In this model, it has been shown that significant vision can be restored to visually impaired dogs using an AAV2/2 vector based gene therapy treatment.(68, 69, 216-220) This demonstrates that strong enough transgene expression to restore working vision can be obtained. These results have been supported in a transgenic RPE knockout mouse model in which AAV gene therapy was able to partially restore vision and morphology when administered in fetal life, and to a lesser extent, when administered in adulthood.(221, 222) It was later shown that the visual restoration was still evident in the RPE dogs up to several years years post-injection, suggesting a long-term effect of the AAV delivered treatment.(70, 223, 224)

Establishment of proof-of-principle in animal models has provided a foundation from which human clinical trials can be conducted. The reports from these trials are promising, as they demonstrate the safety and efficacy of these treatments.(225-231)

Despite the plethora of data concerning AAV based delivery in other animal models however, very limited data has been collected concerning use of these vectors in the feline retina with only one study investigating AAV vectors in the feline retina.(113) With the discoveries and classification of forms of Progressive Retinal Atrophy in the cat

that make important large animal models for human retinal dystrophies the cat has become a new and important tool for studying treatments against these debilitating diseases. However, before studies can investigate therapies in the feline retina, vectors must be identified for the delivery of transgenes or the components required for treatments such as gene therapy or genome editing based therapies.

It is therefore necessary to test vector constructs in the feline retina to study the efficacy of transduction and transgene expression. Similarly, it is important that the cellular tropism of these vectors be elucidated in the feline retina, and that any species differences that may be relevant when studying the cat and extrapolating from feline to the human be determined. To gather this information, it is imperative that adeno-associated virus vector constructs be tested in the wild-type feline retina prior to the use of such vectors for introducing therapeutic genes, which is the focus of Chapter 5 of this dissertation.

1.5 Dissertation aims and hypotheses

The scientific community has made great progress in the understanding of inherited retinal dystrophies in recent years and has made strides towards genetics-based treatments for these debilitating diseases. Animal models have been integral for this progress, with large animal models such as dogs and cats emerging as particularly useful and important tools. The cat provides a unique opportunity to study retinal dystrophies caused by a mutation in the *CEP290* gene, a important gene implicated in about twenty percent of LCA cases.(15) Though the phenotype has been well described for this model, questions remained before the model can be utilized for *in vivo* treatment trials.

A few important questions remained to be answered about the *CEP290* cat model. Though previous studies had suggested a degeneration that affected the peripheral retina greater than the central retina, a characteristic common in people with LCA*CEP290*, it had yet to be determined if the actual rate of degeneration was faster in the periphery than in the central retina. Definitively clarifying this point holds important implications as we move towards treatments. Treatment timing and targeting could be affected by this difference, as it would suggest that the central retina may be sensitive to treatments longer due to the longer availability of viable photoreceptor cells. We therefore aimed to utilize an in vivo monitoring tool, spectral-domain optical coherence tomography (SD-OCT) to investigate retinal degeneration in this model over time and compare regional rates of degeneration. We hypothesized that *CEP290* mutant cats

would show a slower rate of degeneration in the central retina than in the peripheral retina.

Furthermore, previous studies have shown that the mutant cat has a milder phenotype than that typically seen in LCA in people, the most common disease caused by mutations in this gene. Why the phenotype is milder was not well understood. We hypothesized that the mutant cat is a hypomorph, with residual wild-type protein due to some level of useage of the wild-type splice donor site. We therefore aimed to analyze the wild-type and mutant transcript and protein levels to determine what levels of transcript and protein were present in the mutant cat, relative to wild-type and heterozygous carrier cats, that might explain the milder phenotype. If this is correct this has important implications for treatment development. If the shorter mutant protein is translated and is the reason for the milder phenotype, this suggests that a full transcript is not necessary for rescue of some vision and warrants future investigation to determine how much of the transcript is required to improve vision. This is particularly exciting for LCA[CEP290] cases as utilizing a partial transcript is a possible means of overcoming the obstacle that the gene's large size presents. AAV vectors cannot fit the entire *CEP290* transcript but could fit part of the transcript.

Furthermore, as we move towards treatment trials in the feline model it is imperative that we develop tools for treatment testing and identify objective markers for following treatment efficacy. Establishing transcript and protein levels has the added benefit of providing measurable values for this purpose. However, these values can only be obtained following sacrifice of valuable research animals, thus limiting their utility. We therefore also sought measures that could be used *in vivo* as well as aimed to develop

an *in vitro* tool that could be used to optimize treatments prior to use of animals. Utilizing SD-OCT we therefore also aimed to analyze the ellipsoid zone (EZ), an identifiable layer on OCT that has been shown in people to be a valuable marker of photoreceptor health. The EZ is thought to arise from the reflection of mitochondria in the inner segments of photoreceptors and can be visualized as a distinctive line on OCT imaging. (232) It has been shown in previous studies to disappear or lose distinction in regions of photoreceptor loss and be associated with visual loss.(233-235) We therefore aimed to study this zone in the feline retina via OCT and hypothesized that loss of this zone or loss of EZ integrity would correlate to photoreceptor degeneration, as indicated by photoreceptor layer thickness on OCT.

Development of an *in vitro* tool that would allow for testing and optimization of treatments in a faster and more affordable system would provide a valuable advantage that would allow us to save time and money and would allow us to produce faster results to reach towards treatments as well as reduce animal numbers needed for *in vivo* trials. We therefore aimed to develop primary fibroblast cell cultures from wild-type, heterozygous carrier, and homozygous mutant cats that could be utilized for this purpose. We then aimed to induce ciliation in these cells, a potentially useful alteration given the ciliary location and function of the CEP290 protein. To identify an objective functional marker for treatment trials in these cells, we lastly aimed to compare the length of these induced cilia across genotypes. We hypothesized that mutant cat cells would grow shorter cilia than wild-type or carrier cat cells.

Given the significant obstacles to a gene therapy based treatment for *CEP290* diseases, we decided to take a different approach and investigate a genome editing

based treatment. To do this we utilized the CRISPR/Cas-9 nuclease system, a newer genome editing modality that has created great excitement in the scientific community for its more affordable, scalable, and promising utility. Utilizing this system we aimed to delete the feline mutation-introduced splice donor site that deleteriously redirects splicing and then replace that segment with a strong splice donor site in the desired, wild-type location. We utilized the above-mentioned cell cultures to test this construct and hypothesized that we could successfully cause a deletion followed by an insertion that would redirect splicing to the wild-type location. In future studies it is our hope that this editing technique could then be translated to the cat model for testing, either as a method for editing induced pluripotent stem cells or by directly delivering the machinery to the feline retina.

To deliver such a treatment a delivery vector is imperative. We therefore lastly aimed to test adeno-associated viral (AAV) vectors, the vector system of choice for photoreceptor cell transduction, in the wild-type feline retina to study the safety and efficacy of this vector system in the feline retina. Testing four commonly used hybrid vectors, AAVs 2/2, 2/5, 2/8, 2/9, we aimed to determine the cellular tropism, speed of transduction, and safety of these vectors and to determine which vector was most ideal for feline retinal treatments. We hypothesized that all four vectors would lead to successful transduction of feline photoreceptor cells with minimal side effects, and that AAV 2/8 and 2/9 would lead to faster and stronger transduction than 2/2 and 2/5.

The results of these studies are detailed in the proceeding chapters of this dissertation. It is our hope that this body of work can build on previous studies to help better understand this useful model and prepare for use of this model for *in vivo*

treatment trials. Ultimately, we hope these studies will become a part of the body of

work that leads to a treatment for LCA^{CEP290}.

REFERENCES

REFERENCES

1.   Allikmets R. Leber congenital amaurosis: a genetic paradigm. Ophthalmic Genet. 2004;25(2):67-79.

2.   Stone EM. Leber congenital amaurosis - a model for efficient genetic testing of heterogeneous disorders: LXIV Edward Jackson Memorial Lecture. Am J Ophthalmol. 2007;144(6):791-811.

3.   Parmeggiani F. Clinics, epidemiology and genetics of retinitis pigmentosa. Curr Genomics. 2011;12(4):236-7.

4.   Kolb H. Simple Anatomy of the Retina. In: Kolb H, Fernandez E, Nelson R, editors. Webvision: The Organization of the Retina and Visual System. Salt Lake City (UT)1995.

5.   Kolb H. Gross Anatomy of the Eye. In: Kolb H, Fernandez E, Nelson R, editors. Webvision: The Organization of the Retina and Visual System. Salt Lake City (UT)1995.

6.   Kolb H. Photoreceptors. In: Kolb H, Fernandez E, Nelson R, editors. Webvision: The Organization of the Retina and Visual System. Salt Lake City (UT)1995.

7.   Fliegauf M, Benzing T, Omran H. When cilia go bad: cilia defects and ciliopathies. Nat Rev Mol Cell Biol. 2007;8(11):880-93.

8.   Fu Y. Phototransduction in Rods and Cones. In: Kolb H, Fernandez E, Nelson R, editors. Webvision: The Organization of the Retina and Visual System. Salt Lake City (UT)1995.

9.   Sohocki MM, Daiger SP, Bowne SJ, Rodriquez JA, Northrup H, Heckenlively JR, et al. Prevalence of mutations causing retinitis pigmentosa and other inherited retinopathies. Hum Mutat. 2001;17(1):42-51.

10.   Boughman JA, Conneally PM, Nance WE. Population genetic studies of retinitis pigmentosa. Am J Hum Genet. 1980;32(2):223-35.

11.   Hamel C. Retinitis pigmentosa. Orphanet J Rare Dis. 2006;1:40.

12.   Franceschetti A, Dieterle P. [Diagnostic and prognostic importance of the electroretinogram in tapetoretinal degeneration with reduction of the visual field and hemeralopia]. Confin Neurol. 1954;14(2-3):184-6.

13.   Koenekoop RK. An overview of Leber congenital amaurosis: a model to understand human retinal development. Surv Ophthalmol. 2004;49(4):379-98.

14.   den Hollander AI, Roepman R, Koenekoop RK, Cremers FP. Leber congenital amaurosis: genes, proteins and disease mechanisms. Prog Retin Eye Res. 2008;27(4):391-419.

15.   den Hollander AI, Koenekoop RK, Yzer S, Lopez I, Arends ML, Voesenek KE, et al. Mutations in the CEP290 (NPHP6) gene are a frequent cause of Leber congenital amaurosis. Am J Hum Genet. 2006;79(3):556-61.

16.   Moradi P, Davies WL, Mackay DS, Cheetham ME, Moore AT. Focus on Molecules: Centrosomal protein 290 (CEP290). Exp Eye Res. 2011;92(5):316-7.

17.   Coppieters F, Lefever S, Leroy BP, De Baere E. CEP290, a gene with many faces: mutation overview and presentation of CEP290base. Hum Mutat. 2010;31(10):1097-108.

18.   Sayer JA, Otto EA, O'Toole JF, Nurnberg G, Kennedy MA, Becker C, et al. The centrosomal protein nephrocystin-6 is mutated in Joubert syndrome and activates transcription factor ATF4. Nat Genet. 2006;38(6):674-81.

19.   Chang B, Khanna H, Hawes N, Jimeno D, He S, Lillo C, et al. In-frame deletion in a novel centrosomal/ciliary protein CEP290/NPHP6 perturbs its interaction with RPGR and results in early-onset retinal degeneration in the rd16 mouse. Hum Mol Genet. 2006;15(11):1847-57.

20.   Nagase T, Ishikawa K, Nakajima D, Ohira M, Seki N, Miyajima N, et al. Prediction of the coding sequences of unidentified human genes. VII. The complete sequences of 100 new cDNA clones from brain which can code for large proteins in vitro. DNA Res. 1997;4(2):141-50.

21.   Cideciyan AV, Aleman TS, Jacobson SG, Khanna H, Sumaroka A, Aguirre GK, et al. Centrosomal-ciliary gene CEP290/NPHP6 mutations result in blindness with unexpected sparing of photoreceptors and visual brain: implications for therapy of Leber congenital amaurosis. Hum Mutat. 2007;28(11):1074-83.

22.   McEwen DP, Koenekoop RK, Khanna H, Jenkins PM, Lopez I, Swaroop A, et al. Hypomorphic CEP290/NPHP6 mutations result in anosmia caused by the selective loss of G proteins in cilia of olfactory sensory neurons. Proc Natl Acad Sci U S A. 2007;104(40):15917-22.

23.   Kim J, Krishnaswami SR, Gleeson JG. CEP290 interacts with the centriolar satellite component PCM-1 and is required for Rab8 localization to the primary cilium. Hum Mol Genet. 2008;17(23):3796-805.

24. Pazour GJ, Rosenbaum JL. Intraflagellar transport and cilia-dependent diseases. Trends Cell Biol. 2002;12(12):551-5.

25. Badano JL, Mitsuma N, Beales PL, Katsanis N. The ciliopathies: an emerging class of human genetic disorders. Annu Rev Genomics Hum Genet. 2006;7:125-48.

26. Baala L, Audollent S, Martinovic J, Ozilou C, Babron MC, Sivanandamoorthy S, et al. Pleiotropic effects of CEP290 (NPHP6) mutations extend to Meckel syndrome. Am J Hum Genet. 2007;81(1):170-9.

27. Frank V, den Hollander AI, Bruchle NO, Zonneveld MN, Nurnberg G, Becker C, et al. Mutations of the CEP290 gene encoding a centrosomal protein cause Meckel-Gruber syndrome. Hum Mutat. 2008;29(1):45-52.

28. Jha T, Bardhan J, Das B, Patra KK, Dhali B, Seth S. Meckel-Gruber syndrome: a rare clinical entity. J Indian Med Assoc. 2010;108(9):611-2.

29. Waters AM, Beales PL. Bardet-Biedl Syndrome. 1993.

30. Salomon R, Saunier S, Niaudet P. Nephronophthisis. Pediatr Nephrol. 2009;24(12):2333-44.

31. Tory K, Lacoste T, Burglen L, Moriniere V, Boddaert N, Macher MA, et al. High NPHP1 and NPHP6 mutation rate in patients with Joubert syndrome and nephronophthisis: potential epistatic effect of NPHP6 and AHI1 mutations in patients with NPHP1 mutations. J Am Soc Nephrol. 2007;18(5):1566-75.

32. Helou J, Otto EA, Attanasio M, Allen SJ, Parisi MA, Glass I, et al. Mutation analysis of NPHP6/CEP290 in patients with Joubert syndrome and Senior-Loken syndrome. J Med Genet. 2007;44(10):657-63.

33. O'Toole JF, Otto EA, Hoefele J, Helou J, Hildebrandt F. Mutational analysis in 119 families with nephronophthisis. Pediatr Nephrol. 2007;22(3):366-70.

34. Valente EM, Silhavy JL, Brancati F, Barrano G, Krishnaswami SR, Castori M, et al. Mutations in CEP290, which encodes a centrosomal protein, cause pleiotropic forms of Joubert syndrome. Nat Genet. 2006;38(6):623-5.

35. Doherty D. Joubert syndrome: insights into brain development, cilium biology, and complex disease. Semin Pediatr Neurol. 2009;16(3):143-54.

36. Brancati F, Barrano G, Silhavy JL, Marsh SE, Travaglini L, Bielas SL, et al. CEP290 mutations are frequently identified in the oculo-renal form of Joubert syndrome-related disorders. Am J Hum Genet. 2007;81(1):104-13.

37.	Valente EM, Brancati F, Dallapiccola B. Genotypes and phenotypes of Joubert syndrome and related disorders. Eur J Med Genet. 2008;51(1):1-23.

38.	Perrault I, Delphin N, Hanein S, Gerber S, Dufier JL, Roche O, et al. Spectrum of NPHP6/CEP290 mutations in Leber congenital amaurosis and delineation of the associated phenotype. Hum Mutat. 2007;28(4):416.

39.	Littink KW, Pott JW, Collin RW, Kroes HY, Verheij JB, Blokland EA, et al. A novel nonsense mutation in CEP290 induces exon skipping and leads to a relatively mild retinal phenotype. Invest Ophthalmol Vis Sci. 2010;51(7):3646-52.

40.	Pasadhika S, Fishman GA, Stone EM, Lindeman M, Zelkha R, Lopez I, et al. Differential macular morphology in patients with RPE65-, CEP290-, GUCY2D-, and AIPL1-related Leber congenital amaurosis. Invest Ophthalmol Vis Sci. 2010;51(5): 2608-14.

41.	Hanein S, Perrault I, Gerber S, Tanguy G, Barbet F, Ducroq D, et al. Leber congenital amaurosis: comprehensive survey of the genetic heterogeneity, refinement of the clinical definition, and genotype-phenotype correlations as a strategy for molecular diagnosis. Hum Mutat. 2004;23(4):306-17.

42.	Chader GJ. Animal models in research on retinal degenerations: past progress and future hope. Vision Res. 2002;42(4):393-9.

43.	Keeler CE. The Inheritance of a Retinal Abnormality in White Mice. Proc Natl Acad Sci U S A. 1924;10(7):329-33.

44.	Bourne MC, Campbell DA, Tansley K. Hereditary Degeneration of the Rat Retina. Br J Ophthalmol. 1938;22(10):613-23.

45.	Dowling JE, Sidman RL. Inherited retinal dystrophy in the rat. J Cell Biol. 1962;14:73-109.

46.	Pittler SJ, Keeler CE, Sidman RL, Baehr W. PCR analysis of DNA from 70-year-old sections of rodless retina demonstrates identity with the mouse rd defect. Proc Natl Acad Sci U S A. 1993;90(20):9616-9.

47.	van Nie R, Ivanyi D, Demant P. A new H-2-linked mutation, rds, causing retinal degeneration in the mouse. Tissue Antigens. 1978;12(2):106-8.

48.	Naash MI, Hollyfield JG, al-Ubaidi MR, Baehr W. Simulation of human autosomal dominant retinitis pigmentosa in transgenic mice expressing a mutated murine opsin gene. Proc Natl Acad Sci U S A. 1993;90(12):5499-503.

49.	Hong DH, Pawlyk BS, Shang J, Sandberg MA, Berson EL, Li T. A retinitis pigmentosa GTPase regulator (RPGR)-deficient mouse model for X-linked retinitis pigmentosa (RP3). Proc Natl Acad Sci U S A. 2000;97(7):3649-54.

50.	Hageman GS, Gehrs K, Johnson LV, Anderson D. Age-Related Macular Degeneration (AMD). In: Kolb H, Fernandez E, Nelson R, editors. Webvision: The Organization of the Retina and Visual System. Salt Lake City (UT)1995.

51.	Rah H, Maggs DJ, Blankenship TN, Narfstrom K, Lyons LA. Early-onset, autosomal recessive, progressive retinal atrophy in Persian cats. Invest Ophthalmol Vis Sci. 2005;46(5):1742-7.

52.	Menotti-Raymond M, David VA, Schaffer AA, Stephens R, Wells D, Kumar-Singh R, et al. Mutation in CEP290 discovered for cat model of human retinal degeneration. J Hered. 2007;98(3):211-20.

53.	Menotti-Raymond M, Deckman KH, David V, Myrkalo J, O'Brien SJ, Narfstrom K. Mutation discovered in a feline model of human congenital retinal blinding disease. Invest Ophthalmol Vis Sci. 2010;51(6):2852-9.

54.	Ofri R, Reilly CM, Maggs DJ, Fitzgerald PG, Shilo-Benjamini Y, Good KL, et al. Characterization of an Early-Onset, Autosomal Recessive, Progressive Retinal Degeneration in Bengal Cats. Invest Ophthalmol Vis Sci. 2015;56(9):5299-308.

55.	Beltran WA. The use of canine models of inherited retinal degeneration to test novel therapeutic approaches. Vet Ophthalmol. 2009;12(3):192-204.

56.	Tuntivanich N, Petersen-Jones SM, Steibel JP, Johnson C, Forcier JQ. Postnatal development of canine axial globe length measured by B-scan ultrasonography. Vet Ophthalmol. 2007;10(1):2-5.

57.	Gilger BC, Reeves KA, Salmon JH. Ocular parameters related to drug delivery in the canine and equine eye: aqueous and vitreous humor volume and scleral surface area and thickness. Vet Ophthalmol. 2005;8(4):265-9.

58.	McGreevy P, Grassi TD, Harman AM. A strong correlation exists between the distribution of retinal ganglion cells and nose length in the dog. Brain Behav Evol. 2004;63(1):13-22.

59.	Mowat FM, Petersen-Jones SM, Williamson H, Williams DL, Luthert PJ, Ali RR, et al. Topographical characterization of cone photoreceptors and the area centralis of the canine retina. Mol Vis. 2008;14:2518-27.

60.	Beltran WA, Cideciyan AV, Guziewicz KE, Iwabe S, Swider M, Scott EM, et al. Canine retina has a primate fovea-like bouquet of cone photoreceptors which is affected by inherited macular degenerations. PLoS One. 2014;9(3):e90390.

61.   Petersen-Jones SM, Entz DD, Sargan DR. cGMP phosphodiesterase-alpha mutation causes progressive retinal atrophy in the Cardigan Welsh corgi dog. Invest Ophthalmol Vis Sci. 1999;40(8):1637-44.

62.   Dekomien G, Runte M, Godde R, Epplen JT. Generalized progressive retinal atrophy of Sloughi dogs is due to an 8-bp insertion in exon 21 of the PDE6B gene. Cytogenet Cell Genet. 2000;90(3-4):261-7.

63.   Sidjanin DJ, Lowe JK, McElwee JL, Milne BS, Phippen TM, Sargan DR, et al. Canine CNGB3 mutations establish cone degeneration as orthologous to the human achromatopsia locus ACHM3. Hum Mol Genet. 2002;11(16):1823-33.

64.   Winkler PA, Ekenstedt KJ, Occelli LM, Frattaroli AV, Bartoe JT, Venta PJ, et al. A large animal model for CNGB1 autosomal recessive retinitis pigmentosa. PLoS One. 2013;8(8):e72229.

65.   Zeiss CJ, Acland GM, Aguirre GD. Retinal pathology of canine X-linked progressive retinal atrophy, the locus homologue of RP3. Invest Ophthalmol Vis Sci. 1999;40(13):3292-304.

66.   Kijas JW, Cideciyan AV, Aleman TS, Pianta MJ, Pearce-Kelling SE, Miller BJ, et al. Naturally occurring rhodopsin mutation in the dog causes retinal dysfunction and degeneration mimicking human dominant retinitis pigmentosa. Proc Natl Acad Sci U S A. 2002;99(9):6328-33.

67.   Beltran WA, Hammond P, Acland GM, Aguirre GD. A frameshift mutation in RPGR exon ORF15 causes photoreceptor degeneration and inner retina remodeling in a model of X-linked retinitis pigmentosa. Invest Ophthalmol Vis Sci. 2006;47(4): 1669-81.

68.   Acland GM, Aguirre GD, Ray J, Zhang Q, Aleman TS, Cideciyan AV, et al. Gene therapy restores vision in a canine model of childhood blindness. Nat Genet. 2001;28(1):92-5.

69.   Narfstrom K, Katz ML, Bragadottir R, Seeliger M, Boulanger A, Redmond TM, et al. Functional and structural recovery of the retina after gene therapy in the RPE65 null mutation dog. Invest Ophthalmol Vis Sci. 2003;44(4):1663-72.

70.   Acland GM, Aguirre GD, Bennett J, Aleman TS, Cideciyan AV, Bennicelli J, et al. Long-term restoration of rod and cone vision by single dose rAAV-mediated gene transfer to the retina in a canine model of childhood blindness. Mol Ther. 2005;12(6): 1072-82.

71.   Narfstrom K. Hereditary progressive retinal atrophy in the Abyssinian cat. J Hered. 1983;74(4):273-6.

72.   Barnett KC, Curtis R. Autosomal dominant progressive retinal atrophy in Abyssinian cats. J Hered. 1985;76(3):168-70.

73.   Menotti-Raymond M, David VA, Schaffer AA, Stephens R, Wells D, Kumar-Singh R, et al. Mutation in CEP290 discovered for cat model of human retinal degeneration. J Hered. 2007;98(3):211-20.

74.   Narfström K. Hereditary progressive retinal atrophy in the Abyssinian cat. J Hered. 1983;74(4):273-6.

75.   Linberg KA, Lewis GP, Shaaw C, Rex TS, Fisher SK. Distribution of S- and M-cones in normal and experimentally detached cat retina. The Journal of comparative neurology. 2001;430(3):343-56.

76.   Narfstrom K. Progressive retinal atrophy in the Abyssinian cat. Clinical characteristics. Invest Ophthalmol Vis Sci. 1985;26(2):193-200.

77.   Narfstrom K, Nilsson SE. Hereditary retinal degeneration in the Abyssinian cat: correlation of ophthalmoscopic and electroretinographic findings. Doc Ophthalmol. 1985;60(2):183-7.

78.   Narfström K, Wilen M, Andersson BE. Hereditary retinal degeneration in the Abyssinian cat: developmental studies using clinical electroretinography. Doc Ophthalmol. 1988;69(2):111-8.

79.   Jacobson SG, Kemp CM, Narfstrom K, Nilsson SE. Rhodopsin levels and rod-mediated function in Abyssinian cats with hereditary retinal degeneration. Exp Eye Res. 1989;49(5):843-52.

80.   Ekesten B, Narfstrom K. Abnormal dark-adapted ERG in cats heterozygous for a recessively inherited rod-cone degeneration. Vet Ophthalmol. 2004;7(1):63-7.

81.   Hyman JA, Vaegan, Lei B, Narfstrom KL. Electrophysiologic differentiation of homozygous and heterozygous Abyssinian-crossbred cats with late-onset hereditary retinal degeneration. Am J Vet Res. 2005;66(11):1914-21.

82.   Kang Derwent JJ, Padnick-Silver L, McRipley M, Giuliano E, Linsenmeier RA, Narfstrom K. The electroretinogram components in Abyssinian cats with hereditary retinal degeneration. Invest Ophthalmol Vis Sci. 2006;47(8):3673-82.

83.   Narfstrom KL, Nilsson SE, Andersson BE. Progressive retinal atrophy in the Abyssinian cat: studies of the DC-recorded electroretinogram and the standing potential of the eye. Br J Ophthalmol. 1985;69(8):618-23.

84.   Seeliger MW, Narfstrom K. Functional assessment of the regional distribution of disease in a cat model of hereditary retinal degeneration. Invest Ophthalmol Vis Sci. 2000;41(7):1998-2005.

85.   Wiggert B, van Veen T, Kutty G, Lee L, Nickerson J, Si JS, et al. An early decrease in interphotoreceptor retinoid-binding protein gene expression in Abyssinian cats homozygous for hereditary rod-cone degeneration. Cell Tissue Res. 1994;278(2): 291-8.

86.   Narfstrom K, Nilsson SE. Morphological findings during retinal development and maturation in hereditary rod-cone degeneration in Abyssinian cats. Exp Eye Res. 1989;49(4):611-28.

87.   Narfstrom K, Nilsson SE. Progressive retinal atrophy in the Abyssinian cat. Electron microscopy. Invest Ophthalmol Vis Sci. 1986;27(11):1569-76.

88.   Narfstrom K, Ehinger B, Bruun A. Immunohistochemical studies of cone photoreceptors and cells of the inner retina in feline rod-cone degeneration. Vet Ophthalmol. 2001;4(2):141-5.

89.   Narfstrom K, Holland Deckman K, Menotti-Raymond M. The domestic cat as a large animal model for characterization of disease and therapeutic intervention in hereditary retinal blindness. J Ophthalmol. 2011;2011:906943.

90.   Jomary C, Jones SE. Induction of functional photoreceptor phenotype by exogenous Crx expression in mouse retinal stem cells. Invest Ophthalmol Vis Sci. 2008;49(1):429-37.

91.   Lamba DA, Gust J, Reh TA. Transplantation of human embryonic stem cell-derived photoreceptors restores some visual function in Crx-deficient mice. Cell Stem Cell. 2009;4(1):73-9.

92.   Assawachananont J, Mandai M, Okamoto S, Yamada C, Eiraku M, Yonemura S, et al. Transplantation of embryonic and induced pluripotent stem cell-derived 3D retinal sheets into retinal degenerative mice. Stem Cell Reports. 2014;2(5):662-74.

93.   Ng TK, Fortino VR, Pelaez D, Cheung HS. Progress of mesenchymal stem cell therapy for neural and retinal diseases. World J Stem Cells. 2014;6(2):111-9.

94.   Tzameret A, Sher I, Belkin M, Treves AJ, Meir A, Nagler A, et al. Transplantation of human bone marrow mesenchymal stem cells as a thin subretinal layer ameliorates retinal degeneration in a rat model of retinal dystrophy. Exp Eye Res. 2014;118:135-44.

95.   Leow SN, Luu CD, Hairul Nizam MH, Mok PL, Ruhaslizan R, Wong HS, et al. Safety and Efficacy of Human Wharton's Jelly-Derived Mesenchymal Stem Cells Therapy for Retinal Degeneration. PLoS One. 2015;10(6):e0128973.

96.   Nazari H, Zhang L, Zhu D, Chader GJ, Falabella P, Stefanini F, et al. Stem cell based therapies for age-related macular degeneration: The promises and the challenges. Prog Retin Eye Res. 2015;48:1-39.

97.   Tzameret A, Sher I, Belkin M, Treves AJ, Meir A, Nagler A, et al. Epiretinal transplantation of human bone marrow mesenchymal stem cells rescues retinal and vision function in a rat model of retinal degeneration. Stem Cell Res. 2015;15(2):387-94.

98.   Shirai H, Mandai M, Matsushita K, Kuwahara A, Yonemura S, Nakano T, et al. Transplantation of human embryonic stem cell-derived retinal tissue in two primate models of retinal degeneration. Proc Natl Acad Sci U S A. 2016;113(1):E81-90.

99.   Garg A, Yang J, Lee W, Tsang SH. Stem Cell Therapies in Retinal Disorders. Cells. 2017;6(1).

100.   Seiler MJ, Aramant RB, Seeliger MW, Bragadottir R, Mahoney M, Narfstrom K. Functional and structural assessment of retinal sheet allograft transplantation in feline hereditary retinal degeneration. Vet Ophthalmol. 2009;12(3):158-69.

101.   Ivert L, Gouras P, Naeser P, Narfstrom K. Photoreceptor allografts in a feline model of retinal degeneration. Graefes Arch Clin Exp Ophthalmol. 1998;236(11):844-52.

102.   Yan Z, Zhang Y, Duan D, Engelhardt JF. Trans-splicing vectors expand the utility of adeno-associated virus for gene therapy. Proc Natl Acad Sci U S A. 2000;97(12): 6716-21.

103.   Duan D, Yue Y, Engelhardt JF. Expanding AAV packaging capacity with trans-splicing or overlapping vectors: a quantitative comparison. Mol Ther. 2001;4(4):383-91.

104.   Grieger JC, Samulski RJ. Packaging capacity of adeno-associated virus serotypes: impact of larger genomes on infectivity and postentry steps. J Virol. 2005;79(15):9933-44.

105.   Ghosh A, Duan D. Expanding adeno-associated viral vector capacity: a tale of two vectors. Biotechnol Genet Eng Rev. 2007;24:165-77.

106.   Allocca M, Doria M, Petrillo M, Colella P, Garcia-Hoyos M, Gibbs D, et al. Serotype-dependent packaging of large genes in adeno-associated viral vectors results in effective gene delivery in mice. J Clin Invest. 2008;118(5):1955-64.

107.   Ghosh A, Yue Y, Lai Y, Duan D. A hybrid vector system expands adeno-associated viral vector packaging capacity in a transgene-independent manner. Mol Ther. 2008;16(1):124-30.

108.   Baye LM, Patrinostro X, Swaminathan S, Beck JS, Zhang Y, Stone EM, et al. The N-terminal region of centrosomal protein 290 (CEP290) restores vision in a zebrafish model of human blindness. Hum Mol Genet. 2011;20(8):1467-77.

109.   Gaj T, Gersbach CA, Barbas CF, 3rd. ZFN, TALEN, and CRISPR/Cas-based methods for genome engineering. Trends Biotechnol. 2013;31(7):397-405.

110.   Horvath P, Barrangou R. CRISPR/Cas, the immune system of bacteria and archaea. Science. 2010;327(5962):167-70.

111.   Cong L, Ran FA, Cox D, Lin S, Barretto R, Habib N, et al. Multiplex genome engineering using CRISPR/Cas systems. Science. 2013;339(6121):819-23.

112.   Hsu PD, Lander ES, Zhang F. Development and applications of CRISPR-Cas9 for genome engineering. Cell. 2014;157(6):1262-78.

113.   Bainbridge JW, Mistry A, Schlichtenbrede FC, Smith A, Broderick C, De Alwis M, et al. Stable rAAV-mediated transduction of rod and cone photoreceptors in the canine retina. Gene Ther. 2003;10(16):1336-44.

114.   Bainbridge JW, Tan MH, Ali RR. Gene therapy progress and prospects: the eye. Gene Ther. 2006;13(16):1191-7.

115.   Matsuda T, Cepko CL. Electroporation and RNA interference in the rodent retina in vivo and in vitro. Proc Natl Acad Sci U S A. 2004;101(1):16-22.

116.   Hangai M, Kaneda Y, Tanihara H, Honda Y. In vivo gene transfer into the retina mediated by a novel liposome system. Invest Ophthalmol Vis Sci. 1996;37(13):2678-85.

117.   Masuda I, Matsuo T, Yasuda T, Matsuo N. Gene transfer with liposomes to the intraocular tissues by different routes of administration. Invest Ophthalmol Vis Sci. 1996;37(9):1914-20.

118.   del Pozo-Rodriguez A, Delgado D, Solinis MA, Gascon AR, Pedraz JL. Solid lipid nanoparticles for retinal gene therapy: transfection and intracellular trafficking in RPE cells. Int J Pharm. 2008;360(1-2):177-83.

119.   Conley SM, Naash MI. Nanoparticles for retinal gene therapy. Prog Retin Eye Res. 2010;29(5):376-97.

120.   Adijanto J, Naash MI. Nanoparticle-based technologies for retinal gene therapy. Eur J Pharm Biopharm. 2015;95(Pt B):353-67.

121.   Bennett J, Wilson J, Sun D, Forbes B, Maguire A. Adenovirus vector-mediated in vivo gene transfer into adult murine retina. Invest Ophthalmol Vis Sci. 1994;35(5): 2535-42.

122.	Li J, Samulski RJ, Xiao X. Role for highly regulated rep gene expression in adeno-associated virus vector production. J Virol. 1997;71(7):5236-43.

123.	Wu L, Lam S, Cao H, Guan R, Duan R, van der Kooy D, et al. Subretinal gene delivery using helper-dependent adenoviral vectors. Cell Biosci. 2011;1(1):15.

124.	Puppo A, Cesi G, Marrocco E, Piccolo P, Jacca S, Shayakhmetov DM, et al. Retinal transduction profiles by high-capacity viral vectors. Gene therapy. 2014;21(10): 855-65.

125.	Vollrath D, Feng W, Duncan JL, Yasumura D, D'Cruz PM, Chappelow A, et al. Correction of the retinal dystrophy phenotype of the RCS rat by viral gene transfer of Mertk. Proc Natl Acad Sci U S A. 2001;98(22):12584-9.

126.	Chen Y, Moiseyev G, Takahashi Y, Ma JX. RPE65 gene delivery restores isomerohydrolase activity and prevents early cone loss in Rpe65-/- mice. Invest Ophthalmol Vis Sci. 2006;47(3):1177-84.

127.	Kostic C, Chiodini F, Salmon P, Wiznerowicz M, Deglon N, Hornfeld D, et al. Activity analysis of housekeeping promoters using self-inactivating lentiviral vector delivery into the mouse retina. Gene Ther. 2003;10(9):818-21.

128.	Kong J, Kim SR, Binley K, Pata I, Doi K, Mannik J, et al. Correction of the disease phenotype in the mouse model of Stargardt disease by lentiviral gene therapy. Gene therapy. 2008;15(19):1311-20.

129.	Semple-Rowland SL, Coggin WE, Geesey M, Eccles KS, Abraham L, Pachigar K, et al. Expression characteristics of dual-promoter lentiviral vectors targeting retinal photoreceptors and Muller cells. Mol Vis. 2010;16:916-34.

130.	Verrier JD, Madorsky I, Coggin WE, Geesey M, Hochman M, Walling E, et al. Bicistronic lentiviruses containing a viral 2A cleavage sequence reliably co-express two proteins and restore vision to an animal model of LCA1. PLoS One. 2011;6(5):e20553.

131.	Binley K, Widdowson P, Loader J, Kelleher M, Iqball S, Ferrige G, et al. Transduction of photoreceptors with equine infectious anemia virus lentiviral vectors: safety and biodistribution of StarGen for Stargardt disease. Invest Ophthalmol Vis Sci. 2013;54(6):4061-71.

132.	Semple-Rowland SL, Berry J. Use of lentiviral vectors to deliver and express bicistronic transgenes in developing chicken embryos. Methods. 2014;66(3):466-73.

133.	Bartholomae CC, Arens A, Balaggan KS, Yanez-Munoz RJ, Montini E, Howe SJ, et al. Lentiviral vector integration profiles differ in rodent postmitotic tissues. Mol Ther. 2011;19(4):703-10.

134.   Balaggan KS, Duran Y, Georgiadis A, Thaung C, Barker SE, Buch PK, et al. Absence of ocular malignant transformation after sub-retinal delivery of rAAV2/2 or integrating lentiviral vectors in p53-deficient mice. Gene therapy. 2012;19(2):182-8.

135.   Kotin RM. Prospects for the use of adeno-associated virus as a vector for human gene therapy. Hum Gene Ther. 1994;5(7):793-801.

136.   Xie Q, Bu W, Bhatia S, Hare J, Somasundaram T, Azzi A, et al. The atomic structure of adeno-associated virus (AAV-2), a vector for human gene therapy. Proc Natl Acad Sci U S A. 2002;99(16):10405-10.

137.   Laughlin CA, Jones N, Carter BJ. Effect of deletions in adenovirus early region 1 genes upon replication of adeno-associated virus. J Virol. 1982;41(3):868-76.

138.   Lusby E, Fife KH, Berns KI. Nucleotide sequence of the inverted terminal repetition in adeno-associated virus DNA. J Virol. 1980;34(2):402-9.

139.   Ali RR, Reichel MB, De Alwis M, Kanuga N, Kinnon C, Levinsky RJ, et al. Adeno-associated virus gene transfer to mouse retina. Hum Gene Ther. 1998;9(1):81-6.

140.   Calado SM, Oliveira AV, Machado S, Haase R, Silva GA. Sustained gene expression in the retina by improved episomal vectors. Tissue Eng Part A. 2014;20(19-20):2692-8.

141.   Donsante A, Miller DG, Li Y, Vogler C, Brunt EM, Russell DW, et al. AAV vector integration sites in mouse hepatocellular carcinoma. Science. 2007;317(5837):477.

142.   Russell DW, Grompe M. Adeno-associated virus finds its disease. Nat Genet. 2015;47(10):1104-5.

143.   Auricchio A, Kobinger G, Anand V, Hildinger M, O'Connor E, Maguire AM, et al. Exchange of surface proteins impacts on viral vector cellular specificity and transduction characteristics: the retina as a model. Hum Mol Genet. 2001;10(26):3075-81.

144.   Rabinowitz JE, Rolling F, Li C, Conrath H, Xiao W, Xiao X, et al. Cross-packaging of a single adeno-associated virus (AAV) type 2 vector genome into multiple AAV serotypes enables transduction with broad specificity. J Virol. 2002;76(2):791-801.

145.   Surace EM, Auricchio A, Reich SJ, Rex T, Glover E, Pineles S, et al. Delivery of adeno-associated virus vectors to the fetal retina: impact of viral capsid proteins on retinal neuronal progenitor transduction. J Virol. 2003;77(14):7957-63.

146.   Sun L, Li J, Xiao X. Overcoming adeno-associated virus vector size limitation through viral DNA heterodimerization. Nat Med. 2000;6(5):599-602.

147.   Dong JY, Fan PD, Frizzell RA. Quantitative analysis of the packaging capacity of recombinant adeno-associated virus. Hum Gene Ther. 1996;7(17):2101-12.

148.   Wang Q, Dong B, Firrman J, Roberts S, Moore AR, Cao W, et al. Efficient production of dual recombinant adeno-associated viral vectors for factor VIII delivery. Hum Gene Ther Methods. 2014;25(4):261-8.

149.   McClements ME, Charbel Issa P, Blouin V, MacLaren RE. A fragmented adeno-associated viral dual vector strategy for treatment of diseases caused by mutations in large genes leads to expression of hybrid transcripts. J Genet Syndr Gene Ther. 2016;7(5).

150.   Fisher KJ, Gao GP, Weitzman MD, DeMatteo R, Burda JF, Wilson JM. Transduction with recombinant adeno-associated virus for gene therapy is limited by leading-strand synthesis. J Virol. 1996;70(1):520-32.

151.   Ferrari FK, Samulski T, Shenk T, Samulski RJ. Second-strand synthesis is a rate-limiting step for efficient transduction by recombinant adeno-associated virus vectors. J Virol. 1996;70(5):3227-34.

152.   Zhong L, Zhou X, Li Y, Qing K, Xiao X, Samulski RJ, et al. Single-polarity recombinant adeno-associated virus 2 vector-mediated transgene expression in vitro and in vivo: mechanism of transduction. Mol Ther. 2008;16(2):290-5.

153.   McCarty DM, Fu H, Monahan PE, Toulson CE, Naik P, Samulski RJ. Adeno-associated virus terminal repeat (TR) mutant generates self-complementary vectors to overcome the rate-limiting step to transduction in vivo. Gene Ther. 2003;10(26):2112-8.

154.   Chiorini JA, Kim F, Yang L, Kotin RM. Cloning and characterization of adeno-associated virus type 5. J Virol. 1999;73(2):1309-19.

155.   Chiorini JA, Yang L, Liu Y, Safer B, Kotin RM. Cloning of adeno-associated virus type 4 (AAV4) and generation of recombinant AAV4 particles. J Virol. 1997;71(9): 6823-33.

156.   Flotte TR. Adeno-associated virus-mediated gene transfer for lung diseases. Hum Gene Ther. 2005;16(6):643-8.

157.   Gao GP, Alvira MR, Wang L, Calcedo R, Johnston J, Wilson JM. Novel adeno-associated viruses from rhesus monkeys as vectors for human gene therapy. Proc Natl Acad Sci U S A. 2002;99(18):11854-9.

158.   Gao G, Vandenberghe LH, Alvira MR, Lu Y, Calcedo R, Zhou X, et al. Clades of Adeno-associated viruses are widely disseminated in human tissues. J Virol. 2004;78(12):6381-8.

159.   Handa A, Muramatsu S, Qiu J, Mizukami H, Brown KE. Adeno-associated virus (AAV)-3-based vectors transduce haematopoietic cells not susceptible to transduction with AAV-2-based vectors. J Gen Virol. 2000;81(Pt 8):2077-84.

160.   Rutledge EA, Halbert CL, Russell DW. Infectious clones and vectors derived from adeno-associated virus (AAV) serotypes other than AAV type 2. J Virol. 1998;72(1): 309-19.

161.   Summerford C, Samulski RJ. Membrane-associated heparan sulfate proteoglycan is a receptor for adeno-associated virus type 2 virions. J Virol. 1998;72(2): 1438-45.

162.   Qing K, Mah C, Hansen J, Zhou S, Dwarki V, Srivastava A. Human fibroblast growth factor receptor 1 is a co-receptor for infection by adeno-associated virus 2. Nat Med. 1999;5(1):71-7.

163.   Summerford C, Bartlett JS, Samulski RJ. AlphaVbeta5 integrin: a co-receptor for adeno-associated virus type 2 infection. Nat Med. 1999;5(1):78-82.

164.   Kashiwakura Y, Tamayose K, Iwabuchi K, Hirai Y, Shimada T, Matsumoto K, et al. Hepatocyte growth factor receptor is a coreceptor for adeno-associated virus type 2 infection. J Virol. 2005;79(1):609-14.

165.   Lerch TF, Xie Q, Chapman MS. The structure of adeno-associated virus serotype 3B (AAV-3B): insights into receptor binding and immune evasion. Virology. 2010;403(1): 26-36.

166.   Halbert CL, Allen JM, Miller AD. Adeno-associated virus type 6 (AAV6) vectors mediate efficient transduction of airway epithelial cells in mouse lungs compared to that of AAV2 vectors. J Virol. 2001;75(14):6615-24.

167.   Schmidt M, Voutetakis A, Afione S, Zheng C, Mandikian D, Chiorini JA. Adeno-associated virus type 12 (AAV12): a novel AAV serotype with sialic acid- and heparan sulfate proteoglycan-independent transduction activity. J Virol. 2008;82(3):1399-406.

168.   Kaludov N, Brown KE, Walters RW, Zabner J, Chiorini JA. Adeno-associated virus serotype 4 (AAV4) and AAV5 both require sialic acid binding for hemagglutination and efficient transduction but differ in sialic acid linkage specificity. J Virol. 2001;75(15): 6884-93.

169.   Walters RW, Yi SM, Keshavjee S, Brown KE, Welsh MJ, Chiorini JA, et al. Binding of adeno-associated virus type 5 to 2,3-linked sialic acid is required for gene transfer. J Biol Chem. 2001;276(23):20610-6.

170.   Bartlett JS, Wilcher R, Samulski RJ. Infectious entry pathway of adeno-associated virus and adeno-associated virus vectors. J Virol. 2000;74(6):2777-85.

171.   Sanlioglu S, Benson PK, Yang J, Atkinson EM, Reynolds T, Engelhardt JF. Endocytosis and nuclear trafficking of adeno-associated virus type 2 are controlled by rac1 and phosphatidylinositol-3 kinase activation. J Virol. 2000;74(19):9184-96.

172.   Duan D, Li Q, Kao AW, Yue Y, Pessin JE, Engelhardt JF. Dynamin is required for recombinant adeno-associated virus type 2 infection. J Virol. 1999;73(12):10371-6.

173.   Bantel-Schaal U, Hub B, Kartenbeck J. Endocytosis of adeno-associated virus type 5 leads to accumulation of virus particles in the Golgi compartment. J Virol. 2002;76(5):2340-9.

174.   Vihinen-Ranta M, Kalela A, Makinen P, Kakkola L, Marjomaki V, Vuento M. Intracellular route of canine parvovirus entry. J Virol. 1998;72(1):802-6.

175.   Douar AM, Poulard K, Stockholm D, Danos O. Intracellular trafficking of adeno-associated virus vectors: routing to the late endosomal compartment and proteasome degradation. J Virol. 2001;75(4):1824-33.

176.   Yan Z, Zak R, Zhang Y, Ding W, Godwin S, Munson K, et al. Distinct classes of proteasome-modulating agents cooperatively augment recombinant adeno-associated virus type 2 and type 5-mediated transduction from the apical surfaces of human airway epithelia. J Virol. 2004;78(6):2863-74.

177.   Ros C, Burckhardt CJ, Kempf C. Cytoplasmic trafficking of minute virus of mice: low-pH requirement, routing to late endosomes, and proteasome interaction. J Virol. 2002;76(24):12634-45.

178.   Yan Z, Zak R, Luxton GW, Ritchie TC, Bantel-Schaal U, Engelhardt JF. Ubiquitination of both adeno-associated virus type 2 and 5 capsid proteins affects the transduction efficiency of recombinant vectors. J Virol. 2002;76(5):2043-53.

179.   Zerial M, McBride H. Rab proteins as membrane organizers. Nat Rev Mol Cell Biol. 2001;2(2):107-17.

180.   Trischler M, Stoorvogel W, Ullrich O. Biochemical analysis of distinct Rab5- and Rab11-positive endosomes along the transferrin pathway. J Cell Sci. 1999;112 (Pt 24): 4773-83.

181.   Bucci C, Thomsen P, Nicoziani P, McCarthy J, van Deurs B. Rab7: a key to lysosome biogenesis. Mol Biol Cell. 2000;11(2):467-80.

182.   Diaz E, Schimmoller F, Pfeffer SR. A novel Rab9 effector required for endosome-to-TGN transport. J Cell Biol. 1997;138(2):283-90.

183.   Suikkanen S, Antila M, Jaatinen A, Vihinen-Ranta M, Vuento M. Release of canine parvovirus from endocytic vesicles. Virology. 2003;316(2):267-80.

184.   Seisenberger G, Ried MU, Endress T, Buning H, Hallek M, Brauchle C. Real-time single-molecule imaging of the infection pathway of an adeno-associated virus. Science. 2001;294(5548):1929-32.

185.   Ding W, Zhang L, Yan Z, Engelhardt JF. Intracellular trafficking of adeno-associated viral vectors. Gene Ther. 2005;12(11):873-80.

186.   Pang JJ, Lauramore A, Deng WT, Li Q, Doyle TJ, Chiodo V, et al. Comparative analysis of in vivo and in vitro AAV vector transduction in the neonatal mouse retina: effects of serotype and site of administration. Vision Res. 2008;48(3):377-85.

187.   Clement N, Grieger JC. Manufacturing of recombinant adeno-associated viral vectors for clinical trials. Mol Ther Methods Clin Dev. 2016;3:16002.

188.   Hermonat PL, Labow MA, Wright R, Berns KI, Muzyczka N. Genetics of adeno-associated virus: isolation and preliminary characterization of adeno-associated virus type 2 mutants. J Virol. 1984;51(2):329-39.

189.   Samulski RJ, Chang LS, Shenk T. Helper-free stocks of recombinant adeno-associated viruses: normal integration does not require viral gene expression. J Virol. 1989;63(9):3822-8.

190.   Muzyczka N. Use of adeno-associated virus as a general transduction vector for mammalian cells. Curr Top Microbiol Immunol. 1992;158:97-129.

191.   Adamson-Small L, Potter M, Falk DJ, Cleaver B, Byrne BJ, Clement N. A scalable method for the production of high-titer and high-quality adeno-associated type 9 vectors using the HSV platform. Mol Ther Methods Clin Dev. 2016;3:16031.

192.   Xiao X, Li J, Samulski RJ. Production of high-titer recombinant adeno-associated virus vectors in the absence of helper adenovirus. J Virol. 1998;72(3):2224-32.

193.   Grimm D, Kern A, Rittner K, Kleinschmidt JA. Novel tools for production and purification of recombinant adenoassociated virus vectors. Hum Gene Ther. 1998;9(18): 2745-60.

194.   Chadeuf G, Favre D, Tessier J, Provost N, Nony P, Kleinschmidt J, et al. Efficient recombinant adeno-associated virus production by a stable rep-cap HeLa cell line correlates with adenovirus-induced amplification of the integrated rep-cap genome. J Gene Med. 2000;2(4):260-8.

195.   Liu X, Voulgaropoulou F, Chen R, Johnson PR, Clark KR. Selective Rep-Cap gene amplification as a mechanism for high-titer recombinant AAV production from stable cell lines. Mol Ther. 2000;2(4):394-403.

196.   Gao GP, Lu F, Sanmiguel JC, Tran PT, Abbas Z, Lynd KS, et al. Rep/Cap gene amplification and high-yield production of AAV in an A549 cell line expressing Rep/Cap. Mol Ther. 2002;5(5 Pt 1):644-9.

197.   Urabe M, Ding C, Kotin RM. Insect cells as a factory to produce adeno-associated virus type 2 vectors. Hum Gene Ther. 2002;13(16):1935-43.

198.   Grimm D, Kay MA, Kleinschmidt JA. Helper virus-free, optically controllable, and two-plasmid-based production of adeno-associated virus vectors of serotypes 1 to 6. Mol Ther. 2003;7(6):839-50.

199.   Auricchio A, O'Connor E, Hildinger M, Wilson JM. A single-step affinity column for purification of serotype-5 based adeno-associated viral vectors. Mol Ther. 2001;4(4): 372-4.

200.   Auricchio A, Hildinger M, O'Connor E, Gao GP, Wilson JM. Isolation of highly infectious and pure adeno-associated virus type 2 vectors with a single-step gravity-flow column. Hum Gene Ther. 2001;12(1):71-6.

201.   Wu Z, Asokan A, Samulski RJ. Adeno-associated virus serotypes: vector toolkit for human gene therapy. Mol Ther. 2006;14(3):316-27.

202.   Beltran WA, Boye SL, Boye SE, Chiodo VA, Lewin AS, Hauswirth WW, et al. rAAV2/5 gene-targeting to rods:dose-dependent efficiency and complications associated with different promoters. Gene Ther. 2010;17(9):1162-74.

203.   Manfredi A, Marrocco E, Puppo A, Cesi G, Sommella A, Della Corte M, et al. Combined rod and cone transduction by adeno-associated virus 2/8. Hum Gene Ther. 2013;24(12):982-92.

204.   Quiambao AB, Peachey NS, Mangini NJ, Rohlich P, Hollyfield JG, al-Ubaidi MR. A 221-bp fragment of the mouse opsin promoter directs expression specifically to the rod photoreceptors of transgenic mice. Vis Neurosci. 1997;14(4):617-25.

205.   Khani SC, Pawlyk BS, Bulgakov OV, Kasperek E, Young JE, Adamian M, et al. AAV-mediated expression targeting of rod and cone photoreceptors with a human rhodopsin kinase promoter. Invest Ophthalmol Vis Sci. 2007;48(9):3954-61.

206.   Mowat FM, Gornik KR, Dinculescu A, Boye SL, Hauswirth WW, Petersen-Jones SM, et al. Tyrosine capsid-mutant AAV vectors for gene delivery to the canine retina from a subretinal or intravitreal approach. Gene therapy. 2014;21(1):96-105.

207.   Boyd RF, Boye SL, Conlon TJ, Erger KE, Sledge DG, Langohr IM, et al. Reduced retinal transduction and enhanced transgene-directed immunogenicity with intravitreal delivery of rAAV following posterior vitrectomy in dogs. Gene therapy. 2016;23(6): 548-56.

208.   Woodard KT, Liang KJ, Bennett WC, Samulski RJ. Heparan Sulfate Binding Promotes Accumulation of Intravitreally Delivered Adeno-associated Viral Vectors at the Retina for Enhanced Transduction but Weakly Influences Tropism. J Virol. 2016;90(21): 9878-88.

209.   Kay CN, Ryals RC, Aslanidi GV, Min SH, Ruan Q, Sun J, et al. Targeting photoreceptors via intravitreal delivery using novel, capsid-mutated AAV vectors. PLoS One. 2013;8(4):e62097.

210.   Qing K, Hansen J, Weigel-Kelley KA, Tan M, Zhou S, Srivastava A. Adeno-associated virus type 2-mediated gene transfer: role of cellular FKBP52 protein in transgene expression. J Virol. 2001;75(19):8968-76.

211.   Qing K, Li W, Zhong L, Tan M, Hansen J, Weigel-Kelley KA, et al. Adeno-associated virus type 2-mediated gene transfer: role of cellular T-cell protein tyrosine phosphatase in transgene expression in established cell lines in vitro and transgenic mice in vivo. J Virol. 2003;77(4):2741-6.

212.   Zhong L, Li B, Mah CS, Govindasamy L, Agbandje-McKenna M, Cooper M, et al. Next generation of adeno-associated virus 2 vectors: point mutations in tyrosines lead to high-efficiency transduction at lower doses. Proc Natl Acad Sci U S A. 2008;105(22): 7827-32.

213.   Yokoi K, Kachi S, Zhang HS, Gregory PD, Spratt SK, Samulski RJ, et al. Ocular gene transfer with self-complementary AAV vectors. Invest Ophthalmol Vis Sci. 2007;48(7):3324-8.

214.   Natkunarajah M, Trittibach P, McIntosh J, Duran Y, Barker SE, Smith AJ, et al. Assessment of ocular transduction using single-stranded and self-complementary recombinant adeno-associated virus serotype 2/8. Gene Ther. 2008;15(6):463-7.

215.   Petersen-Jones SM, Bartoe JT, Fischer AJ, Scott M, Boye SL, Chiodo V, et al. AAV retinal transduction in a large animal model species: comparison of a self-complementary AAV2/5 with a single-stranded AAV2/5 vector. Mol Vis. 2009;15:1835-42.

216.   Ford M, Bragadottir R, Rakoczy PE, Narfstrom K. Gene transfer in the RPE65 null mutation dog: relationship between construct volume, visual behavior and electroretinographic (ERG) results. Doc Ophthalmol. 2003;107(1):79-86.

217.   Narfstrom K, Bragadottir R, Redmond TM, Rakoczy PE, van Veen T, Bruun A. Functional and structural evaluation after AAV.RPE65 gene transfer in the canine model of Leber's congenital amaurosis. Adv Exp Med Biol. 2003;533:423-30.

218.   Annear MJ, Bartoe JT, Barker SE, Smith AJ, Curran PG, Bainbridge JW, et al. Gene therapy in the second eye of RPE65-deficient dogs improves retinal function. Gene Ther. 2011;18(1):53-61.

219.   Annear MJ, Mowat FM, Bartoe JT, Querubin J, Azam SA, Basche M, et al. Successful gene therapy in older Rpe65-deficient dogs following subretinal injection of an adeno-associated vector expressing RPE65. Hum Gene Ther. 2013;24(10):883-93.

220.   Mowat FM, Breuwer AR, Bartoe JT, Annear MJ, Zhang Z, Smith AJ, et al. RPE65 gene therapy slows cone loss in Rpe65-deficient dogs. Gene Ther. 2013;20(5):545-55.

221.   Dejneka NS, Surace EM, Aleman TS, Cideciyan AV, Lyubarsky A, Savchenko A, et al. In utero gene therapy rescues vision in a murine model of congenital blindness. Mol Ther. 2004;9(2):182-8.

222.   Lai CM, Yu MJ, Brankov M, Barnett NL, Zhou X, Redmond TM, et al. Recombinant adeno-associated virus type 2-mediated gene delivery into the Rpe65-/- knockout mouse eye results in limited rescue. Genet Vaccines Ther. 2004;2(1):3.

223.   Narfstrom K, Katz ML, Ford M, Redmond TM, Rakoczy E, Bragadottir R. In vivo gene therapy in young and adult RPE65-/- dogs produces long-term visual improvement. J Hered. 2003;94(1):31-7.

224.   Narfstrom K, Vaegan, Katz M, Bragadottir R, Rakoczy EP, Seeliger M. Assessment of structure and function over a 3-year period after gene transfer in RPE65-/- dogs. Doc Ophthalmol. 2005;111(1):39-48.

225.   Bainbridge JW, Smith AJ, Barker SS, Robbie S, Henderson R, Balaggan K, et al. Effect of gene therapy on visual function in Leber's congenital amaurosis. N Engl J Med. 2008;358(21):2231-9.

226.   Hauswirth WW, Aleman TS, Kaushal S, Cideciyan AV, Schwartz SB, Wang L, et al. Treatment of leber congenital amaurosis due to RPE65 mutations by ocular subretinal injection of adeno-associated virus gene vector: short-term results of a phase I trial. Hum Gene Ther. 2008;19(10):979-90.

227.   Maguire AM, Simonelli F, Pierce EA, Pugh EN, Jr., Mingozzi F, Bennicelli J, et al. Safety and efficacy of gene transfer for Leber's congenital amaurosis. N Engl J Med. 2008;358(21):2240-8.

228.   Bainbridge JW, Mehat MS, Sundaram V, Robbie SJ, Barker SE, Ripamonti C, et al. Long-term effect of gene therapy on Leber's congenital amaurosis. N Engl J Med. 2015;372(20):1887-97.

229.   Bennett J, Wellman J, Marshall KA, McCague S, Ashtari M, DiStefano-Pappas J, et al. Safety and durability of effect of contralateral-eye administration of AAV2 gene

therapy in patients with childhood-onset blindness caused by RPE65 mutations: a follow-on phase 1 trial. Lancet. 2016;388(10045):661-72.

230.   Ghazi NG, Abboud EB, Nowilaty SR, Alkuraya H, Alhommadi A, Cai H, et al. Treatment of retinitis pigmentosa due to MERTK mutations by ocular subretinal injection of adeno-associated virus gene vector: results of a phase I trial. Hum Genet. 2016;135(3):327-43.

231.   Weleber RG, Pennesi ME, Wilson DJ, Kaushal S, Erker LR, Jensen L, et al. Results at 2 Years after Gene Therapy for RPE65-Deficient Leber Congenital Amaurosis and Severe Early-Childhood-Onset Retinal Dystrophy. Ophthalmology. 2016;123(7): 1606-20.

232.   Spaide RF, Curcio CA. Anatomical correlates to the bands seen in the outer retina by optical coherence tomography: literature review and model. Retina. 2011;31(8):1609-19.

233.   Hood DC, Zhang X, Ramachandran R, Talamini CL, Raza A, Greenberg JP, et al. The inner segment/outer segment border seen on optical coherence tomography is less intense in patients with diminished cone function. Invest Ophthalmol Vis Sci. 2011;52(13):9703-9.

234.   Wu Z, Ayton LN, Guymer RH, Luu CD. Relationship between the second reflective band on optical coherence tomography and multifocal electroretinography in age-related macular degeneration. Invest Ophthalmol Vis Sci. 2013;54(4):2800-6.

235.   Wu Z, Ayton LN, Guymer RH, Luu CD. Second reflective band intensity in age-related macular degeneration. Ophthalmology. 2013;120(6):1307-8 e1.

CHAPTER 2

ALTERNATIVE SPLICING IN *CEP290* MUTANT CATS RESULTS IN A MILDER PHENOTYPE THAN LCA^{CEP290} PATIENTS

Author contributions

Conceived and designed the experiments: ALM, SMP-J. Performed the experiments: ALM. Analyzed the data: ALM. Wrote the chapter: ALM, SMP-J.

2.1 Introduction

Leber Congenital Amaurosis (LCA) is a group of debilitating inherited retinal diseases that cause retinal degeneration and eventual blindness in children.(1) There are currently no treatments outside of clinical trials for these devastating conditions, however, experimental procedures aimed at replacing or repairing the causative genetic defect show great promise.(2-4)

For such treatments to reach clinical trials in people, animal models are imperative for achieving optimal efficacy and to ensure safety. Rodent models have been widely utilized and are useful for initial development of therapeutic approaches but studies using large animal models such as the cat that have eyes with critical similarities to those of humans, can build on data collected in such models. The feline eye is close in size and proportions to the human eye, allowing for optimization of surgical delivery techniques and greater ease of detailed *in vivo* imaging. Importantly, the feline retina also has a similar photoreceptor topography to the human retina with an *area centralis*, a region semi-homologous to the human macula, that could allow for greater translational analysis of treatment to this crucial region.(5)

About 20% of LCA cases are caused by mutations in the centrosomal 290kDa (*CEP290*) gene.(1) Mutations in this gene have been associated with a broad spectrum of diseases, ranging from neonatal lethal syndromes to retina-only phenotypes.(6-13) The most common retinal phenotype caused by mutations in this gene is LCA, with the commonest mutation being an intronic mutation that creates a strong splice donor site, leading to the introduction of a cryptic exon in the *CEP290* transcript.(1)

A spontaneous mutation in the *CEP290* gene in the cat resulting in an autosomal recessive retinal degeneration has provided a naturally-occurring feline model for LCA caused by *CEP290* mutations known as the *rdAc* cat.(14-33) The feline defect arises from an intronic T to G substitution 9 base-pairs downstream from the wild-type splice donor site.(34) . This is predicted to result in a canonical GT splice donor site 4 base-pairs downstream of the wild-type GC donor site that is preferentially used. Use of the alternative splice site in mutant cats results in a frameshift and a premature termination codon following two altered codons.(35) The predicted effect on the protein, if translated, would be a truncation of 159 amino acids out of the total 2,479. This feline mutation offers an opportunity to study splice-altering mutations, how they affect transcript levels relative to the wild-type state, and what types of molecular intervention could reverse the dysfunction. This model therefore provides a valuable tool for better understanding this commonly mutated gene, as well as for the development and testing of treatments.

Cats show a significantly milder phenotype than most human *CEP290* retinopathy patients, with a later-onset and slowly-progressing photoreceptor degeneration.(14, 15) The underlying mechanism for this milder phenotype may shed light on *CEP290*-associated *retinopathies* and for the development of treatments. This mutation in felines occurs further downstream than the similar mutation in people, suggesting that a possible mechanism could be the translation of a longer, more functional, protein due to a less severe truncation. Furthermore, the wild-type splice site remains, raising the question of whether some amount of full-length protein is still produced in homozygous mutant cats.

The *CEP290* gene encodes a ciliary protein that localizes to the interconnecting cilium of rod and cone photoreceptors and is integral for protein transport between the inner and outer segments.(36) The large size of this gene precludes packaging of the full-length cDNA into the most effective retinal vector system; adeno-associated virus (AAV) vectors, and other vector types have shown poor retinal transduction, making gene therapy based treatments challenging. However, a possible method to circumvent this obstacle to gene therapy could be to deliver a partial *CEP290* transcript if this provides some protein function. A study in zebrafish supports this approach with rescue of vision noted after injection of a partial transcript.(37) However, the effect of a truncated protein has not been studied in mammals, leaving a significant information gap before this form of treatment could reach human clinical trials. The *CEP290* mutant feline may provide information on the retinal phenotype associated with a truncated protein. However, detailed characterization of the *rdAc* mutation on retinal *CEP290* transcripts in affected cats has not been reported. We therefore analyzed *CEP290* transcript levels and the protein profile in *rdAc* cats versus wild-type and heterozygous carrier cats aiming to investigate whether the canonical splice site resulting from the intronic mutation is used exclusively and whether the mutant mRNA avoids nonsense-mediated decay to result in a truncated protein.

2.2 Methods

2.2.1 Animals and tissue processing

All cats were purpose bred as part of a *CEP290* retinopathy breeding colony maintained at Michigan State University. All animal practices were approved by the Michigan State University Institutional Animal Care and Use Committee and conducted according to the Association for Research in Vision and Ophthalmology Statement for the Use of Animals in Ophthalmic and Vision Research. Colony cats were genotyped utilizing a standard assay developed by our laboratory. A 240 base-pair genomic region spanning the mutation site was amplified by polymerase chain reaction. The amplicons were then differentially cut by restriction enzyme digestion with the TasI/Tsp509I enzyme (NEB, Beverly, MA, USA). (Figure 2.1)

A. Step 1: PCR			
Forward primer	TCAATGAATTATTTCCATGTCTACACT		
Reverse primer	ATGCCAAGAAGTGGCTTGAG		
B. STEP 2: Restriction enzyme digestion			
Enzyme	TasI/Tsp509I (NEB)		
Differential Digestion			
Band size	Wild-type	Heterozygous	Homozygous Mutant

Figure 2.1: Feline *CEP290* genotyping assay. A. A 240 base-pair region spanning the mutation site is amplified by PCR. B. The amplicon is digested for differential cutting of the wild-type versus mutant alleles, resulting in a larger band present for mutant alleles for clear genotype confirmation.

Following euthanasia by intravenous pentobarbital overdose (Fatal-Plus, Vortech

Pharmaceuticals, Dearborn, MI, USA), retinas were collected from nine 16 week-old

cats, three from each genotype; homozygous wild-type, *CEP290* mutation

heterozygous, and *CEP290* mutation homozygous,flash frozen and stored at -80°C until

use. RNA was extracted using the 5 Prime PerfectPure RNA Tissue Kit (Fisher Scientific

Co., Fair Lawn, NJ, USA) following the standard kit protocol. RNA quality and quantity

was analyzed using the Agilent BioAnalyzer 2100 (Agilent Technologies, Palo Alto, CA,

USA) with a minimum RNA Integrity Number (RIN) set at 6 (Table 2.1). cDNA was

synthesized using the Transcriptor First Strand cDNA synthesis kit (Roche Diagnostics,

Basel, Switzerland) following standard kit protocol using the provided random primers

and including a DNase step to prevent DNA contamination.

Sample Number	Genotype	RIN
1	Wild-type	7.5
2	Wild-type	7.3
3	Wild-type	7
4	Heterozygous	7.9
5	Heterozygous	7.1
6	Heterozygous	6.9
7	Homozygous mutant	7.9
8	Homozygous mutant	6.1
9	Homozygous mutant	8.2

Table 2.1: RNA Integrity Data. RNA integrity data for RNA samples used to create cDNA for transcript analysis.

2.2.2 Transcript analysis

For quantitative real-time polymerase chain reactions (qRT-PCRs), custom TaqMan assays were designed (Applied Biosystems, Foster City, CA, USA) to detect the wild-type *CEP290* transcript, the mutation-created alternative *CEP290* transcript, and *Tuba1b* transcript as an endogenous control (Table 2.2). qRT-PCR was carried out on a ABI 7500 Fast qRT-PCR system (Applied Biosystems) under standard conditions which included a 2 minute UNG incubation at $50°C$, a 10 minute polymerase activation step at $95°C$, and then 40 cycles of a denature and anneal protocol of $95°C$ for 15 seconds and $60°C$ for 1 minute, respectively. All samples were run in triplicate and technical replicates were analyzed and only used if within 0.3 Ct of each other. Samples were re-run if outside of this level of consistency. *CEP290* data was normalized to the *Tuba1b* data and analyzed using the comparative delta delta Ct method with the wild-type samples set as the reference. Data was analyzed for normality using the Shapiro-Wilk test for normality. Since the datasets did not pass normality testing, non-parametric tests were used to compare genotypes. For wild-type transcript level data, in which three genotypes were compared, the Kruskal-Wallis One Way Analysis of Variance on ranks was used. To compare the two genotypes in which the truncated transcript was analyzed, the Mann-Whitney Rank Sum test was used. Statistical significance was set at $p < 0.05$ for all testing. All statistical analysis and graphing was completed in SigmaPlot12 statistical software (Systat Software Inc., Chicago, IL, USA).

Forward Primer	Reverse Primer	Reporter
Full length wild-type transcript assay		
AGAGAGGGAGCAAAAAGCTAAGAAA	GCACCTTCAGGAACATGTTTGAGA	CCTTGAGCAACAAATTGA
Truncated mutant transcript assay		
AGAGAGGGAGCAAAAAGCTAAGAAA	GCACCTTCAGGAACATGTTTGAGA	TTGAGCAACAAGCAAATTG
Tuba1b endogenous control assay		
GCCCCAACCTACACTAACCTAAATAG	ACATTCAGGGCTCCATCAAATCTG	TCCATCACTGCTTCCC

Table 2.2: TaqMan Primers and Probes. Primers and probes designed by Applied Biosystems for Taqman assays, designed to differentially target the wild-type and mutant alleles as well as Tuba1b as an endogenous control.

2.2.3 Protein analysis

Protein was extracted from retinal tissue as follows: Retinal tissue was immersed in a Tris-Triton cell lysis buffer and homogenized with a pestle. Samples were then vigorously mixed on a vortex machine and centrifuged, saving the supernatant sample. Protein was quantified by spectrophotometry using a ND-1000 NanoDrop machine (NanoDrop Technologies, Wilmington, DE, USA) and stored at -20°C.

Relative quantification of CEP290 protein across genotypes was determined by automated capillary western blot utilizing the WES system (ProteinSimple, San Jose, CA, USA) following standard kit protocols. All samples were run in duplicate and were run against a calnexin control. Relative protein concentration was compared across genotypes. To do this, the area under the curve of the CEP290 peaks for each sample was generated by the WES Compass software (ProteinSimple, San Jose, CA, USA). Genotypes were then statistically compared using the Kruskal-Wallis One Way Analysis of Variance on ranks using SigmaPlot12 software (Systat Software Inc.) (Table 2.3)

Antibody	Host	Target	Use and concentration	Source
Primary Antibodies				
CEP290	Rabbit	CEP290 in interconnecting cilium	1:50, WES 1:500, IHC	Thermo Fisher Scientific
Calnexin	Rabbit	Calnexin protein	1:500, WES	Novus Biologicals
Secondary Antibodies				
Goat anti-Mouse IgG (H+L) Cross-Adsorbed Secondary Antibody. Alexa Fluor 488	Goat	Rabbit primary antibody	1:500, IHC	Thermo Fisher Scientific
Goat anti-rabbit HRP conjugate	Goat	Rabbit primary antibody	1:50, WES	Protein Simple
Nuclear counterstain				
DAPI (4',6-Diamidino-2-Phenylindole, Dihydrochloride)	NA	Nuclei	1:10,000, IHC	Thermo Fisher Scientific

Table 2.3: Antibodies Used for Protein Analysis. The same CEP290 antibody was used for both WES western blotting and IHC. Different secondary antibodies appropriate to the assays were used, with the WES-provided secondary antibody used for the WES and an IHC verified antibody used for the IHC. A nuclear counterstain was used on all IHC slides.

2.2.4 Immunohistochemistry

One eye from each of four mid-stage (four year-old) *CEP290* mutant cats and one eye from an adult wild-type cat were processed for immunohistochemistry (IHC) as previously described.(38) Briefly, eyes were promptly enucleated, fixed in 4% paraformaldehyde, and dissected along the limbus to separate the posterior eye cup which was then embedded in optimal cutting temperature gel (OCT. Sakura Finetek USA, Inc., Torrance, CA, USA) and flash frozen in liquid nitrogen.

For visualization of CEP290 protein in retinal sections, serial 14 micron vertical retinal sections were taken from the above eyes and stained with a CEP290 specific antibody (Table 2.3). Immunohistochemistry was performed as previously reported by our laboratory to label CEP290 protein against a nuclear counterstain and images were collected on a Nikon Eclipse 80i microscope (Nikon instruments Inc., Melville, NY, USA) equipped with a CoolSnap ESv camera (Photometrics, Tuscon, AZ, USA).(38)

2.3 Results

qRT-PCR revealed that *CEP290* homozygous mutant felines produce both full-length wild-type and truncated mutant transcript. Mutant cats produce 17.4% as much full-length transcript as wild-type cats ($p < 0.001$), a statistically significant difference that shows that mutant cat cells do utilize the wild-type splice site at a low level. Heterozygous mutant (carrier) cats produce 67.8% as much full-length transcript as wild-type cats, a difference which was not statistically significant ($p = 0.125$). Mutant cats also showed usage of the mutant splice site, with heterozygous cats showing 48% as much mutant transcript as mutant cats ($p = 0.026$). Taken together, these data suggest that homozygous mutant cats produce a combination of shortened mutant transcript and full-length wild-type transcript. (Figure 2.2)
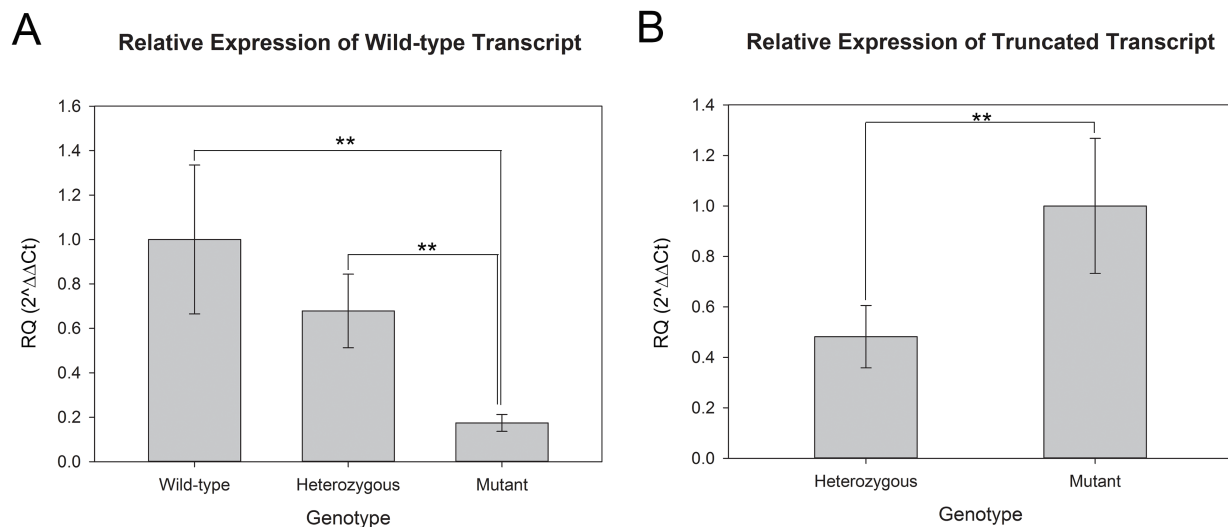
Figure 2.2: Relative expression of full-length wild-type and truncated mutant transcripts. A. Mutant cats produce 17.4% as much full-length transcript as wild-type cats. B. Mutant cats show production of truncated transcript and heterozygous cats show 48% as much truncated transcript as mutant cats. ** = $p < 0.005$

WES analysis shows production of CEP290 protein in cats of all genotypes. The homozygous mutant *CEP290* cats showed a protein blot that appeared as a smear with a wider band that extends from 290kDa to slightly lower. Because the truncated protein is only shortened by 159 of 2,479 amino acids (approximately 6%), it is difficult to separate the truncated and full-length proteins on western blot. The area under the CEP290 peaks show a stronger CEP290 signal for wild-type cats (average area = 24,917.5 chemiluminescence) than the other genotypes, with heterozygous cats having an intermediate protein signal (average area = 16,140.8 chemiluminescence) and homozygous mutant cats having the weakest signal (average area = 13,466.25 chemiluminescence). Statistical comparison of the genotypes shows a significant difference between the protein signals of mutant cats and wild-type cats ($p= 0.005$) and between wild-type cats and heterozygous cats ($p = 0.01$). (Figure 2.3)
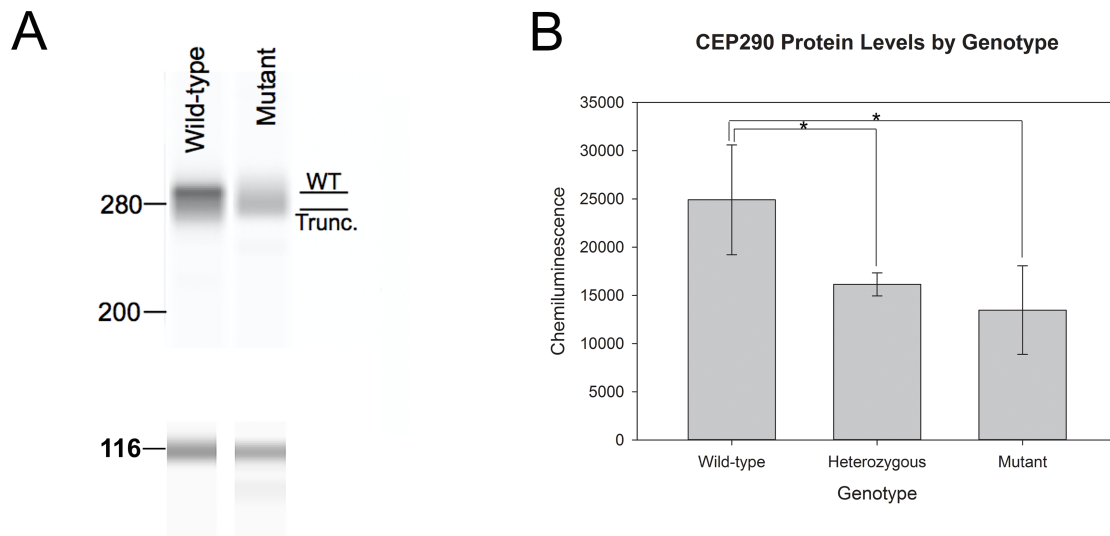
Figure 2.3: Automated capillary western blot shows detectable CEP290 signal in mutant cats. A. Representative blots generated by the WES software showing the shift towards a lower band in a *CEP290* homozygous mutant cat. The band at 116 shows the calnexin loading control. B. Relative quantitation shows a significant difference between CEP290 protein levels in wild-type cats versus heterozygous or homozygous mutant cats. * = $p < 0.05$

Immunohistochemistry (IHC) in wild-type cats showed strong labeling of the photoreceptors at the inner segment/outer segment junction. IHC on sections from mid-stage (4 year-old) *CEP290* mutant cats also shows immunolabeling for CEP290 in the region of the connecting cilium. (Figure 2.4)

CEP290, DAPI
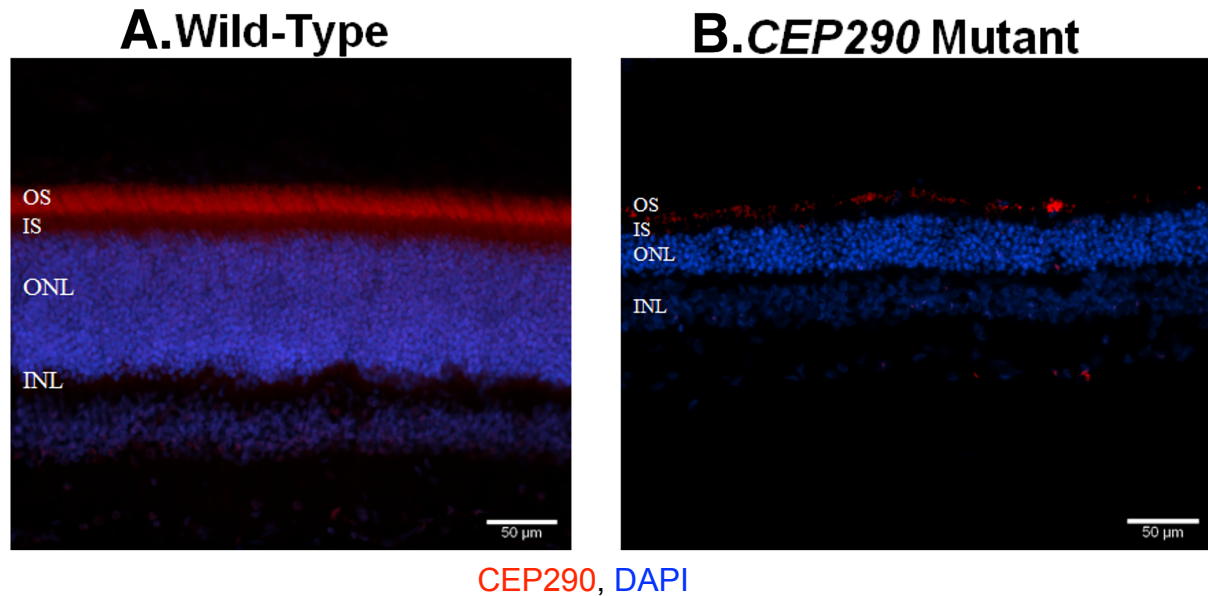
Figure 2.4: Immunohistochemistry shows detectable CEP290 protein in CEP290 mutant cats. A. Wild-type cats show significant CEP290 protein signal in the inner/ outer segment junction extending into the outer segments. B. CEP290 mutant cats show a low but detectable signal for CEP290, which appropriately localizes to the region of the connecting cilium.

2.4 Discussion

CEP290 mutant cats have a milder phenotype than is typical for people with LCA^CEP290. Our results show that this is likely to be due to a combination of some production of full-length CEP290 due to use of the wild-type splice site and some production of truncated protein due to use of the introduced splice site. Western blot resulted in a wider band in CEP290 cats compared to wild-type cats that likely represented the presence of both full-length and truncated CEP290 protein. The protein signal was 54% as strong as seen in wild-type cats but the wild-type transcript levels were only 17.4% that detected in wild-type cats, suggesting the production of a significant amount of truncated protein. The CEP290 protein produced by mutant cats is visualized in the correct retinal location on IHC of retinal sections. The predicted truncated protein resulting from this mutation would be shortened by 159 out of the 2,479 amino acids.(34) The truncation would remove two kinase inducible domains but leaves the rest of the protein, including other functional domains and localization signals, intact. This taken together with our IHC findings of appropriate localization and studies in other species showing truncated CEP290 can be functional, supports likely residual function of this shortened protein.(37) Taken together, these results suggest that the milder phenotype seen in CEP290 mutant felines is because of the production wild-type protein and a significant production of shortened but semi-functional protein.

It is important to note that the antibody used in this study is a polyclonal antibody that targets upstream of the truncation at amino acids 781-830 of the human protein. This antibody would therefore label both the full-length protein as well as the truncated

protein produced by the shortened transcript. In future studies it would be valuable to create antibodies to differentiate between the full-length and truncated proteins..

These findings in *CEP290* cats have important implications for the development of treatments against LCA^{CEP290}. Since the full *CEP290* transcript cannot fit into an AAV vector, packing a partial transcript into an AAV is one possible approach to lessen the severity of the phenotype While the shortened transcript produced in these mutant cats is still too large to fit into an AAV vector, a previous study in a zebrafish model showed that only the N-terminal region of the protein was required to rescue vision in this model suggesting that a shorter transcript than that produced in mutant cats may be therapeutic.(37)

This study also holds interesting implications for nonsense-mediated decay (NMD) in the retina as it shows that a significant amount of truncated transcript is translated. Future studies investigating this anomaly may hold additional insights into retinopathy mechanisms and treatments against these diseases.

Lastly, when studying animal models, objective markers for monitoring disease progression and treatment efficacy are integral. This study provides new information about this important model of LCA^{CEP290} and also provides new markers that could be used for objectively measuring treatment efficacy in treatment trials using this model. Transcript and protein levels relative to wild-type cats could be analyzed to determine level of rescue, which could then be combined with visual function assays for a thorough picture of treatment efficacy.

In summary, we present here evidence that translation of a truncated protein along with a low level of wild-type protein is the likely reason for the comparatively mild phenotype seen in the *CEP290* mutant feline.

2.5 Acknowledgments

REFERENCES

REFERENCES

1.   den Hollander AI, Koenekoop RK, Yzer S, Lopez I, Arends ML, Voesenek KE, et al. Mutations in the CEP290 (NPHP6) gene are a frequent cause of Leber congenital amaurosis. American journal of human genetics. 2006;79(3):556-61.

2.   Bainbridge JW, Mehat MS, Sundaram V, Robbie SJ, Barker SE, Ripamonti C, et al. Long-term effect of gene therapy on Leber's congenital amaurosis. N Engl J Med. 2015;372(20):1887-97.

3.   Ghazi NG, Abboud EB, Nowilaty SR, Alkuraya H, Alhommadi A, Cai H, et al. Treatment of retinitis pigmentosa due to MERTK mutations by ocular subretinal injection of adeno-associated virus gene vector: results of a phase I trial. Hum Genet. 2016;135(3):327-43.

4.   Weleber RG, Pennesi ME, Wilson DJ, Kaushal S, Erker LR, Jensen L, et al. Results at 2 Years after Gene Therapy for RPE65-Deficient Leber Congenital Amaurosis and Severe Early-Childhood-Onset Retinal Dystrophy. Ophthalmology. 2016;123(7): 1606-20.

5.   Linberg KA, Lewis GP, Shaaw C, Rex TS, Fisher SK. Distribution of S- and M-cones in normal and experimentally detached cat retina. The Journal of comparative neurology. 2001;430(3):343-56.

6.   Valente EM, Silhavy JL, Brancati F, Barrano G, Krishnaswami SR, Castori M, et al. Mutations in CEP290, which encodes a centrosomal protein, cause pleiotropic forms of Joubert syndrome. Nat Genet. 2006;38(6):623-5.

7.   Baala L, Audollent S, Martinovic J, Ozilou C, Babron MC, Sivanandamoorthy S, et al. Pleiotropic effects of CEP290 (NPHP6) mutations extend to Meckel syndrome. American journal of human genetics. 2007;81(1):170-9.

8.   Brancati F, Barrano G, Silhavy JL, Marsh SE, Travaglini L, Bielas SL, et al. CEP290 mutations are frequently identified in the oculo-renal form of Joubert syndrome-related disorders. American journal of human genetics. 2007;81(1):104-13.

9.   Helou J, Otto EA, Attanasio M, Allen SJ, Parisi MA, Glass I, et al. Mutation analysis of NPHP6/CEP290 in patients with Joubert syndrome and Senior-Loken syndrome. J Med Genet. 2007;44(10):657-63.

10.   Frank V, den Hollander AI, Bruchle NO, Zonneveld MN, Nurnberg G, Becker C, et al. Mutations of the CEP290 gene encoding a centrosomal protein cause Meckel-Gruber syndrome. Hum Mutat. 2008;29(1):45-52.

11.   Travaglini L, Brancati F, Attie-Bitach T, Audollent S, Bertini E, Kaplan J, et al. Expanding CEP290 mutational spectrum in ciliopathies. Am J Med Genet A. 2009;149A(10):2173-80.

12.   Ghaffari SR, Rafati M, Ghaffari G, Morra M, Tekin M. Familial intellectual disability in an Iranian family with a novel truncating mutation in CEP290. Clin Genet. 2014;86(4):387-90.

13.   Wang L, Yang Y, Song J, Mao L, Wei X, Sun Y, et al. Two novel mutations in the C-terminal region of centrosomal protein 290 (CEP290) result in classic Joubert syndrome. J Child Neurol. 2015;30(6):772-6.

14.   Narfstrom K. Hereditary progressive retinal atrophy in the Abyssinian cat. J Hered. 1983;74(4):273-6.

15.   Narfstrom K. Progressive retinal atrophy in the Abyssinian cat. Clinical characteristics. Invest Ophthalmol Vis Sci. 1985;26(2):193-200.

16.   Narfstrom KL, Nilsson SE, Andersson BE. Progressive retinal atrophy in the Abyssinian cat: studies of the DC-recorded electroretinogram and the standing potential of the eye. Br J Ophthalmol. 1985;69(8):618-23.

17.   Narfstrom K, Nilsson SE. Hereditary retinal degeneration in the Abyssinian cat: correlation of ophthalmoscopic and electroretinographic findings. Doc Ophthalmol. 1985;60(2):183-7.

18.   Narfstrom K, Nilsson SE. Hereditary rod-cone degeneration in a strain of Abyssinian cats. Prog Clin Biol Res. 1987;247:349-68.

19.   Narfstrom K, Wilen M, Andersson BE. Hereditary retinal degeneration in the Abyssinian cat: developmental studies using clinical electroretinography. Doc Ophthalmol. 1988;69(2):111-8.

20.   Jacobson SG, Kemp CM, Narfstrom K, Nilsson SE. Rhodopsin levels and rod-mediated function in Abyssinian cats with hereditary retinal degeneration. Exp Eye Res. 1989;49(5):843-52.

21.   Narfstrom K, Arden GB, Nilsson SE. Retinal sensitivity in hereditary retinal degeneration in Abyssinian cats: electrophysiological similarities between man and cat. Br J Ophthalmol. 1989;73(7):516-21.

22.   Narfstrom K, Nilsson SE. Morphological findings during retinal development and maturation in hereditary rod-cone degeneration in Abyssinian cats. Exp Eye Res. 1989;49(4):611-28.

23.	Anderson RE, Maude MB, Nilsson SE, Narfstrom K. Plasma lipid abnormalities in the abyssinian cat with a hereditary rod-cone degeneration. Exp Eye Res. 1991;53(3): 415-7.

24.	Ehinger B, Narfstrom K, Nilsson SE, van Veen T. Photoreceptor degeneration and loss of immunoreactive GABA in the Abyssinian cat retina. Exp Eye Res. 1991;52(1):17-25.

25.	Ekesten B, Narfstrom K. Cone positive off-response in normal and dystrophic cats. Doc Ophthalmol. 1998;97(1):9-21.

26.	Seeliger MW, Narfstrom K. Functional assessment of the regional distribution of disease in a cat model of hereditary retinal degeneration. Invest Ophthalmol Vis Sci. 2000;41(7):1998-2005.

27.	Narfstrom K, Ehinger B, Bruun A. Immunohistochemical studies of cone photoreceptors and cells of the inner retina in feline rod-cone degeneration. Vet Ophthalmol. 2001;4(2):141-5.

28.	Nilsson SF, Maepea O, Alm A, Narfstrom K. Ocular blood flow and retinal metabolism in abyssinian cats with hereditary retinal degeneration. Invest Ophthalmol Vis Sci. 2001;42(5):1038-44.

29.	Kang Derwent JJ, Padnick-Silver L, McRipley M, Giuliano E, Linsenmeier RA, Narfstrom K. The electroretinogram components in Abyssinian cats with hereditary retinal degeneration. Invest Ophthalmol Vis Sci. 2006;47(8):3673-82.

30.	Padnick-Silver L, Kang Derwent JJ, Giuliano E, Narfstrom K, Linsenmeier RA. Retinal oxygenation and oxygen metabolism in Abyssinian cats with a hereditary retinal degeneration. Invest Ophthalmol Vis Sci. 2006;47(8):3683-9.

31.	May CA, Narfstrom K. Choroidal microcirculation in Abyssinian cats with hereditary rod-cone degeneration. Exp Eye Res. 2008;86(3):537-40.

32.	Thompson S, Whiting RE, Kardon RH, Stone EM, Narfstrom K. Effects of hereditary retinal degeneration due to a CEP290 mutation on the feline pupillary light reflex. Vet Ophthalmol. 2010;13(3):151-7.

33.	Narfstrom K, Menotti Raymond M, Seeliger M. Characterization of feline hereditary retinal dystrophies using clinical, functional, structural and molecular genetic studies. Vet Ophthalmol. 2011;14 Suppl 1:30-6.

34.	Menotti-Raymond M, David VA, Schaffer AA, Stephens R, Wells D, Kumar-Singh R, et al. Mutation in CEP290 discovered for cat model of human retinal degeneration. J Hered. 2007;98(3):211-20.

35.   Menotti-Raymond M, David VA, Schaffer AA, Stephens R, Wells D, Kumar-Singh R, et al. Mutation in CEP290 discovered for cat model of human retinal degeneration. J Hered. 2007;98(3):211-20.

36.   Betleja E, Cole DG. Ciliary trafficking: CEP290 guards a gated community. Curr Biol. 2010;20(21):R928-31.

37.   Baye LM, Patrinostro X, Swaminathan S, Beck JS, Zhang Y, Stone EM, et al. The N-terminal region of centrosomal protein 290 (CEP290) restores vision in a zebrafish model of human blindness. Hum Mol Genet. 2011;20(8):1467-77.

38.   Minella AL, Mowat FM, Willett KL, Sledge D, Bartoe JT, Bennett J, et al. Differential targeting of feline photoreceptors by recombinant adeno-associated viral vectors: implications for preclinical gene therapy trials. Gene therapy. 2014;21(10): 913-20.

CHAPTER 3

CENTRAL RETINA PRESERVATION IN rdAc CATS

In review with the Veterinary Ophthalmology journal.

3.1 Abstract

Objective. Children with Leber Congenital Amaurosis (LCA) due to *CEP290* mutations show characteristic macular preservation. Spectral domain optical coherence tomography (SD-OCT) is a non-invasive technique to investigate retinal structural changes. Loss of integrity of the ellipsoid zone (EZ) on OCT in people with retinal disease has been associated with loss of visual function and is a useful measure of retinal disease progression. We hypothesized that *rdAc* felines with *Cep290* mutation would have a similar pattern of degeneration, with relative central retinal preservation associated with maintenance of the EZ. **Procedures.** Fundus imaging, confocal scanning laser ophthalmoscopy, and SD-OCT cross sectional imaging was performed on 11 *rdAc* cats ranging from 6 months to 10 years of age. Images were collected from the *area centralis*, visual streak, and the mid-superior and mid-inferior retina. Receptor plus (REC+, encompassing the entire length of photoreceptors) thicknesses were measured. Regional rates of degeneration were determined by regression analysis and compared using unpaired t-tests. The EZ was evaluated for presence, absence, or loss of definition. **Results.** *RdAc* cats showed REC+ thinning over time in all regions. The *area centralis* and visual streak had a slower rate of thinning than the mid-peripheral retina. There was loss of integrity of the EZ initially in the more peripheral regions while its integrity was maintained in the *area centralis* and visual streak at all ages studied. **Conclusions.** *rdAc* cats show preservation of the central retina with maintenance of EZ integrity, which recapitulates findings in human patients.

3.2 Introduction

Progressive Retinal Atrophy (PRA) is a group of genetically heterogenous retinal degenerative diseases that cause blindness in cats and dogs. Though more common in dogs, a well-described form of autosomal recessive PRA, designated *rdAc*, segregates in the feline population across several breeds and is the result of a mutation in the centrosomal protein 290kDa (*Cep290*) gene.(1-3) The affected cats have a relatively late-onset, slowly progressing retinal degeneration eventually leading to blindness.(4-8)

Mutations in *CEP290* in people are associated with a wide spectrum of phenotypes dependent on the effect of the mutation on gene function. The most severe result in early lethality or syndromic conditions (such as Joubert syndrome, Meckel syndrome and Senior-Løken syndrome).(9-16) Milder phenotypes are of a non-syndromic retinal dystrophy.(17-19) The most common retinal phenotype is Leber Congenital Amaurosis (LCA), which is a devastating disease and a leading cause of childhood blindness.(20) Mutations in *CEP290* are the commonest cause of LCA accounting for about 20% of cases.(21) There are currently no treatments for LCA outside of clinical trials, and no clinical trials aimed at LCA[CEP290]. The *rdAc* cat therefore is a valuable model for this human retinal dystrophy, allowing for the study of molecular mechanisms, phenotype, and treatments that may benefit both veterinary and human patients.

A thorough characterization of disease phenotype and identification of biomarkers of disease progression, which can be used to assess treatment efficacy, are necessary for animal models intended for use in the development of translational therapies. Several modalities are available for this purpose, with electroretinographic, histological,

and ultrastructural changes well described in the *rdAc* cat.(4, 6-8, 22-40) However, investigations using a newer modality, spectral domain optical coherence tomography (SD-OCT), have not been published for this model. SD-OCT provides a valuable imaging technique that allows for the *in vivo* monitoring of retinal health by enabling visualization of retinal layers and retinal architecture. The images can match those of low power histological sections. Changes in layer thickness and in the visualization of the reflective zones from photoreceptor inner and outer segments can be used for longitudinal monitoring of disease progression, photoreceptor health, and for targeting therapeutic interventions and monitoring treatment efficacy. In the normal retina, a series of zones can be distinguished between the external limiting membrane (ELM) and the interdigitation zone (IZ). The IZ represents the tips of outer segments with enveloping retinal pigment epithelial cell processes.(41) Loss of definition of one of these zones, the ellipsoid zone (EZ), has been correlated with functional vision loss in people with retinal disease.(42-44) This zone represents the ellipsoid region of photoreceptor inner segments and is thought to arise from laser light reflection from mitochondria in this region.(45) EZ integrity has been suggested as a marker to monitor disease progression and could also be used to select regions to target with therapies such as gene augmentation therapy in human patients.(46-49) The EZ has not been studied in detail in the cat but could be a valuable tool for the same purposes in feline models.

Humans with LCA[CEP290] have a distinctive pattern of retinal degeneration with sparing of the central retina (i.e. macula) until later stages of disease.(17) SD-OCT can be used to monitor these changes and has implications for judging whether there are still photoreceptors remaining and if so their location to target with treatment.(50) The

central retina in humans contains the macula within which is the fovea and foveola. These are regions of high photoreceptor, in particular cone, density with the centermost part, the foveola, containing exclusively cones, that are important for high visual acuity. Degeneration of this macular region causes severe impairment of vision. Therefore therapy aiming to conserve that retinal area is of particular importance.

Laboratory rodents are commonly used in the study of hereditary retinal disease but they do not have a central region of higher photoreceptor density that is similar to the macula. This is a serious limitation of these species for translational studies. Cats and dogs on the other hand have a semi-homologous region known as the *area centralis* that allows for the study of regions of high photoreceptor density making them important models of human disease. Given the central, macular preservation seen in LCA^{CEP290}, a large animal model with a homologous retinal region is imperative for understanding disease mechanisms and studying treatments. Previous studies in the *rdAc* cat have suggested that the central retina degenerated at a slower rate than the peripheral retina and that there is functional preservation, as assessed by multifocal ERG, in the central retinal region.(6, 30)

The tapetal reflectivity changes in *rdAc* cats includes the appearance of patchy hyporeflectivity in earlier disease stages prior to the development of more extensive hyperreflectivity. The central retina, including the *area centralis* and visual streak, will often appear hyporeflective compared to the more peripheral retina suggestive of a relative preservation of the central region (Figure 3.1). SD-OCT is an ideal tool for longitudinal comparison of regional rates of degeneration and for further detailed investigation of regional differences in rate of photoreceptor degeneration.

Figure 3.1: Tapetal reflectivity changes in the *rdAC* feline. A. The wild-type feline fundus shows the distinctive feline tapetum lucidum and well defined vasculature. B. A fundus image from a 1.5 year-old *rdAC* feline. In earlier stages of disease the *rdAC* fundus often shows patchy changes in tapetal reflectivity. C. A fundus image from a 6 year-old *rdAC* feline. In later stages of disease the fundus shows blood vessel attenuation and a characteristic tapetal hyporeflectivity of the central fundus that extends across the *area centralis* and visual streak.

In this study, we used SD-OCT to study the regional rates of degeneration to determine if *rdAc* cats show the same pattern of degeneration as people with LCA[CEP290] and to evaluate the EZ as a possible biomarker of retinal preservation in the *rdAc* feline. We hypothesized that *rdAc* cats will show central retinal sparing on SD-OCT with corresponding maintenance of EZ definition. If true, this would further validate and direct future studies utilizing this feline disease as a model to test therapies aimed at preserving photoreceptors and vision in patients with *CEP290* mutations.

3.3 Methods

3.3.1 Animals

RdAc cats maintained as a breeding colony at Michigan State University were utilized in this study . The genotypes of colony cats was confirmed utilized a standard genotyping assay developed in our laboratory that includes a polymerase chain reaction (PCR) to amplify the mutant region followed by a restriction enzyme digestion to result in differential cutting of the mutant region. Cutting with the TasI/Tsp509I enzyme (NEB, Beverly, MA, USA) results in cutting of the wild-type allele but not the mutant allele, allowing for definitive identification of wild-type, heterozygous, and homozygous mutant animals. They were maintained under 12:12hr light dark cycles and fed *ad libitum* with Purina Cat Chow (Nestlé Purina, Wilkes-Barre, PA). Standard complete eye examinations including indirect ophthalmoscopy and wide-field fundus imaging (RetCam II. Clarity Medical Systems, Pleasanton, CA, USA) were performed at regular intervals. All procedures were approved by the Michigan State University Institutional Animal Care and Use committee and were conducted in accordance with the Association for Research in Vision and Ophthalmology statement on the use of animals.

3.3.2 Scanning laser ophthalmoscopy and spectral domain optical coherence tomography imaging

A standardized spectral domain-optical coherence tomography (SD-OCT; Spectralis OCT+HRA, Heidelberg Engineering Inc., Heidelberg, Germany) protocol was developed and performed on the right eye of 11 *RdAc* cats under general anesthesia. A

total of 23 OCT examinations were performed covering ten time-points from 6 months of age to 10 years of age (Table 3.1).

Age (years)	0.5	0.75	1	2	3	4	5	6	8	10
A. n, sex	n = 2 2M	n = 3 2M, 1F	n = 2 1M, 1F	n = 3 1M, 2F	n = 3 2F, 1M	n = 4 1M, 3F	n = 1 1F	n = 2 1M, 1F	n = 2 2M	n = 1 1M
B. Distribution of SD-OCT scans by cat										
Cat 1 (F)					X	X				
Cat 2 (F)							X	X		
Cat 3 (F)						X				
Cat 4 (F)				X	X	X				
Cat 5 (F)		X	X	X						
Cat 6 (M)	X	X	X	X						
Cat 7 (M)	X	X								
Cat 8 (M)						X		X		
Cat 9 (M)									X	X
Cat 10 (M)									X	
Cat 11 (M)					X					

Table 3.1: Animal numbers and design. 11 mutant cats that were part of an rdAc breeding colony were used to collect 23 SD-OCT scans over an age range of 6 months to 10 years old. A. The numbers of cats in each age group and sex of those cats. B. A visual depiction of the distribution of the scans collected.

Anesthesia was induced by isoflurane delivered by mask or induction box (IsoFlo, Abbott Laboratories, North Chicago, IL, USA). Following anesthesia induction, cats were intubated and maintained on isoflurane delivered in oxygen for the entire procedure. They were positioned in sternal recumbency on a heating pad for thermoregulation and monitored with a pulse oximeter (Vet/Ox 4400, Heska Corporation, Fort Collins, CO). Mydriasis was induced by topical application of tropicamide (Tropicamide Ophthalmic

106

Solution UPS 1%®, Falcon Pharmaceuticals Ltd., Fort Worth, TX, USA). The eyes were maintained in primary gaze using a stay suture placed in the perilimbal conjunctiva. Confocal scanning laser ophthalmoscopy (cSLO) followed by SD-OCT was performed. The corneas were kept constantly moist with sterile eye wash applied regularly throughout the procedure. For all scans, the retinal vasculature was used for orientation. The Heidelberg Eye Explorer Software (Heidelberg Engineering Inc., Heidelberg, Germany), which has a function to align scans was used to allow the same region to be imaged in repeat scans.

3.3.3 Receptor plus thickness evaluation

The standard SD-OCT protocol used includes cross-sectional volume scan images collected from the *area centralis*, visual streak, and the inferior and superior mid-peripheries (Figure 3.2A). The photoreceptor structural preservation was evaluated by measuring the thickness of the receptor plus (REC+). The REC+ extends from the outer plexiform layer to the IZ and therefore represents the full length of the photoreceptor cell (Figure 3.2B). The REC+ layer was measured for each cat, in each region, at each time-point, in triplicate and the measurements from each region averaged. All measurements were conducted manually by the same investigator and areas under major blood vessels were avoided.
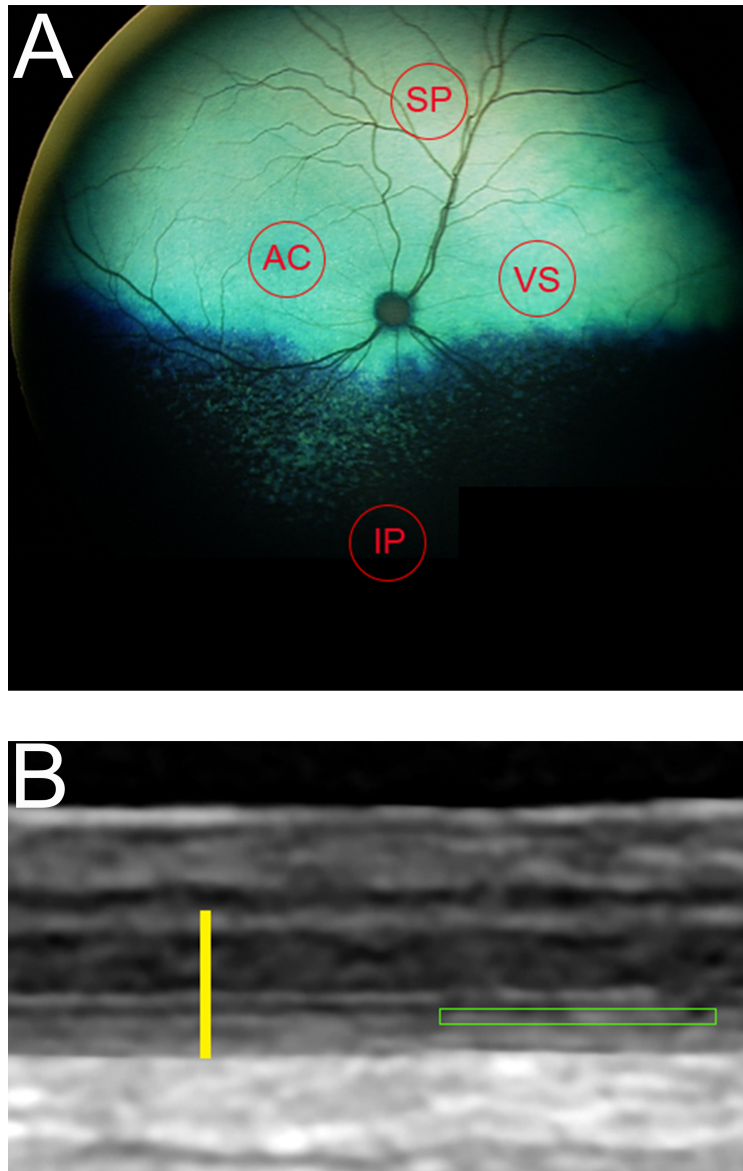
Figure 3.2: Regional and SD-OCT Measurements. A. Circles indicate where measurements were taken for REC+ evaluation. Measurements were taken from the *area centralis* (AC) with retinal vasculature utilized as landmarks. The visual streak (VS) was then assessed as the mirror image region on the opposite side of the vasculature. The superior and inferior mid-peripheries (SP and IP) were measured superior or inferior to the optic nerve head, respectively, at a distance of 5,000 microns from the edge of the optic nerve head. B. Photoreceptor degeneration was assessed using the receptor plus (REC+) layer indicated in by the yellow line. This layer represents the entire length of the photoreceptor cell as it extends from the outer plexiform layer to the interdigitation between the photoreceptor cells and the retinal pigment epithelium. The ellipsoid zone, indicated by the green box, was monitored for presence or absence across all retinal sections.

The rate of degeneration over time was calculated for each region by performing a linear regression on the REC+ thickness measurements. Analysis of differences between the rates of degeneration across different retinal regions was performed by comparing the slopes of the regressions using un-paired two-tailed Student's t-tests with significance set at $p < 0.05$, after all data passed the Shapiro-Wilk test for normality. Bonferroni correction was applied to account for the multiple comparisons. All regions were compared separately against the measurements from the *area centralis*. The *area centralis* and visual streak measurements were then averaged to represent the central retina and compared against the mid-peripheral retina, calculated by averaging the values for the superior and inferior mid-peripheries. Data was then graphed using Sigma-Plot12 statistical software (Systat Software Inc., Chicago, IL, USA).

Color heat maps to illustrate REC+ thickness across the fundus were developed using the Heidelberg Eye Explorer Software (Heidelberg Engineering Inc., Heidelberg, Germany). Heat maps were created by tracing two lines, the proximal line following the outer plexiform layer and a distal line following the IZ. The software could then calculate the REC+ thickness across the entire section. This was performed for all sections within each selected volume scan.

3.3.4 Ellipsoid zone assessment

The EZ was visually assessed for presence, absence, or loss of definition, in all cats for all time-points (Figure 3.2B). It was mapped by following the layer across sections and marking on the corresponding cSLO fundus image where the layer was no longer discernible. This was performed in all sections across a chosen volume scan of

109

61 sections. The marks for each section were then connected to create a map of the region over which there was discernible uninterrupted EZ. This was then visually compared to the heat map created from the same volume scan.

3.4 Results

Color fundus images and infrared cSLO images captured from cats at various disease stages showed an initial patchy tapetal hyporeflectivity as one of the earliest changes. With progression, they developed blood vessel attenuation and more obvious taptetal hyperreflectivity in the peripheral regions. With more advanced disease a hyporeflective band involving the *area centralis* and visual streak became more apparent (Figure 3.1).

The REC+ layer thickness of *rdAc* cats decreased over time in all regions (Figure 3.3 and 3.4). However, the central retina (*area centralis* and visual streak) showed a significantly slower rate of thinning of the REC+ layer than the combined mid-peripheral retinal regions (superior and inferior mid-peripheries) (p=0.00016). When broken down by region, the superior mid-periphery was found to have a significantly faster rate of thinning than the *area centralis* (p=$7.20e^{-5}$). Though the difference was not statistically significant (p=0.14), the slope indicating thinning of the inferior mid-periphery REC+ was also steeper than that of the central retinal regions. The rates of degeneration of the two central retinal regions, the *area centralis* and visual streak, were similar over the time period studied. (Figure 3.4)
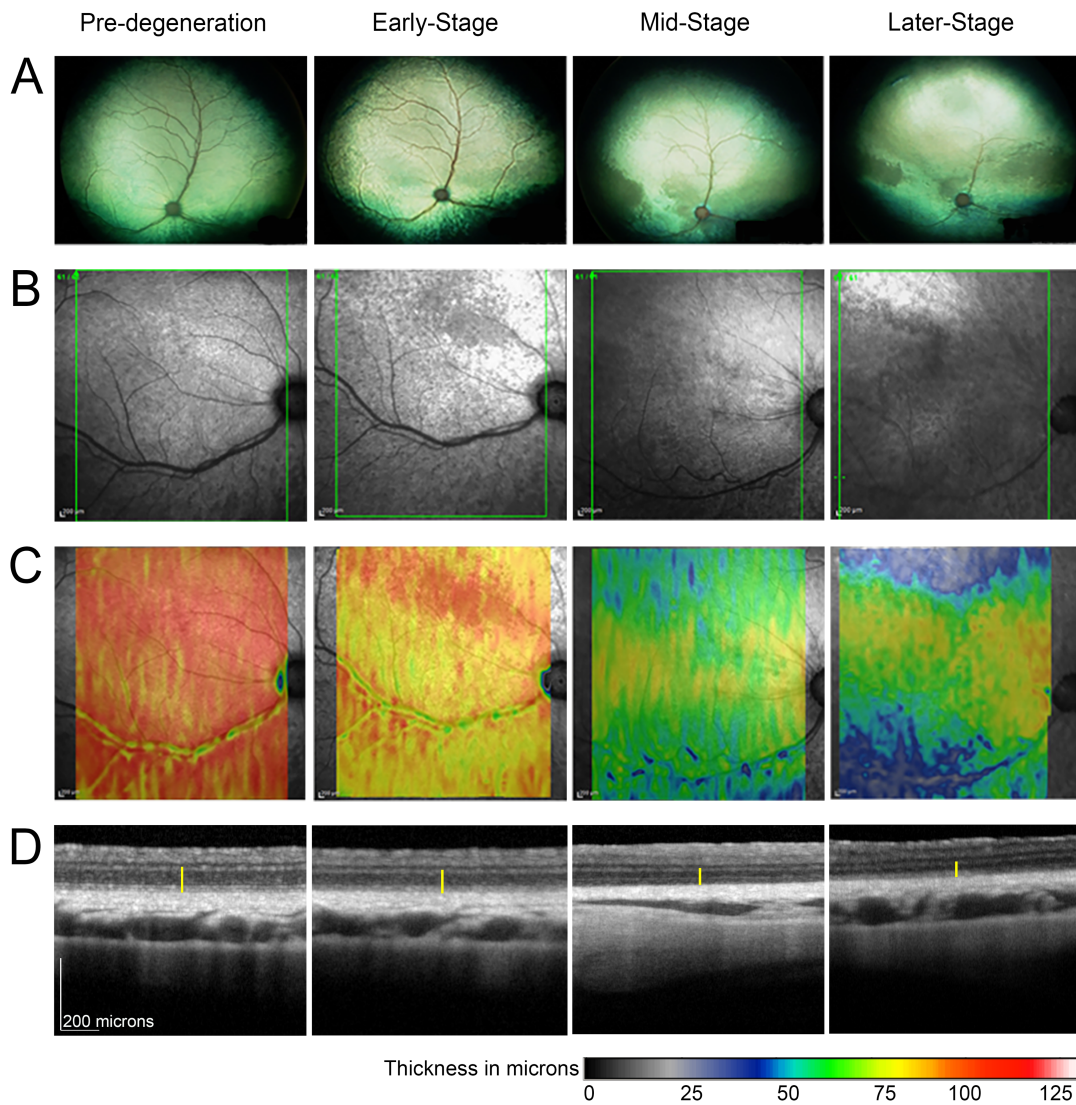
Figure 3.3: Preservation of the central retina. A. Wide-field color fundus images of the corresponding eyes and time-points (6 month-old pre-degeneration, 2 year-old early-stage, 6 year-old mid-stage, and 9 year-old later-stage) in B, C, and D, taken from four different cats. Patchy tapetal reflectivity changes in earlier stages of disease progress to hyporeflectivity in the central retina (extending across the *area centralis* and visual streak) and hyperreflectivity in the peripheral fundus, with eventual hyperreflectivity of the central fundus as well in late stages of disease. Progressive blood vessel attenuation, a hallmark of progressive retinal atrophy, can also be seen. B. cSLO images corresponding to the heat maps in C without color overlay. The changes in reflectivity noted in A are also apparent here. C. Heat maps derived from the REC+ layer thickness show that despite pan retinal degeneration there is preservation of REC+ thickness in the central retina even in later stages of disease. D. Representative cross-sectional images taken from the *area centralis* show REC+ layer thinning over time but with remaining measurable REC+ in this area even in later stages of disease. Yellow vertical lines indicate the REC+ layer and illustrate progressive thinning, from 108 microns at the earliest stage, down to 103 microns, then 74 microns, and finally 67 microns in subsequent stages in these examples.

A: Rate of Degeneration in the Central versus Mid-Peripheral Retina

Central retina (AV,VS): m=-3.69, R²=0.93
Peripheral retina (SP, IP): m=-6.14, R²=0.94

B: Rate of Degeneration Across all Regions

AC: m=-4.14, R²=0.78
VS: m=-3.24, R²=0.91
SP: m=-7.12, R²=0.96
IP: m=-5.17, R²=0.87

*** = p< 0.0005

C

Area Centralis REC+ Thickness

Visual Streak REC+ Thickness

Superior Periphery REC+ Thickness

Inferior Periphery REC+ Thickness

Figure 3.4: Regional rates of degeneration. A. The central retina (combined *area centralis* and visual streak) degenerates at a slower rate than the mid-peripheral retina (combined superior and inferior mid-peripheries). B. There is no difference in the rate of degeneration between the *area centralis* and visual streak, however, the superior and inferior mid-peripheries degenerate at faster rates than the *area centralis* based on slope, with a significant difference in rate of degeneration between the *area centralis* and superior mid-periphery. C. The range of data is shown for the *area centralis*, visual streak, superior periphery, and inferior periphery REC+ thickness data sets.

113

The EZ could be clearly seen on cross sectional images in young cats with early stages of disease (Figure 3.5A). With progression, patchy loss of integrity became apparent in some retinal regions. This patchy loss in integrity was first apparent in the mid-peripheral retina while in the central retina the EZ remained clearly discernible. Once cats reached a later stage of disease characterized by more significant pan retinal thinning, there was severe to complete loss of EZ integrity in the mid-peripheral retina, however, even at this late stage of disease the integrity of the EZ was readily visualized within the central region (Figure 3.5B). This area of retained EZ integrity closely corresponded to the region of preserved REC+ thickness as illustrated by superimposition of the extent of the EZ integrity on the REC+ thickness heat map (Figure 3.6).
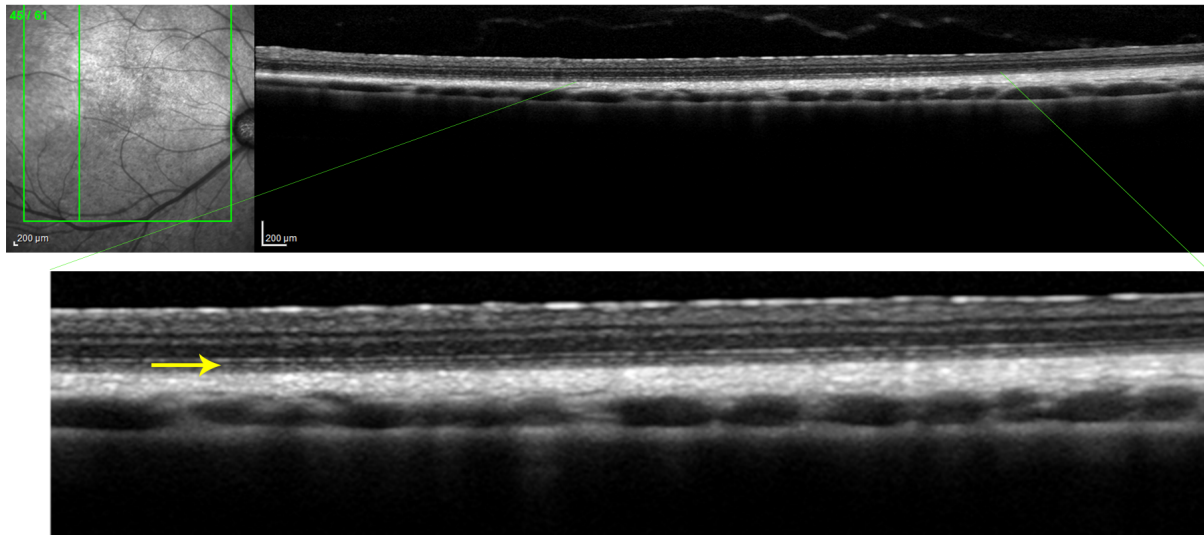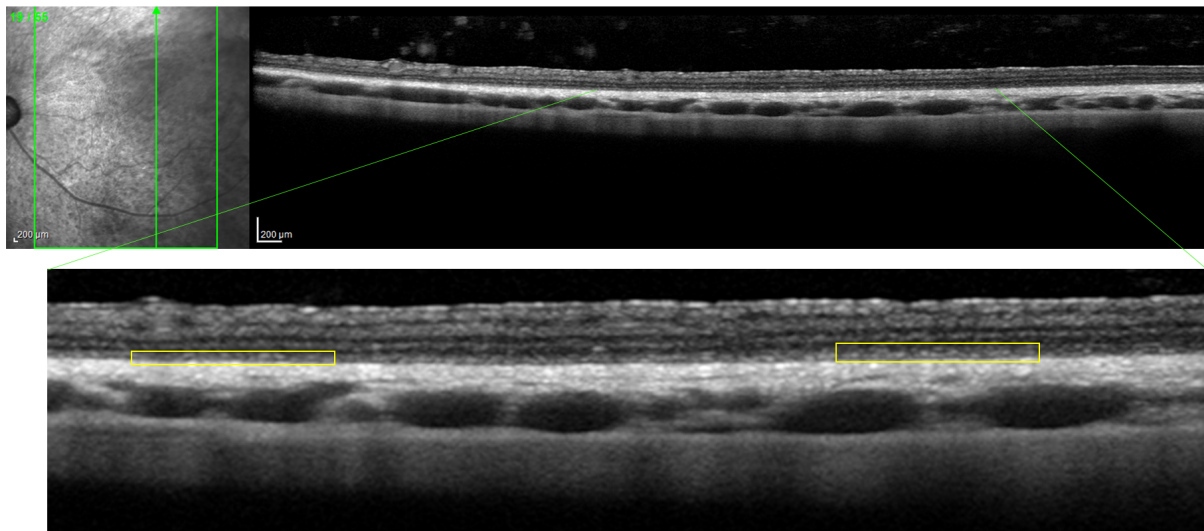
Figure 3.5: Ellipsoid zone integrity deteriorates with progressive stages of disease. A. In early stages of disease the ellipsoid zone (EZ) can be visualized and followed across all sections, showing well preserved integrity across the entire length of the example scan (yellow arrow). B. In later stages of disease, patchy or complete loss of EZ integrity is apparent in the peripheral retina (towards the left of the image with the left yellow box indicating a region of EZ loss) . However, the EZ was visible in the central retina even in this later stage of disease despite pan retinal thinning (right of the image with the right yellow box indicating a region of EZ preservation).
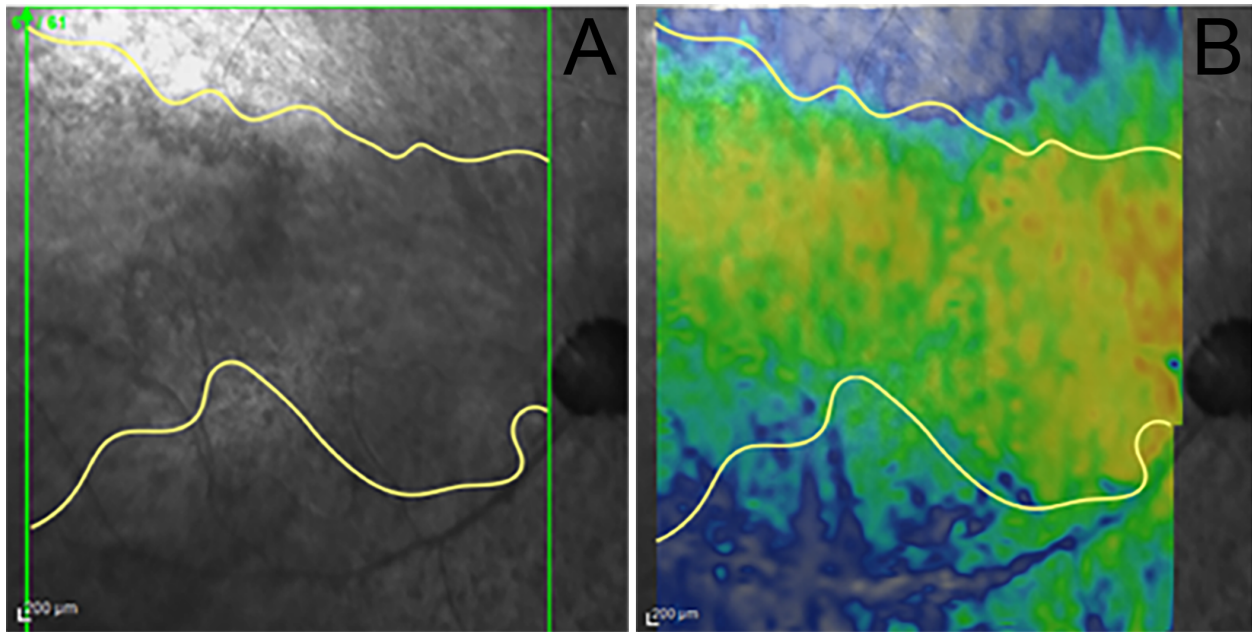
Figure 3.6: Preserved ellipsoid zone integrity corresponds to preserved central REC+ thickness. A. When the region of continuous ellipsoid zone (EZ) integrity is mapped across the fundus of a 9 year-old late-stage cat, central maintenance is apparent. B. This region corresponds closely with the region of REC+ thickness preservation, suggesting that preservation of EZ integrity can be used as a marker of regions of preserved photoreceptor cells.

3.5 Discussion

Measurement of the thickness of the REC+ layer and construction of heat maps of the REC+ clearly demonstrate that in the *rdAc* cat with advancing disease this layer remains notably thicker in the *area centralis* and visual streak than in the more peripheral retinal regions. This is in keeping with previous descriptions of the phenotype and confirms the clinical impression from indirect ophthalmoscopy and wide-angle color fundus photography where the difference in tapetal reflectivity between the central and peripheral tapetal fundus suggests central retinal preservation.(6, 30) The central retina in normal cats is thicker than the more peripheral retina so it is conceivable that the apparent preservation of REC+ thickness simply reflects that the region had a greater number of starting photoreceptors and that the rate of thinning was not different from the more peripheral retina. However, plotting the REC+ thickness against age shows that in fact the rate of thinning in the central retina is significantly slower than that in the combined mid-peripheral retinal regions. When the rate of REC+ thinning of the four regions that were measured are examined separately the superior mid-peripheral retina shows the greatest rate of thinning and is significantly different to that in the area *centralis* or visual streak. However, the rate of thinning in the inferior mid-peripheral region was not significantly different to that of the central retinal regions. Study of larger numbers of animals would be required to be sure that this latter finding was not a type II statistical error. The central retinal preservation in the *rdAc* cat mirrors the finding in people with LCA due to *CEP290* mutations thus supporting the cat as a model for this devastating disease.

The relative preservation of the *area centralis* and visual streak may be because these regions have a higher cone density than the more peripheral retina and cones degenerate at a slower rate than rods in *CEP290* retinopathies.(51, 52) An investigation of the relative rod and cone numbers over time in the area of preservation would be required to see if there were larger numbers of surviving cones than rods and that another factor such as a protective effect of having a higher number of photoreceptors was not playing a role in the slower rate of degeneration in this region. Furthermore, given the innate difference in photoreceptor density between the central retina and regions outside of the central retina, proper identification of the central retina as well as accurate alignment of scans from one session to the next is important to ensure accurate longitudinal evaluation. Utilizing retinal vasculature to orient the investigator to the central retina and then utilizing the OCT software's ability to align scans across sessions for example, are therefore important study design components to consider.

This study also showed that the EZ is preserved in the central retina until late stages of disease, corresponding to the region of REC+ preservation. In human patients the preserved continuity of the EZ correlates with remaining visual function.(42-44) In human patients with established retinal degeneration therapeutic interventions such as gene augmentation therapy must target remaining photoreceptors that can still be rescued. Retinal imaging (such as SD-OCT) to identify the location of such photoreceptors is important.(53) Large animal models that have similar changes detectable by SD-OCT afford the opportunity to evaluate the safety and efficacy of such therapies in a retina with established disease. This will more closely reflect the situation in clinical patients

rather than treating young animals where there has been little or no loss of photoreceptors.

These parameters, differences in rate of degeneration of the REC+ layer and EZ integrity changes, may be valuable in pre-clinical studies as markers of disease progression and/or treatment success. It is important to note however that inter-observer and inter-session reproducibility should be considered. In this study a single investigator conducted all measurements to eliminate the possible effects of inter-observer differences and maximize reproducibility. For maximum utility of these parameters in future studies we suggest similar efforts to ensure consistency across measurements. Moreover, in longer-term studies in which study cats age significantly throughout the course of the study, age-related retinal changes should also be considered as a possible confounding factor. If the study length is extensive enough that normal age-related changes may be present, we suggest that measurements also be taken in wild-type cats such that changes in mutant cats can be normalized to wild-type changes.

In conclusion, we have further defined the central retinal preservation in the *rdAc* cat, which shows a similar pattern of degeneration to that reported in the literature in human LCA[CEP290] patients. Furthermore, we show that integrity of the EZ is maintained in the better preserved retinal regions providing the opportunity to use this as a marker of photoreceptor morphological preservation. This further supports the cat as a useful large animal model for studies of retinal dystrophy including future translational studies investigating potential therapies.

3.6 Acknowledgements

REFERENCES

REFERENCES

1.   Menotti-Raymond M, David VA, Schaffer AA, Stephens R, Wells D, Kumar-Singh R, et al. Mutation in CEP290 discovered for cat model of human retinal degeneration. J Hered. 2007;98(3):211-20.

2.   Narfstrom K, David V, Jarret O, Beatty J, Barrs V, Wilkie D, et al. Retinal degeneration in the Abyssinian and Somali cat (rdAc): correlation between genotype and phenotype and rdAc allele frequency in two continents. Vet Ophthalmol. 2009;12(5):285-91.

3.   Menotti-Raymond M, David VA, Pflueger S, Roelke ME, Kehler J, O'Brien SJ, et al. Widespread retinal degenerative disease mutation (rdAc) discovered among a large number of popular cat breeds. Vet J. 2010;186(1):32-8.

4.   Narfstrom K. Hereditary progressive retinal atrophy in the Abyssinian cat. J Hered. 1983;74(4):273-6.

5.   Narfstrom LK, Nilsson SE. Progressive retinal atrophy in the Abyssinian cat: an update. Vet Rec. 1983;112(22):525-6.

6.   Narfstrom K. Progressive retinal atrophy in the Abyssinian cat. Clinical characteristics. Invest Ophthalmol Vis Sci. 1985;26(2):193-200.

7.   Narfstrom K, Nilsson SE. Hereditary rod-cone degeneration in a strain of Abyssinian cats. Prog Clin Biol Res. 1987;247:349-68.

8.   Kang Derwent JJ, Padnick-Silver L, McRipley M, Giuliano E, Linsenmeier RA, Narfstrom K. The electroretinogram components in Abyssinian cats with hereditary retinal degeneration. Invest Ophthalmol Vis Sci. 2006;47(8):3673-82.

9.   Valente EM, Silhavy JL, Brancati F, Barrano G, Krishnaswami SR, Castori M, et al. Mutations in CEP290, which encodes a centrosomal protein, cause pleiotropic forms of Joubert syndrome. Nat Genet. 2006;38(6):623-5.

10.   Baala L, Audollent S, Martinovic J, Ozilou C, Babron MC, Sivanandamoorthy S, et al. Pleiotropic effects of CEP290 (NPHP6) mutations extend to Meckel syndrome. American journal of human genetics. 2007;81(1):170-9.

11.   Brancati F, Barrano G, Silhavy JL, Marsh SE, Travaglini L, Bielas SL, et al. CEP290 mutations are frequently identified in the oculo-renal form of Joubert syndrome-related disorders. American journal of human genetics. 2007;81(1):104-13.

12.   Helou J, Otto EA, Attanasio M, Allen SJ, Parisi MA, Glass I, et al. Mutation analysis of NPHP6/CEP290 in patients with Joubert syndrome and Senior-Loken syndrome. J Med Genet. 2007;44(10):657-63.

13.   Frank V, den Hollander AI, Bruchle NO, Zonneveld MN, Nurnberg G, Becker C, et al. Mutations of the CEP290 gene encoding a centrosomal protein cause Meckel-Gruber syndrome. Hum Mutat. 2008;29(1):45-52.

14.   Travaglini L, Brancati F, Attie-Bitach T, Audollent S, Bertini E, Kaplan J, et al. Expanding CEP290 mutational spectrum in ciliopathies. Am J Med Genet A. 2009;149A(10):2173-80.

15.   Ghaffari SR, Rafati M, Ghaffari G, Morra M, Tekin M. Familial intellectual disability in an Iranian family with a novel truncating mutation in CEP290. Clin Genet. 2014;86(4):387-90.

16.   Wang L, Yang Y, Song J, Mao L, Wei X, Sun Y, et al. Two novel mutations in the C-terminal region of centrosomal protein 290 (CEP290) result in classic Joubert syndrome. J Child Neurol. 2015;30(6):772-6.

17.   Cideciyan AV, Aleman TS, Jacobson SG, Khanna H, Sumaroka A, Aguirre GK, et al. Centrosomal-ciliary gene CEP290/NPHP6 mutations result in blindness with unexpected sparing of photoreceptors and visual brain: implications for therapy of Leber congenital amaurosis. Hum Mutat. 2007;28(11):1074-83.

18.   Coppieters F, Lefever S, Leroy BP, De Baere E. CEP290, a gene with many faces: mutation overview and presentation of CEP290base. Hum Mutat. 2010;31(10): 1097-108.

19.   Littink KW, Pott JW, Collin RW, Kroes HY, Verheij JB, Blokland EA, et al. A novel nonsense mutation in CEP290 induces exon skipping and leads to a relatively mild retinal phenotype. Invest Ophthalmol Vis Sci. 2010;51(7):3646-52.

20.   Perrault I, Delphin N, Hanein S, Gerber S, Dufier JL, Roche O, et al. Spectrum of NPHP6/CEP290 mutations in Leber congenital amaurosis and delineation of the associated phenotype. Hum Mutat. 2007;28(4):416.

21.   den Hollander AI, Koenekoop RK, Yzer S, Lopez I, Arends ML, Voesenek KE, et al. Mutations in the CEP290 (NPHP6) gene are a frequent cause of Leber congenital amaurosis. American journal of human genetics. 2006;79(3):556-61.

22.   Narfstrom KL, Nilsson SE, Andersson BE. Progressive retinal atrophy in the Abyssinian cat: studies of the DC-recorded electroretinogram and the standing potential of the eye. Br J Ophthalmol. 1985;69(8):618-23.

23.   Narfstrom K, Nilsson SE. Hereditary retinal degeneration in the Abyssinian cat: correlation of ophthalmoscopic and electroretinographic findings. Doc Ophthalmol. 1985;60(2):183-7.

24.   Narfstrom K, Nilsson SE. Progressive retinal atrophy in the Abyssinian cat. Electron microscopy. Invest Ophthalmol Vis Sci. 1986;27(11):1569-76.

25.   Narfstrom K, Wilen M, Andersson BE. Hereditary retinal degeneration in the Abyssinian cat: developmental studies using clinical electroretinography. Doc Ophthalmol. 1988;69(2):111-8.

26.   Jacobson SG, Kemp CM, Narfstrom K, Nilsson SE. Rhodopsin levels and rod-mediated function in Abyssinian cats with hereditary retinal degeneration. Exp Eye Res. 1989;49(5):843-52.

27.   Narfstrom K, Arden GB, Nilsson SE. Retinal sensitivity in hereditary retinal degeneration in Abyssinian cats: electrophysiological similarities between man and cat. Br J Ophthalmol. 1989;73(7):516-21.

28.   Ehinger B, Narfstrom K, Nilsson SE, van Veen T. Photoreceptor degeneration and loss of immunoreactive GABA in the Abyssinian cat retina. Exp Eye Res. 1991;52(1):17-25.

29.   Ekesten B, Narfstrom K. Cone positive off-response in normal and dystrophic cats. Doc Ophthalmol. 1998;97(1):9-21.

30.   Seeliger MW, Narfstrom K. Functional assessment of the regional distribution of disease in a cat model of hereditary retinal degeneration. Invest Ophthalmol Vis Sci. 2000;41(7):1998-2005.

31.   Narfstrom K, Ehinger B, Bruun A. Immunohistochemical studies of cone photoreceptors and cells of the inner retina in feline rod-cone degeneration. Vet Ophthalmol. 2001;4(2):141-5.

32.   Nilsson SF, Maepea O, Alm A, Narfstrom K. Ocular blood flow and retinal metabolism in abyssinian cats with hereditary retinal degeneration. Invest Ophthalmol Vis Sci. 2001;42(5):1038-44.

33.   Ekesten B, Narfstrom K. Abnormal dark-adapted ERG in cats heterozygous for a recessively inherited rod-cone degeneration. Vet Ophthalmol. 2004;7(1):63-7.

34.   Vaegan, Narfstrom K. Optimal discrimination of an Abyssinian cat recessive retinal degeneration: a short electroretinogram protocol is more efficient than a long one. Clin Exp Ophthalmol. 2004;32(6):619-25.

35.   Hyman JA, Vaegan, Lei B, Narfstrom KL. Electrophysiologic differentiation of homozygous and heterozygous Abyssinian-crossbred cats with late-onset hereditary retinal degeneration. Am J Vet Res. 2005;66(11):1914-21.

36.   May CA, Lutjen-Drecoll E, Narfstrom K. Morphological changes in the anterior segment of the Abyssinian cat eye with hereditary rod-cone degeneration. Curr Eye Res. 2005;30(10):855-62.

37.   Vaegan, Narfstrom K. A(max) is the best a-wave measure for classifying Abyssinian cat rod/cone dystrophy. Doc Ophthalmol. 2005;111(1):33-8.

38.   May CA, Narfstrom K. Choroidal microcirculation in Abyssinian cats with hereditary rod-cone degeneration. Exp Eye Res. 2008;86(3):537-40.

39.   Vaegan, Narfstrom K. Amax to scotopic Imax diagnoses feline hereditary rod cone degeneration more efficiently than any other combination of long protocol electroretinogram parameters. Doc Ophthalmol. 2008;117(1):1-12.

40.   May CA, Narfstrom K. Retinal capillary morphology in the Abyssinian cat with hereditary retinal degeneration. Exp Eye Res. 2012;99:45-7.

41.   Banaee T. Re: Staurenghi et al.: Proposed lexicon for anatomic landmarks in normal posterior segment spectral-domain optical coherence tomography: the IN*OCT consensus (Ophthalmology 2014;121:1572-8). Ophthalmology. 2015;122(7):e40.

42.   Hood DC, Zhang X, Ramachandran R, Talamini CL, Raza A, Greenberg JP, et al. The inner segment/outer segment border seen on optical coherence tomography is less intense in patients with diminished cone function. Invest Ophthalmol Vis Sci. 2011;52(13):9703-9.

43.   Wu Z, Ayton LN, Guymer RH, Luu CD. Relationship between the second reflective band on optical coherence tomography and multifocal electroretinography in age-related macular degeneration. Invest Ophthalmol Vis Sci. 2013;54(4):2800-6.

44.   Wu Z, Ayton LN, Guymer RH, Luu CD. Second reflective band intensity in age-related macular degeneration. Ophthalmology. 2013;120(6):1307-8 e1.

45.   Spaide RF, Curcio CA. Anatomical correlates to the bands seen in the outer retina by optical coherence tomography: literature review and model. Retina. 2011;31(8):1609-19.

46.   Fischer MD, Fleischhauer JC, Gillies MC, Sutter FK, Helbig H, Barthelmes D. A new method to monitor visual field defects caused by photoreceptor degeneration by quantitative optical coherence tomography. Invest Ophthalmol Vis Sci. 2008;49(8):3617-21.

47.   Birch DG, Locke KG, Wen Y, Locke KI, Hoffman DR, Hood DC. Spectral-domain optical coherence tomography measures of outer segment layer progression in patients with X-linked retinitis pigmentosa. JAMA Ophthalmol. 2013;131(9):1143-50.

48.   Mathew R, Richardson M, Sivaprasad S. Predictive value of spectral-domain optical coherence tomography features in assessment of visual prognosis in eyes with neovascular age-related macular degeneration treated with ranibizumab. Am J Ophthalmol. 2013;155(4):720-6, 6 e1.

49.   Sujirakul T, Lin MK, Duong J, Wei Y, Lopez-Pintado S, Tsang SH. Multimodal Imaging of Central Retinal Disease Progression in a 2-Year Mean Follow-up of Retinitis Pigmentosa. Am J Ophthalmol. 2015;160(4):786-98 e4.

50.   Jacobson SG, Aleman TS, Cideciyan AV, Sumaroka A, Schwartz SB, Windsor EA, et al. Identifying photoreceptors in blind eyes caused by RPE65 mutations: Prerequisite for human gene therapy success. Proc Natl Acad Sci U S A. 2005;102(17): 6177-82.

51.   Pasadhika S, Fishman GA, Stone EM, Lindeman M, Zelkha R, Lopez I, et al. Differential macular morphology in patients with RPE65-, CEP290-, GUCY2D-, and AIPL1-related Leber congenital amaurosis. Invest Ophthalmol Vis Sci. 2010;51(5):2608-14.

52.   Cideciyan AV, Rachel RA, Aleman TS, Swider M, Schwartz SB, Sumaroka A, et al. Cone photoreceptors are the main targets for gene therapy of NPHP5 (IQCB1) or NPHP6 (CEP290) blindness: generation of an all-cone Nphp6 hypomorph mouse that mimics the human retinal ciliopathy. Human molecular genetics. 2011;20(7):1411-23.

53.   Jacobson SG, Aleman TS, Cideciyan AV, Sumaroka A, Schwartz SB, Windsor EA, et al. Identifying photoreceptors in blind eyes caused by RPE65 mutations: Prerequisite for human gene therapy success. ProcNatlAcadSciUSA. 2005;102(17):6177-82.

CHAPTER 4

EVALUATION OF A CRISPR-CAS9 NUCLEASE GENOME EDITING TREATMENT AGAINST THE FELINE *CEP290* MUTATION USING A NEWLY DEVELOPED *IN VITRO* TOOL

Author Contributions

Conceived and designed the experiments: Andrea L. Minella (ALM), Marie-Claude Senut (M-CS), Steve Suhr (SS), Simon M. Petersen-Jones (SMP-J) . Performed the experiments: ALM, M-CS, SS. Analyzed the data: ALM, SS. Wrote the chapter: ALM, SS, SMP-J.

4.1. Introduction

The *CEP290* gene encodes a ciliary protein that localizes to the interconnecting cilium of rod and cone photoreceptors and is integral for proper transport between the inner and outer segments.(1) The large size of this gene precludes packaging of the transcript into the gene therapy vector of choice for retinal therapies, the adeno-associated viral (AAV) vector. Other vector types that could accommodate larger payloads have shown poor retinal transduction, making gene therapy based treatments for *CEP290* retinopathies challenging. Alternatively, genome editing techniques that could allow direct "repair" of the *CEP290* gene show promise while circumventing the size limitations of AAV packaging.

A method of genome editing, the Clustered Regularly Interspersed Short Palindromic Repeats (CRISPR) Cas9 nuclease system has been shown to be able to correct defects in human cell lines and provides a more easily engineered, scalable, and affordable method of genome manipulation. The CRISPR system is a component of bacterial-immunity that has been repurposed as a promising genome editing tool. This method of editing is an appealing option for LCA treatments, including LCA*CEP290*. Before such treatments can reach human clinical trials, however, extensive *in vitro* and animal model testing is necessary for proof-of-principle and safety assurance.(2)

A spontaneous *CEP290* mutation in cats causes a retinal degeneration that has been well characterized and shows promise as a model for LCA*CEP290*.(3-6) This mutation is an intronic T>G substitution that allows for the usage of a GT downstream of the wild-type splice donor site of Exon 50 to be used as a new donor site (Figure 4.1).

This results in a four base-pair insert in the transcript, a frameshift, and a premature stop codon.(7) This leads to a slow autosomal recessively-inherited retinal degeneration. All human *CEP290* phenotypes are recessively inherited, including *null* mutations, indicating that 50% of normal transcript levels will rescue the phenotype (https://cep290base.cmgg.be). This suggests that for phenotype rescue, a treatment that results in cellular wild-type transcript levels of 50%, and potentially less, should be successful.
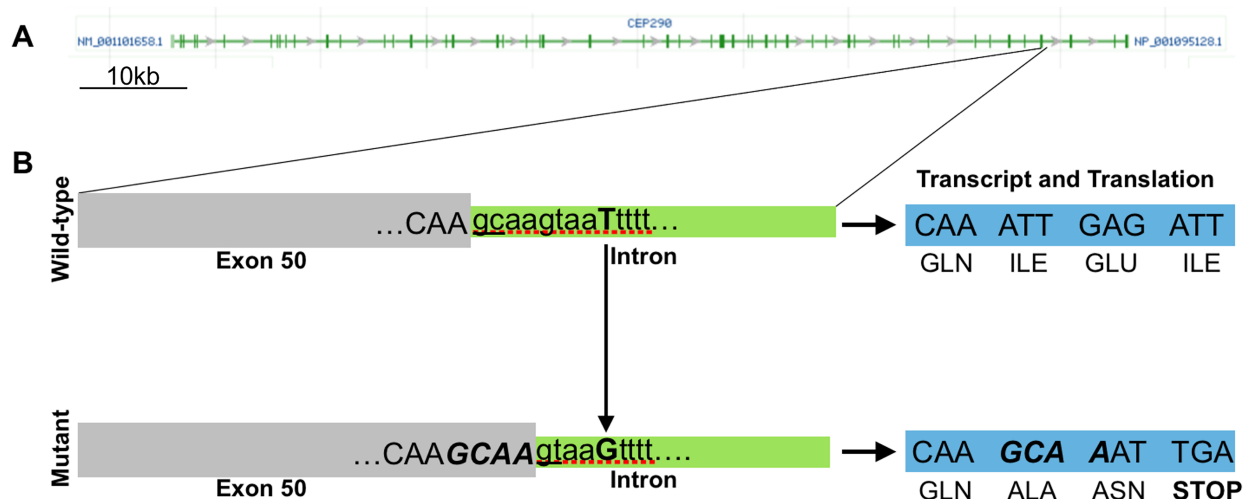
Figure 4.1: The feline *CEP290* mutation. A. The feline *CEP290* gene (NCBI) showing the large gene size and exon number. B. Magnified view of exon 50 and the following intron in the wild-type and mutant alleles. A single base-pair T > G substitution (vertical arrow) in the mutant allele makes the upstream GT (underlined) a stronger splice donor site, altering splicing such that a 4 base-pair insert is incorporated into the transcript (bold italics). this results in a frameshift and premature stop codon.

The cat offers a unique and useful model for studying retinopathies given the large eye size and ocular anatomy that shares similarities to the human eye such as proportional components and a similar distribution of rods and cones with a central region semi-homologous to the human macula.(8) These advantages combined with the

CEP290 mutation make the *CEP290* mutant cat a valuable model for testing the safety and efficacy of *CEP290* based therapies.

The feline *CEP290* model could also be utilized for the development of an *in vitro* model for preliminary treatment testing of a variety of therapy modalities including genome editing therapies. This would allow for extensive testing of different treatment constructs before implementation in animal models, providing a valuable tool for reducing animal numbers and animal trial costs. A treatment could then be taken to the animal model once optimized in the cells. Although fibroblasts from human patients can be grown and used for *in vitro* testing of CRISPR-Cas9 therapy, the developed treatment would require animal testing before they could be used in clinical trials. Attempts at creating a rodent knock-in model containing the common human *CEP290* splice-altering mutation have shown differences in splicing in the mouse than in the human, limiting its usefulness as a model and reiterating the need for a naturally-occurring splice mutation model such as the cat.(9) We therefore aimed to develop an *in vitro* tool for this purpose by growing primary fibroblast cells from *CEP290* wild-type, mutant, and heterozygous carrier cats and to utilize this tool to test CRISPR-Cas 9 nuclease editing to remove the mutation in the mutant cells.

Given the localization and proposed function of the CEP290 protein within cilia, we further speculated that defects in *CEP290* could impact cilia formation. To test this possibility, we sought to induce ciliation in cultured cells and compare cilia length across genotypes to determine whether *CEP290* mutant cells would show altered ciliation which could then be used as an objective marker for treatment assessment. Furthermore, we reasoned that even if differences are not observed in cilia length

between experimental groups, induced ciliation in fibroblasts is a relatively well-established technique that could be exploited to better understand the function of *CEP290* and its role in the ciliation process in on-going studies and the development of future therapies for application to both animal and human LCA^{CEP290} patients.

4.2 Methods

4.2.1 Animals and tissue collection

Eighteen cats from a purpose-bred *CEP290* retinopathy breeding colony maintained at Michigan State University were utilized for this study, six from each genotype: *CEP290* wild-type, heterozygous carrier, and homozygous mutant. Cats were housed under 12:12hr lightdark cycles and were fed Purina Cat Chow (Nestlé Purina, Wilkes-Barre, PA) *ad libitum*. All animal practices were carried out in accordance with the Association for Research in Vision and Ophthalmology Statement for the Use of Animals in Ophthalmic and Vision Research and were approved by the Michigan State University Institutional Animal Care and Use Committee.

Skin biopsies were performed on each cat under general anesthesia. Anesthesia induction was performed with isoflurane (IsoFlo, Abbott Laboratories, North Chicago, IL, USA) delivered by mask or induction box. Cats were maintained in a light plane of anesthesia by flow-by isoflurane. A small area on the flank was shaved and cleaned thoroughly with alcohol. A sterile 4mm biopsy punch (Acuderm Inc., Ft. Lauderdale, FL, USA) was then used to remove a piece of skin, which was immediately placed into a vial of sterile Dulbecco's Modified Eagle Medium (DMEM, Thermo Fisher Scientific, Waltham, MA, USA) with 10% fetal bovine serum (FBS, Thermo Fisher Scientific) and 1% penicillin (Gibco, Grand Island, NY, USA) for culture. Hemostasis of the biopsy site was achieved by applying pressure with medical gauze when needed and a single simple interrupted suture was placed to close the defect. Cats were given a single

injection of meloxicam (0.3mg/kg dose, Boehringer Ingelheim Vetmedica Inc., St.

Joseph, MO, USA) to relieve pain or discomfort and then recovered from anesthesia.

4.2.2 Establishment of cultured cell lines

Skin samples were cultured to develop primary fibroblast cells as previously

described.(10) Briefly, samples were aseptically dissected in a cell culture hood into 6

small even pieces, each of which was placed in a single well of a 6-well cell-culture

plate containing DMEM media (Thermo Fisher Scientific). Cells were incubated under

standard cell culture conditions at 37C and 5% carbon dioxide and imaged on an

Olympus IX71 microscope (Olympus America Inc., Melville, NY, USA) daily to monitor

for adherence and growth. Cells were fed or passed every few days with the same

media. Once microscopic visualization showed outgrowth of cells with fibroblastic

morphology, immunocytochemistry (ICC) was performed to confirm cell type. (Table 4.1)

Antibody	Host	Target	Concentration and Use	Source
Primary Antibodies				
Anti vimentin	Chicken	Fibroblast marker	1:5000	Millipore, Billerica, MA, USA
Wide spectrum anti cytokeratin	Rabbit	Keratinocyte marker	1:100	Abcam, Cambridge, MA, USA
Anti acetylated alpha-tubulin	Mouse	Cilia marker	1:5000	Sigma Aldrich, St. Louis, MO, USA
Secondary Antibodies				
Goat anti-chicken alexa fluor 594	Goat	Chicken primary antibody	against vimentin	Abcam
Goat anti-rabbit IgG (H+L) Cross-Adsorbed Secondary Antibody, Alexa Fluor 488	Goat	Rabbit primary antibody	1:500, against cytokeratin	Thermo Fisher Scientific, Waltham, MA, USA
Goat anti-mouse IgG (H+L) Cross-Adsorbed Secondary Antibody, Alexa Fluor 489	Goat	Mouse primary antibody	1:500, against alpha-tubulin	Thermo Fisher Scientific
Nuclear counterstain				
DAPI (4',6-Diamidino-2-Phenylindole, Dihydrochloride)	NA	Nuclei	1:10,000	Thermo Fisher Scientific

Table 4.1: Antibodies used for immunocytochemistry.

ICC was performed as previously described.(11) Briefly, cells were fixed with methanol/acetone and stained for vimentin and cytokertatin overnight. Slides were incubated with secondary antibody for one hour, mounted, and then imaged on a Nikon Eclipse 80i microscope (Nikon instruments Inc., Melville, NY, USA) equipped with a CoolSnap ESv camera (Photometrics, Tuscon, AZ, USA). Cultured cells were examined for the marker proteins vimentin (indicative of fibroblasts) and cytokeratin, (inducative of keratinocytes) to confirm that they were fibroblasts. (Table 4.1)

4.2.3. Investigation of ciliation

Fibroblast cultures were induced to form cilia as previously reported.(10) Cells were serum starved for 24 hours by incubating in DMEM media with no FBS added to induce ciliation. ICC against acetylated alpha-tubulin (Table 4.1) was then performed based on an established protocol to confirm ciliation and collect images for cilia analysis.(11) Cells from each cat were stained in three separate ICC reactions and a fluorescent image was taken from each reaction for analysis on the same Nikon Eclipse 80i microscope. Images were randomized by an investigator not involved in this study. A different investigator, masked to the genotype of the cats from which the images were taken, then measured all cilia in each image. Cilia were measured as a function of pixels using ImageJ software (NIH, Bethesda, MD, USA) on all images. To do this, ImageJ pixels were calibrated to the pixel:micron ratio of the microscope used (above). Cilia were then manually measured by the investigator using the straight line tool to measure each cilia from end to end. Cilia measurements from the three images of ciliated cells for each cat were averaged and then measurements were compared

134

across genotypes. Data was tested for normality using the Shapiro-Wilk test and passed. A Student's two-tailed unpaired t-test was therefore performed with significance set at $p < 0.05$ and Bonferroni correction was applied to account for multiple comparisons. All statistical analysis and graphing was completed using SigmaPlot12 statistical software (Systat Software Inc., Chicago, IL, USA).

4.2.4 Targeting of the feline *CEP290* gene

Targeting of the feline *CEP290* gene defect entailed several steps: 1) determine if cultured feline primary fibroblasts were amenable to transduction, 2) determine the efficiency of this process, 3) confirm the sequence of the feline *CEP290* gene in DNA isolated from our mutant cat cells, 4) identify potential Cas9 recognition sites proximal to the mutated region, 5) design gRNAs recognizing these sites, 6) determine conditions for most efficient transduction of factors into cultured feline fibroblasts, 7) determine an optimal time for post-transduction recombination to occur, 8) test methods for detection of mutation events at the target locus, and 9) determination of the relative efficiency of targeting at different loci.

4.2.5 Transduction of primary feline fibroblasts

To determine the parameters for optimal transduction of mutant feline fibroblasts we transduced fibroblast lines derived from three different cats with varying amounts of capped-polyadenylated mRNA for eGFP (Trilink Biotech, San Diego, CA, USA) using the liposome-based transduction reagents Lipofectamine 2000 or Lipofectamine RNAiMAX (Invitrogen, Carlsbad, CA, USA) that had proven effective on primary canine

cells of similar origin previously used by our laboratory. Green fluorescence indicative of

production of the eGFP protein 16-48 hours post-transduction was used as an indicator

of relative efficiency. Both Lipofectamine reagents were determined to be approximately

equally efficient on the feline cells, but since short RNAs were to be the ultimate

payload, Lipofectamine RNAmax was selected as the reagent of choice (see Results).

4.2.6 Sequence of the feline *CEP290* gene in DNA from mutant cat cells

To confirm the sequence of the *CEP290* mutation in the cells derived from the

mutant cats, DNA was isolated from each line using the Promega Genomic DNA

isolation kit (Promega, Madison, WI, USA) following the manufacturer's protocol. 100 ng

of purified DNA from each line was amplified by PCR using two alternate sets of primers

(CEP2901F – 5'gtgcaatgacttgaactggc/CEP2901R – 5'gcaccgacagcagaagctcc or

CEP2902F – 5'gaagcagtgtaagatactg/CEP2902R – 5'ggaacagaggatctgaag) flanking the

putative mutation site. Amplification with Set 1 was predicted to return a 405 bp

fragment and amplification with Set 2 a 463 bp fragment. The Promega GoTaq Kit

(Promega) using enclosed default buffers and reaction conditions was used to produce

PCR products in an Applied Biosystems GenaAmp thermocycler (Applied Biosystems,

Foster City, CA, USA) using prolonged denaturation for 5min at 95oC, cycled for 40

cycles using 1 min. 95°C, 1 min. 55°C, 1 min 72°C, and polished with a 5 min.

incubation at 72°C. The amplified PCR products were visualized on a 3% agarose gel,

the band excised and purified using centrifugation through sterile nylon fiber, and the

flow through sent to the MSU RTSF core with either the 5' or 3' primer for sequence

analysis. The returned sequence confirmed that the sequence of the feline *CEP290* gene in our cultured lines matched the published sequence of the mutated allele.

4.2.7 Identification of Cas9 target sites

The CRISPR guide design engines maintained by MIT (http://crispr.mit.edu) and Harvard (https://crispr.med.harvard.edu/) were used to identify potential Cas9 binding sites within an approximately 250 bp region surrounding the mutation. More in depth scrutiny of these sites and comparison of their relative positions was performed using the Lasergene suite of programs on license from the Michigan State University Research Technology Support Facility genomics core.

Eleven sites were identified by the Harvard sgSCORER1.0 website that allowed off-target analysis using the cat FC5 genome (see Results). Of the 11 sites, two sites (referred to as Target 1 and 2) had relatively few off-targets that did not reside within coding or known control regions of transcribed genes and were proximal to the point mutation in the *CEP290* gene. These two gRNAs were selected for production of synthetic gRNAs for direct targeting by Cas9.

4.2.8 Production and testing of CRISPR reagents

Previous work in our laboratory using CRISPR/Cas9 to target genes in canine primary fibroblasts indicated that the Alt-R system available from IDT (Integrated DNA Technologies Inc., Coralville, Iowa, USA) displayed a high-efficiency of targeting in our hands, so this system that uses a synthetic gRNA, a separate tracerRNA, and purified Cas9 protein was utilized. One advantage of this system is that since no DNA

components are used, there is no possibility of incorporation of foreign DNA into target cells that could complicate future analysis. Target 1 (PAM underlined) (ACTTACTTGCTTGTTGCTCA<u>AGG</u>) and Target 2 (TTTCATCTCAAGCCACTTCT<u>TGG)</u> on either side of the mutation region were synthesized by IDT and received for testing. The RNAs and Cas9 protein were complexed in different ratios and amounts as described in the Results Section to determine functionality and efficiency. Cells from each of the three lines were transduced in wells of a 96-well plate with 40K cells/well and left for 1-7 days post-transduction until DNA harvest to determine efficiency.

4.2.9 Detection of CRISPR activity

To determine the efficiency of disruption at the individual target sites, PCR products produced using the flanking primer sets described above were subjected to two types of analysis: 1) digestion with restriction endonuclease, or 2) digestion with the ssDNA cutter T7 endonuclease. The disadvantage of using specific restriction endonucleases is that the restriction site must overlap the cut site of Cas9 within the target but has the advantage that any change in the recognition sequence will prevent digestion. T7 endonuclease, on the other hand is advantageous in that any mismatch of >1 base can potentially act as a cleavage site, however, single-base mismatches will not be detected. Target 1 had an Sml I site proximal to the predicted cut site and Target 2 had a Bsl I restriction site directly on top of the predicted cleavage position in TAR2. Targeting at both loci was determined by incubation of PCR products with the appropriate restriction enzyme or with T7endo following procedures outline by the enzyme manufacturer (New England BioLabs Inc., Ipswich, MA, USA). Digested PCR

products were examined on a 3% agarose gel and imaged using and EagleEye imaging system (BioRad, Hercules, CA, USA).

4.2.10 *CEP290* repair using single-stranded DNA (ssDNA)

A long single-stranded synthetic DNA oligonucleotide ("ultramer") was co-transfected along with the CRISPR reagents into feline fibroblasts. The success of recombination measured by the loss of regional restriction sites within the target region (as described above) and by the introduction of novel restriction sites within the newly integrated DNA. Design of the ssDNA ultramer was performed using the Lasergene suite licensed from the MSU RTSF Core along with the WatCut engine at the University of Waterloo (http://watcut.uwaterloo.ca/template.php). The sequence of the 154bp *CEP290* repair ultramer was

5'AGAGAGGGAGCAAAAGCTAAGAAATACACTGAAGACCTTGAGCAACAAGTAATT AATTTTATCAAATTAGAAAATAATGCATTTCATCTCGAGCCACTTCTTTGCATTATCTTA TGTATATAAAAATGAACTCTTGGGGCAACTGGGTGGCTC 3'. The optimal amount of Target2 gRNA, trRNA, and Cas9 protein were combined with different amounts of the ultramer oligonucleotide and co-transfected into recipient cells using both Lipofectamine 2000 and RNAiMAX reagents.

4.3 Results

4.3.1 Fibroblast production and ciliation

Primary cultures of fibroblast cells were successfully created from all 18 cats, with no more than two passages necessary to reach pure fibroblast culture, as confirmed by vimentin and cytokeratin staining (Figure 4.2 A). Cells from all 18 cats were also successfully ciliated via serum starvation, as confirmed by acetylated alpha-tubulin staining (Figure 4.2 B).
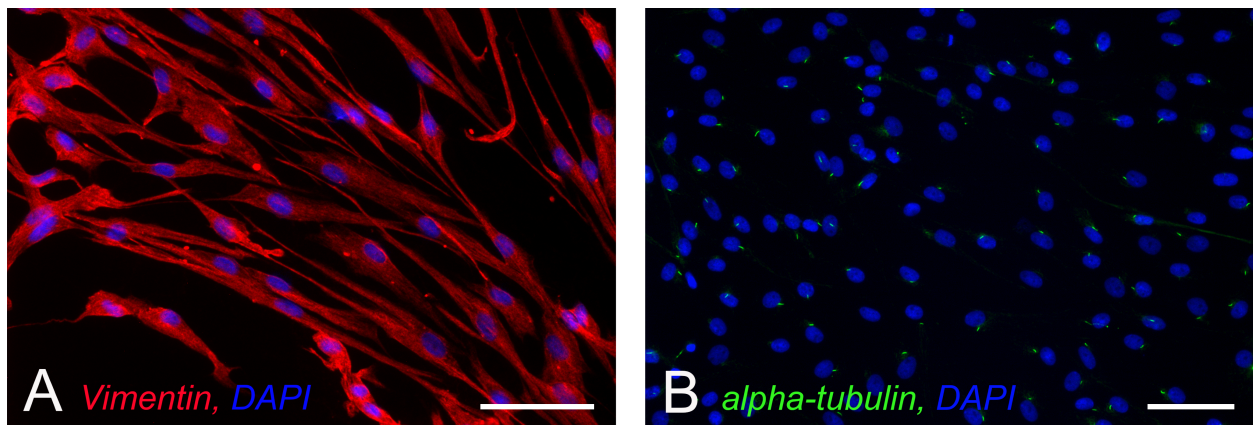
Figure 4.2: Representative ICC images show growth of pure fibroblast culture and successful induction of cilia growth. A. Positive vimentin staining supports the growth of fibroblast culture. B. Immunolabeling against acetylated alpha-tubulin shows the presence of cilia extending from cultured cells following serum starvation. Scale = 100 microns

4.3.2 Cilia analysis

There were no significant differences in cilia length across genotypes. Wild-type, heterozygous, and homozygous mutant cells grew cilia of nearly identical average lengths (3.8 +/- 0.36 SD microns, 3.7 +/- 0.46 SD microns, and 3.7 +/- 0.38 SD microns, respectively). (Figure 4.3)

Cilia Length by Genotype
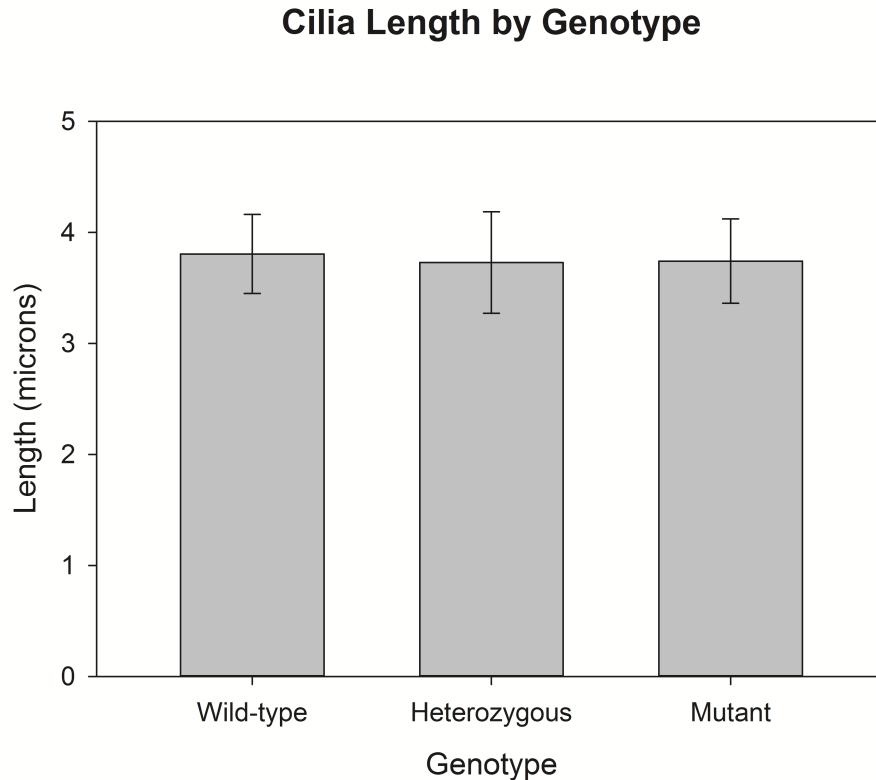
Figure 4.3: Cilia show no significant difference in length across genotypes. Cilia lengths were nearly identical across genotypes with wild-type cells having an average cilia length of 3.8 microns and heterozygous and homozygous mutant cells having average lengths of 3.7 microns each. Student's t-test showed no significant differences. Bars = standard deviation.

4.3.3 Targeting and repair of the feline *CEP290* gene using CRISPR/Cas9

4.3.3.1 Transduction of feline fibroblasts

Establishment of methods to induce changes at the feline *CEP290* mutation site started with testing methods of transduction. Fibroblasts from three mutant cat fibroblasts that displayed the best growth were used in transfection tests. An example of these lines transduced with 100ng of eGFP mRNA is shown in Figure 4.4.
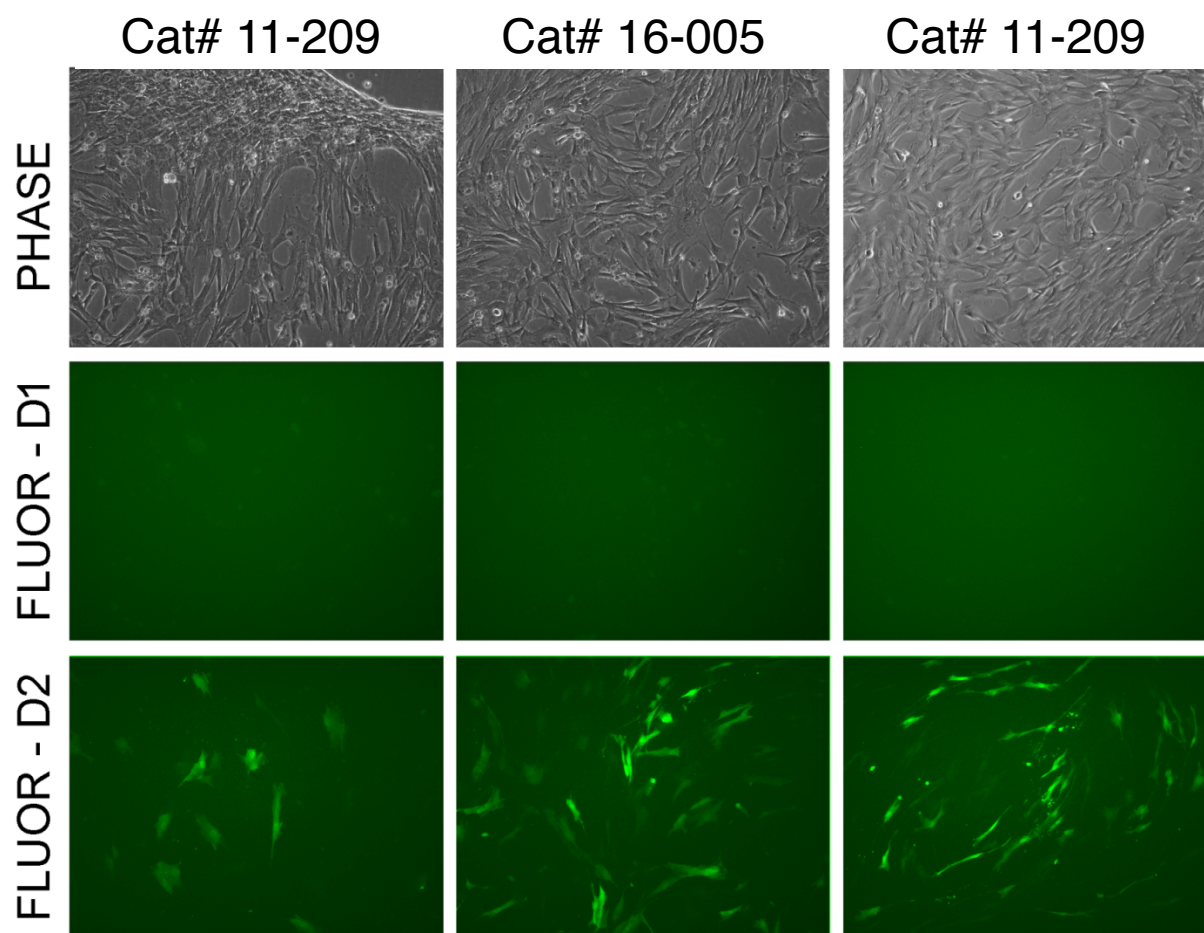
Figure 4.4: Example of transfection of three feline primary fibroblast lines with eGFP mRNA. Cells from three cats with good growth characteristics were used. Fluorescence indicative of eGFP expression from the transduced mRNA was imaged at 16 and 24 hour post-transfection, as labeled.

Transfection was scalable with more mRNA and Lipofectamine RNAiMax producing more intense fluorescence and more transduced cells (>50%). Expression of eGFP was found to peak 20-30 hours post-transduction, and although this does not necessarily mean that transduced CRISPR reagents would display maximum activity along the same time-course, based on these results, published reports in other animal systems, and our experiences with canine fibroblasts, we thought that 48-72 hours would likely be

sufficient time for targeting to be completed. Overall, these results gave us confidence that we could transduce a significant population of our feline fibroblasts.

4.3.3.2 The *CEP290* mutation and design of CRISPR reagents

Since efficient targeting of genomic loci with Cas9 is dependent on precise recognition of 23-base pair sequences, we decided to first confirm the sequence of the *CEP290* gene proximal to the reporter mutation in our cat cell lines. Using two primer sets flanking the putative location of the mutation, we amplified DNA fragments from genomic DNA of each cell line (Figure 4.5).
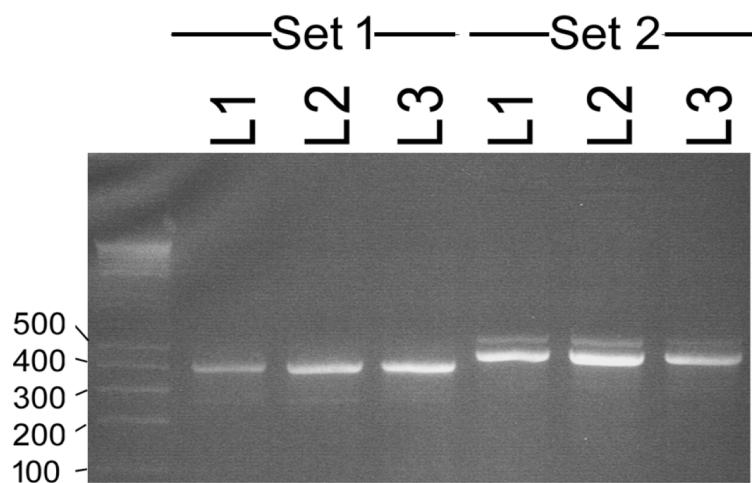
Figure 4.5: PCR products from genomic DNA amplified from three cat fibroblast lines. Sequences were amplified using Primer Sets 1 and 2 (as labeled) flanking the putative *CEP290* mutation region. Primer Sets 1 and 2 were predicted to produce bands of 405 and 463 base pairs, respectively. Relative to molecular weight markers, the PCR products appeared to match the predicted size. The bands in this gel were excised, purified, and sent for sequence analysis that revealed that they were a match for the published sequence (genome browser accession number: GCA_000181335.3).

The confirmed sequence was submitted to Cas9 target finder engines at MIT and Harvard for analysis. The Harvard engine provided analysis against the feline Fc5 genome and ultimately was used. Eleven targets were found and two were selected for their relatively low off-target prediction and the fact that no off-targets for these gRNAs were found to reside within protein coding regions except for *CEP290* (Figure 4.6A). TAR1 and TAR2 bracketed the region with the *CEP290* mutation with TAR1 slightly overlapping, and the TAR2 cleavage site roughly 40 bp downstream (Figure 4.6B). Both sites were within the distance limits suggested for insertion of single-stranded DNAs for replacement and repair. TAR1 and 2 gRNAs were produced and used in the CRISPR/ Cas9 Alt-R system from IDT as outlined in Methods.

A

TARGET ID	SeqID	Sequence	Rank	#ofHits in Feline FC5
	cep90_FASTA:7-29	TGAAACCAAGCTGAAAGAATTGG	35.1	9
	cep90_FASTA:78-100	TTGTAAAACAAGCAACAGAGAGG	90.3	16
TARGET 2	cep90_FASTA:176-198	TTTCATCTCAAGCCACTTCTTGG	18.6	9
	cep90_FASTA:209-231	TGTATATAAAAATGAACTCTTGG	19.1	30
	cep90_FASTA:210-232	GTATATAAAAATGAACTCTTGGG	61.8	25
	cep90_FASTA:211-233	TATATAAAAATGAACTCTTGGGG	73.8	36
	cep90_FASTA:12-34	AGTTTCCAATTCTTTCAGCTTGG	30.1	9
	cep90_FASTA:79-101	TGTAAAACAAGCAACAGAGAGGG	66.4	14
TARGET 1	cep90_FASTA:130-152	ACTTACTTGCTTGTTGCTCAAGG	15.8	7
	cep90_FASTA:188-210	CATAAGATAATGCCAAGAAGTGG	71.4	6
	cep90_FASTA:58-80	CAAGCTGTTTAAGATCAGTAAGG	82.1	2

B
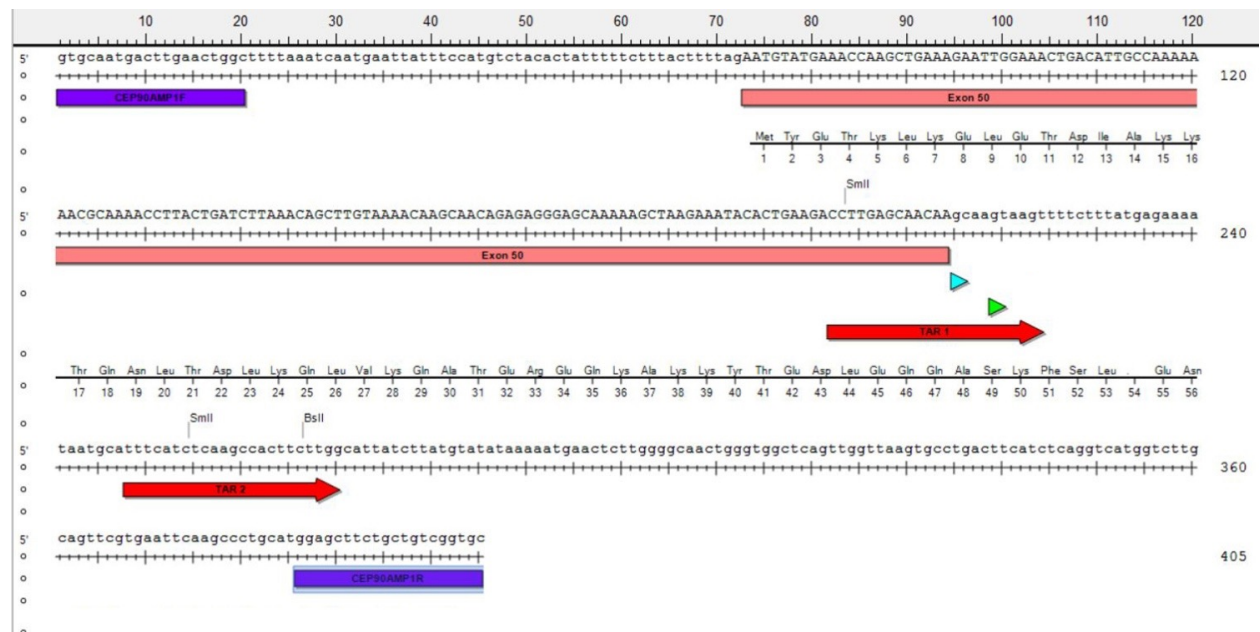
Figure 4.6: gRNA targets within the *CEP290* gene region surrounding Exon 50 and the mutation. A. Highlighted targets labeled 1 and 2 displayed relatively few off-targets using the sgSCORER 1.0 website. B. Location of TAR1 and TAR2 within the 405 bp PCR product amplified with primer Set 1. The amplification primers are shown in purple, Exon 50 in light red, and the two gRNAs in dark red, as labeled. The weak splice donor site (light blue) and stronger splice donor site created by the mutation (green), are shown at the end of Exon 50 between the two gRNA targets.

145

4.3.3.3. Transduction of primary cat fibroblasts with CRISPR reagents and assay of targeting

Previous work in our laboratory suggested that the Alt-R system worked best at concentrations ranging from 3-30nM gRNA. These three (3, 10, 30 nM) concentrations were tested on the most transfectable feline cell lines along with 100ng/well of eGFP gRNA to allow monitoring of transfection efficiency. As shown in Figure 4.7, we observed only slight toxicity in transduced wells compared to untransduced controls, and based on fluorescence, transduction efficiency in both lines exceeded approximately 80%. Cells were allowed to continue growth for 3-5 days post transduction and tested for modification of their genomic DNA.
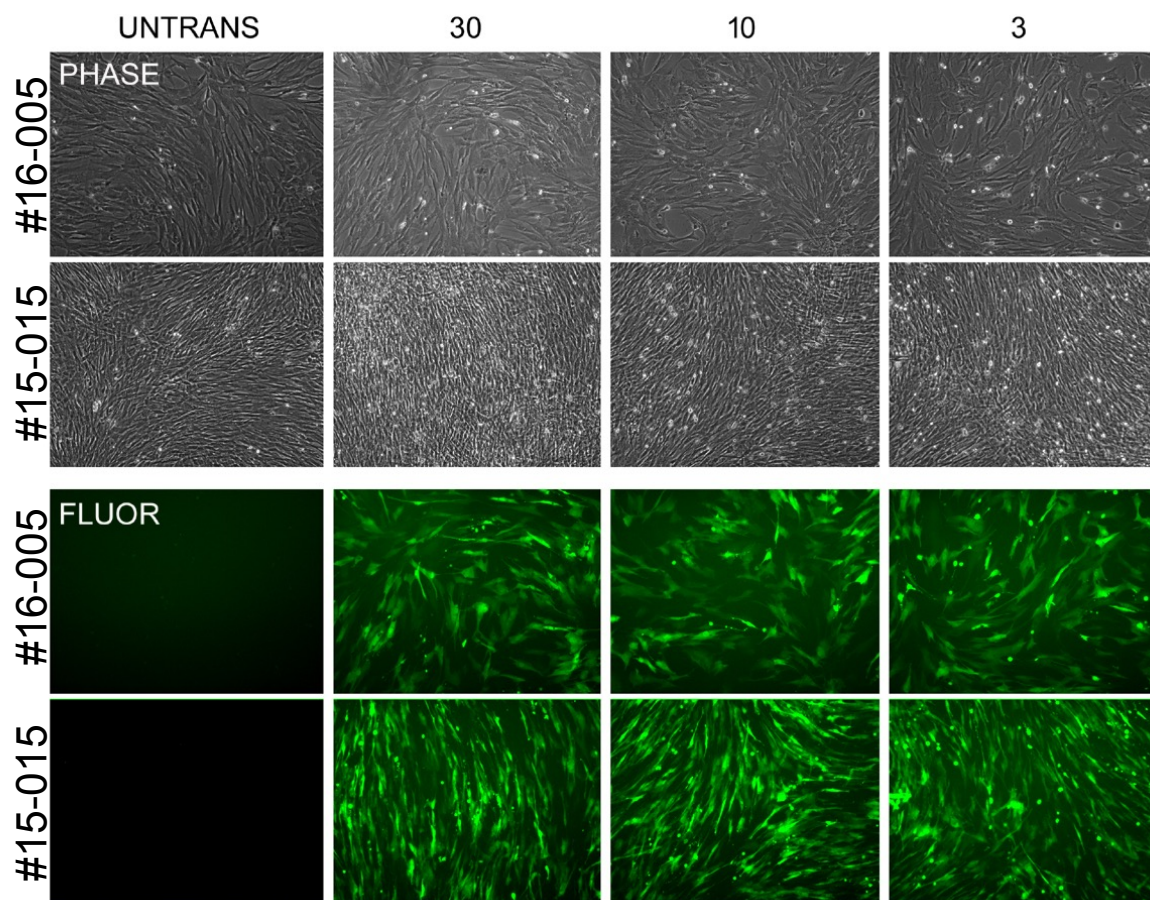
Figure 4.7: Example of transfection of primary cat fibroblasts with 30, 10, and 3 nM gRNA (as labeled) complexed with the trRNA and Cas9 protein. 100ng of eGFP RNA was included to allow visualization of transduced cells. Cellular toxicity as indicated by phase-bright rounded cells was slightly higher in transfected cells compared to un-transfected cell (far left) but did not appear to differ with changing concentration of CRISPR reagents. Transfection efficiency appeared high over-all (based on visible fluorescence, >80%), and increased slightly in wells receiving more reagent. Cells were imaged at 24-hours post transduction.

As described in Methods, two approaches were used to look for mutations in targeted DNA – T7 endonuclease digestion and restriction enzyme digestion. Figure 4.8 shows the results of digestion with these reagents on PCR fragments generated from each DNA sample using the primer sets shown in Figure 4.8. Figure 4.8A shows digestion of DNA from cat # 15-015 targeted with either TAR1 or TAR2 at the different

concentrations. Despite repeated attempts to generate a "clean" digest and image, the results invariably looked hazy and indistinct. Our interpretation was that there was some activity at the TAR2 locus as evidenced by fragments in the T7endo-digested lanes approximating the sizes (around 145bp and 270bp) predicted for digestion of the 405bp PCR fragment if disruption occurred at the TAR2 position. Bands corresponding to digestion at the TAR1 locus, however, were not observed. The haziness of the bands may suggest that digestion of TAR2 by Cas9 is quite variable, perhaps ranging from a single base indel (which would not digest with T7endo) to 2-10 base indels that would produce dozens of bands of various sizes. In short, this expriment suggested activity at TAR2 and much less at TAR1.

Further investigation of mutation at TAR1 was performed by Sml I digestion of the 405bp PCR product. As shown in Figure 4.8B, Sml I digestion, which is more complex given that there are multiple Sml I sites within the PCR fragment, was difficult to interpret, but showed no difference in cut pattern between DNAs targeted with the TAR1 gRNA or the TAR2 gRNA. Successful targeting by TAR1 should result in an increase in a 273bp band in TAR1 transduced cells, but we observed no difference regardless of which gRNA was used. Digestion under different conditions, different concentrations of agarose gel, and running the gels further did not produce any results indicating a difference between the use of either gRNA or no gRNA at all. This result coupled with the results of T7endo digestion, suggested to us that TAR1 gRNA activity was low.

Better results were obtained with TAR2 using digestion with the restriction endonuclease Bsl I. Bsl I cuts only at a single site in the PCR product, almost directly on top of the TAR2 Cas9 cleavage site, and creates bands of approximately 160 and 300

bp (using the 463 Primer Set 2 fragment). As shown in Fig. 4.8C distinct bands of this size are observed in the TAR1 transduced cells or cell transduced with no gRNA, but in cells transduced with the TAR2 gRNA, an undigested band corresponding to the uncut 460-bp band is observed. We estimate the relative ratio of uncut DNA:cut DNA to be approximately 50%. If 100% of cells were transduced, this suggests that essentially all cells have targeting of one *CEP290* allele. Since transduction was estimated at closer to 80%, this suggests that there is a population of 10-20% of total cells that likely have disruption of both alleles in the mutant *CEP290* gene. The same result was observed using either PCR primer set and was reproduced over several experiments. Curiously 3nM gRNA appeared slightly more efficient at targeting than higher amounts, so this amount was used in ongoing experiments aimed at inserting DNA correcting the splice donor mutation proximal to the *CEP290* TAR2 site.
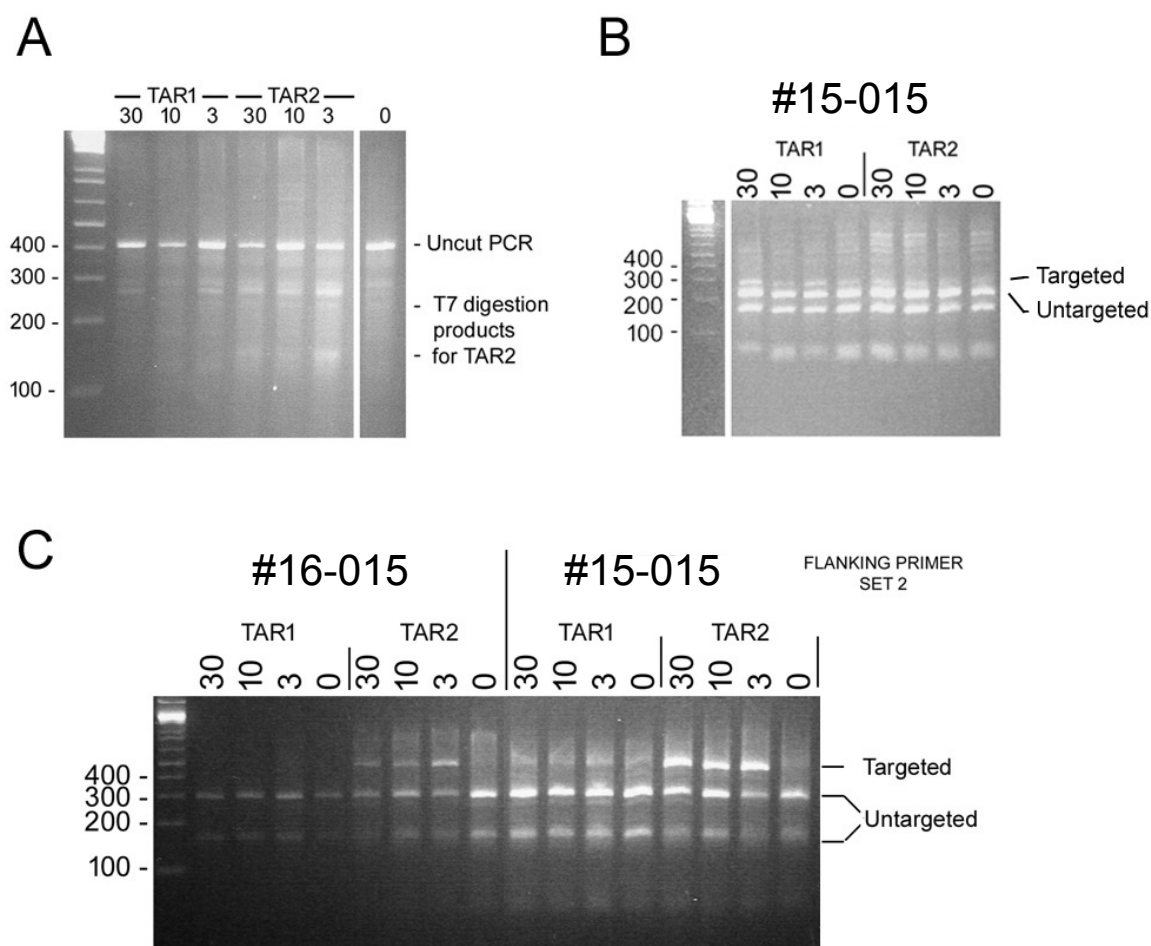
Figure 4.8: Detection of Cas9 activity at the *CEP290* TAR1 and TAR2 loci. A. Digest of PCR amplified Primer Set 1 (405bp) DNA, melted, re-annealed, and digested with T7endo. Spurious digestion and haziness of bands complicates interpretation, but sizes suggest some activity at TAR2 but little at TAR1. B. Sml I digest of PCR products (Primer set 2) indicative of activity at TAR1 likewise showed no clear difference between TAR1, TAR2, or untargeted PCR products, further suggesting a lack of activity at TAR1. C. Digest of PCR products (from Primer Set 2) with Bsl I indicating activity at the TAR2 locus. Uncut bands (Targeted) and cut bands (untargeted) clearly differ between TAR2 and other gRNAs. 30, 10, 3, and 0 indicates the nanomolar amount used of individual gRNAs. Labels on the left edge of gels indicate the size of the DNA ladder. See text for further detail.

4.3.3.4 Attempt to repair the *CEP290* mutation

It has been reported that new replacement DNA can be integrated into genomic loci using disruption of DNA with Cas9 and homologous recombination.(12-14) It has further been reported that short single-stranded DNAs (ssDNAs) can be used for this process with double-digit efficiencies of insertion. Given the efficiency of Cas9 cleavage at TAR2, we elected to try to repair the *CEP290* gene defect by co-introducing a long ssDNA (ultramer) of 154bp synthesized by IDT. This ultramer had several features designed to both repair the splicing defect at Exon 50 and to facilitate detection of the integrated ssDNA (Figure 4.9). First, the ultramer had over-all homology with the original 154bp region just downstream of *CEP290* Exon 50 of >92% with perfectly matched homology arms of ~50bp on either end. This high level of similarity should favor correct homologous recombination. The size was slightly longer than the preferred length of 100-120bp, however, to replace the splice donor and eliminate competing mis-splice sites, we felt that the length was justified. We used the splice donor of a downstream *CEP290* Exon (Exon 53) as a template for replacing the low-efficiency splice donor of Exon 50. We reasoned that if this splice donor worked well elsewhere in the feline *CEP290* gene, it should also work here. The Exon 53 splice donor also contained an Ase I site that was not in the original Exon 50 sequence, so this further justified the strategy. Finally, we incorporated an Xho I site slightly further downstream that required the change of only two base pairs from the original sequence.
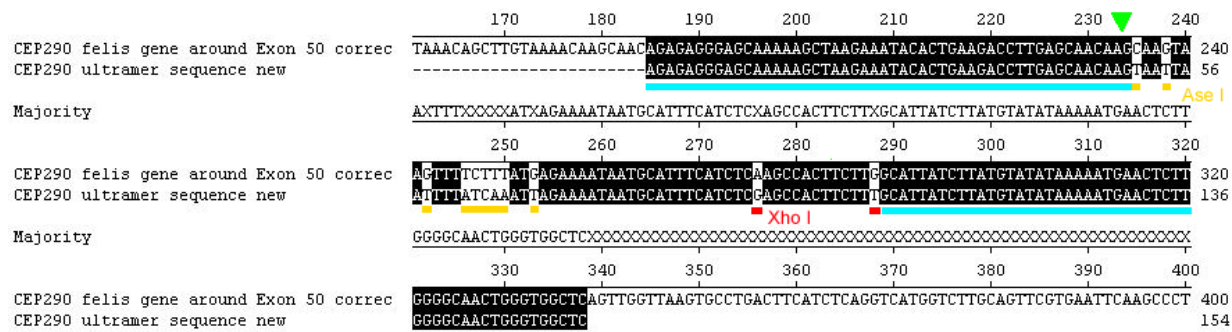
Figure 4.9: Comparison of the feline *CEP290* Exon 50 mutant sequence with the modified ssDNA ultramer. Sequence underlined in blue indicated the homology arms. Black shading indicates identical bases in both sequences. Yellow boxes indicate ultramer sequence matching the splice donor copied from Exon 52. The Ase I and introduced Xho I sites are also shown. Mismatches in red were introduced to prevent cleavage of TAR2 by Cas9 in the repaired sequence. Green arrow indicates splice site corrected from GC to GT.

We tested co-transfection of 100, 50, 10, 3, 1 and 0 nM concentrations of ultramer in combination with the TAR2 targeting conditions worked out in the experiments of Figure 4.8 and assayed the amplified PCR products for cleavage by either the Xho I or Ase I enzymes in a similar fashion to our analysis with Bsl I. Even though we observed transfection efficiencies and targeting efficiencies somewhat attenuated in the presence of ultramer compared to zero co-transduced ultramer (variable, but ~50% reduction), we still felt that they were high enough to produce a usable result. In short, we were not able to detect cleavage of the PCR products with either Primer set 1 or 2 by either Ase I or Xho I. Repeats of this experiment altering parameters or using increased gRNA (TAR2 gRNA was increased from 3nM to 30nM) still did not yield evidence of incorporation of the ssDNA. Since individual targeting DNAs, both single and double-stranded are variably able to function efficiently (most likely based on sequence composition), we have concluded that the ultramer we tested

152

is not a high-efficiency integrator. We predict that integration at <5% of alleles could

probably not be detected with confidence using our assay methods. Since this method

also affords us no way to select or identify repaired cells that had undergone

recombination, an efficiency below 10-20% would probably been of little use in most

assays.

4.4 Discussion

Fibroblast cells were successfully grown from all cats with minimal passages required to establish pure fibroblast culture. This creates a useful *in vitro* tool that is easy to develop and quick to grow, allowing for fast and efficient downstream analysis in future studies. Successful cilia induction further increases the utility of this tool for analysis of *CEP290* mutations. Since the protein produced by this gene is a ciliary protein, assays investigating ciliation and ciliary effects may be useful for better describing this model and for establishing objective markers for treatment efficacy analysis.

Our attempt at establishing one such marker by measuring cilia length did not produce a useful marker as cells from all genotypes produce cilia of similar same length. This is not surprising given the milder nature of the phenotype seen in cats, suggesting that more severe changes such as disruption of cilia growth is unlikely to be an issue in this model.(15) However, this does not exclude use of this *in vitro* tool but simply highlights the need for further investigation to identify objective markers. Though cilia length is not affected by the feline *CEP290* mutation, the presence of a retinal phenotype in cats shows that the mutation has deleterious effects on protein levels and/ or function and therefore suggests that abnormalities in mutant cells are likely to be present. Future studies should be aimed at identifying these abnormalities such that they can be utilized as markers in treatment trials. Alternatively, it may be possible to utilize genome editing to alter the cells to make the phenotype more severe, perhaps by

154

knocking down or out another gene involved in ciliation. This would result in more obvious abnormalities in mutant cells that could be identified as objective markers.

CRISPR/Cas9 editing of *CEP290* mutant feline fibroblast cells proved challenging and requires further optimization and studies to reach a useable treatment. It is important to note that before proceeding with the above-mentioned methods, a "nickase" method was attempted. The nickase method is a modified editing technique that utilizes a mutated Cas9 enzyme to introduce single-stranded cuts instead of double-stranded cuts. In theory, this should result in a lower risk of off-target mutagenesis as naturally present cell repair machinery will detect and repair single-stranded disruptions with high fidelity by homology-directed repair.(16) Off-target breaks, which will be single-stranded, will therefore be repaired while double stranded breaks directed by the gRNA pairs will only occur at the chosen target site. Unfortunately, pilot studies showed insufficient transfection efficiency using this method, precluding its use for our desired purposes. We therefore switched to the described pre-made kit that includes the wild-type Cas9 enzyme and does not employ a nickase method. This method could lead to significant off-target mutagenesis, a potentially significant safety concern as we moves towards an *in vivo* treatment. However, there are methods to overcome this obstacle. The same CRISPR engines used to design our CRISPR constructs can also analyze these constructs for possible off-target sites. We can then use this information to determine the possible effects cuts in these off-target sites could cause, gauge the safety of the treatment, and make adjustments as needed. If off-target sites occur in oncogenes for example, new gRNAs can be analyzed until a construct that does not target important genes is found. Once a construct that has

minimal off-target sites of less importance (non-coding regions, for example) is designed, pilot studies can be conducted to analyze the percentage of target hit versus off-target hit utilizing assays such as T7 endonuclease or restriction enzyme digestion.

As treatments move closer to *in vivo* models and human clinical trials, other methods can be employed to even further reduce the possible effects of off-target mutagenesis and improve treatment safety. Treatments utilizing this machinery will likely employ one of two methods; either direct *in vivo* delivery of the CRISPR machinery, or correction of induced pluripotent stem cells (iPSCs) for transplantation. Direct delivery of the machinery, likely utilizing a vehicle such as adeno-associated viral (AAV) vectors, could result in off-target mutagenesis. However, though off-target sites should be avoided as much as possible in pre-delivery construct design as described above, remaining off-target breaks are likely to be repaired by cell repair machinery, further reducing possible deleterious effects. Treatments utilizing corrected iPSCs could be verified as safe pre-treatment by sequence analysis. iPSCs corrected could be sequenced to definitively determine all sites targeted and then a cell that has no or minimal off-target mutagenesis could be identified and clonally expanded to create a line of cells known to contain no potentially hazardous off-target sites.

Though we achieved high-efficiency of cell transfection and showed good cutting with one of our gRNA pairs, our diagnostic assays for insert integration showed no detectable integration of the insertion oligonucleotide. We are not able to determine if this is due to no integration at all, or more likely, integration that is occurring but at too low of a level for our diagnostic assays to detect. It is unclear why we did not achieve integration of the insert at detectable levels but there are several possibilities. DNA does

not transfect with nearly as strong an efficiency as RNA.(17) Therefore, while our RNAs transfected cells effectively it is possible that the DNA oligonucleotide insert did not transfect the cells with these RNAs and the Cas9 enzyme with detectably high efficiency. This could be compounded by our CRISPR efficiency; though 50% transfection efficiency is relatively strong, that indicates that whatever oligo transfection efficiency we achieved would only be appreciated at 50% of that level. If we for example achieved 10% insert integration, the overall integration is then only 5%. Alternatively, the lack of detectable integration could be an issue with the oligonucleotide, warranting further optimization such as pilot studies investigating a variety of oligo lengths and alternative sequences. A likely explanation therefore is that different targeting fragments and genomic targets possess intrinsically different capacities for recombination and by chance the target we had to work with is not a site of high-efficiency. Expansion of testing to more ssDNAs or dsDNAs with different length homology arms and compositions is necessary to explore this possibility.

A strategy that may overcome the obstacles faced in this study could be based on the recently described process for precise integration of non-homologous DNA fragments termed "homology-independent targeted integration", or HITI.(18) If the technique described in this report can be successfully adapted to feline cells, it is a superior method for repair of the feline *CEP290* mutation because it would also allow for easy identification and selection of cells with mutation-correcting recombination. (Figure 4.10)
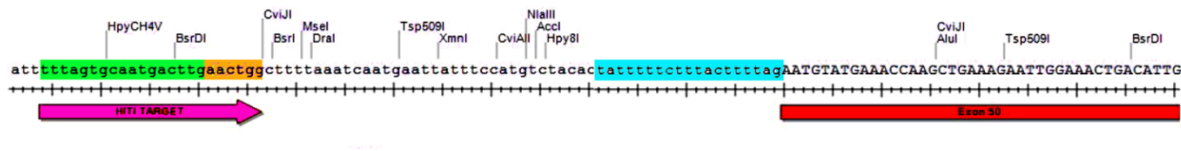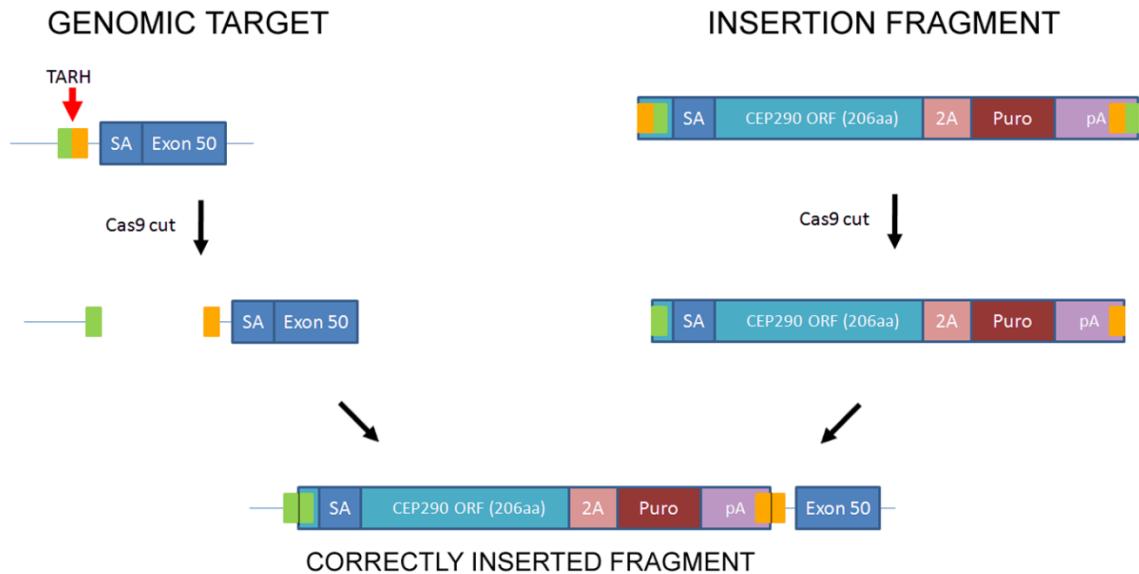
Figure 4.10: Schematic of feline *CEP290* repair using HITI. A. Sequence proximal to the splice acceptor of *CEP290* Exon 50. The proposed guide RNA sequence labeled HITI TARGET on the left. Green shading indicates sequence upstream of the putative Cas9 cleavage site and orange shading indicates sequence downstream. Blue shading indicates sequence within the proximal splice acceptor (ending in AG). Red bar indicates exon mRNA for *CEP290* Exon 50. B. Schematic of the insertion of the synthetic DNA fragment into the HITI TARGET (TARH) site. Note that the two "halves" of the recognition site on genomic DNA and the DNA fragment for insertion are flipped relative to each other such that correct insertion of the DNA fragment juxtaposes to "green" halves and two "orange" halves, effectively destroying the recognition site, stopping further digestion by the Cas9 enzyme, and completing the recombination reaction. Insertions in reverse are subject to continued digest by Cas9, thus favoring eventual correctly oriented insertion events.

As suggested above, one severe limitation of the ssDNA recombination method of repair is that unless insertion of the repair region is quite efficient (we estimate >5-10% of all alleles), detection of the insertion events will be difficult and isolation and enrichment of repaired cells will be impractical. HITI could solve this problem by permitting the relatively efficient integration of larger payloads into the *CEP290* defect region and allowing selection of correctly recombined cells using standard antibiotic resistance genes.

The HITI strategy is based on: 1) a high-efficiency and unique Cas9 target, 2) high-level Cas9 expression, 3) an abundance of a double-stranded DNA insert of moderate length (<10Kb) with reverse Cas9 target sequences (relative to the genomic target) such that the insert DNA is cut on the 5' and 3' ends by Cas9 and insertion in the correct orientation destroys the target sequences on both ends. Insertion of the DNA insert in the incorrect (reverse) orientation re-creates the Cas9 target site that continues to be cleaved by Cas9 until the target is destroyed by indel creation or by insertion of the foreign DNA fragment in the correct orientation into the genomic site. Consequently, three classes of allele are generated in the target cell population: wild-type, indel mutated, and correctly inserted "repaired" alleles. By including a selectable marker such as a drug-resistance gene in the insertion cassette, only those cells with correct integration of the repair fragment will be returned.

In the case of feline *CEP290*, the high-efficiency gRNA Target 2 that we identified would not be ideal for use with HITI. The reason for this is that TAR2 resides just downstream of the Exon 50 splice site and insertion of a new fragment would leave the non-canonical splice intact. Although there are possible work-arounds for using the

159

TAR2 site, we have concluded that the simplest and likely best approach for repairing the defect using HITI is to insert a fragment just upstream of the Exon 50 splice acceptor that will essentially replace the coding portion of *CEP290* from Exon 50 downstream, adding a puromycin-resistance ORF attached to the C-terminus of the completed CEP290 protein using a 2A element. This new CEP290-2A-Puro ORF would then be transcriptionally-terminated by a foreign polyadenylation signal immediately following the inserted fragment such that the remainder of the gene downstream (including the splice donor mutation) not utilized. A schematic of this process is shown in Figure 4.10. This is a good experimental design that has a high probability of success and would be a worthwhile effort for future studies.

While we did not complete successful integration of an oligonucleotide insert to repair the defect in feline *CEP290* mutant cells, we achieved the initial steps to reach this aim, including RNA and Cas9 enzyme transfection of cells and cutting with gRNAs, with strong efficiency. We are confident that with further trials and optimizations editing of the *CEP290* feline mutation can be achieved and are particularly hopeful that the HITI method could be employed with a successful outcome. Future studies should aim to reach this goal as well as identify differences between mutant and non-mutant cells for utilization as objective markers of treatment success.

4.5 Acknowledgments

REFERENCES

REFERENCES

1.   Betleja E, Cole DG. Ciliary trafficking: CEP290 guards a gated community. Curr Biol. 2010;20(21):R928-31.

2.   Mali P, Yang L, Esvelt KM, Aach J, Guell M, DiCarlo JE, et al. RNA-guided human genome engineering via Cas9. Science. 2013;339(6121):823-6.

3.   Narfström K. Hereditary progressive retinal atrophy in the Abyssinian cat. J Hered. 1983;74(4):273-6.

4.   Narfström K. Progressive retinal atrophy in the Abyssinian cat. Clinical characteristics. Invest Ophthalmol Vis Sci. 1985;26(2):193-200.

5.   Menotti-Raymond M, David VA, Schaffer AA, Stephens R, Wells D, Kumar-Singh R, et al. Mutation in CEP290 discovered for cat model of human retinal degeneration. J Hered. 2007;98(3):211-20.

6.   Menotti-Raymond M, David VA, Pflueger S, Roelke ME, Kehler J, O'Brien SJ, et al. Widespread retinal degenerative disease mutation (rdAc) discovered among a large number of popular cat breeds. Vet J. 2010;186(1):32-8.

7.   Menotti-Raymond M, David VA, Schaffer AA, Stephens R, Wells D, Kumar-Singh R, et al. Mutation in CEP290 discovered for cat model of human retinal degeneration. J Hered. 2007;98(3):211-20.

8.   Linberg KA, Lewis GP, Shaaw C, Rex TS, Fisher SK. Distribution of S- and M-cones in normal and experimentally detached cat retina. The Journal of comparative neurology. 2001;430(3):343-56.

9.   Garanto A, van Beersum SE, Peters TA, Roepman R, Cremers FP, Collin RW. Unexpected CEP290 mRNA splicing in a humanized knock-in mouse model for Leber congenital amaurosis. PLoS One. 2013;8(11):e79369.

10.   Vangipuram M, Ting D, Kim S, Diaz R, Schule B. Skin punch biopsy explant culture for derivation of primary human fibroblasts. J Vis Exp. 2013(77):e3779.

11.   Rao KN, Li L, Zhang W, Brush RS, Rajala RV, Khanna H. Loss of human disease protein retinitis pigmentosa GTPase regulator (RPGR) differentially affects rod or cone-enriched retina. Hum Mol Genet. 2016;25(7):1345-56.

12.   Ran FA, Hsu PD, Wright J, Agarwala V, Scott DA, Zhang F. Genome engineering using the CRISPR-Cas9 system. Nat Protoc. 2013;8(11):2281-308.

13.   Sander JD, Joung JK. CRISPR-Cas systems for editing, regulating and targeting genomes. Nat Biotechnol. 2014;32(4):347-55.

14.   Hoshijima K, Jurynec MJ, Grunwald DJ. Precise genome editing by homologous recombination. Methods Cell Biol. 2016;135:121-47.

15.   Narfstrom K. Hereditary progressive retinal atrophy in the Abyssinian cat. J Hered. 1983;74(4):273-6.

16.   Shen B, Zhang W, Zhang J, Zhou J, Wang J, Chen L, et al. Efficient genome modification by CRISPR-Cas9 nickase with minimal off-target effects. Nat Methods. 2014;11(4):399-402.

17.   Wiedenheft B, Sternberg SH, Doudna JA. RNA-guided genetic silencing systems in bacteria and archaea. Nature. 2012;482(7385):331-8.

18.   Suzuki K, Tsunekawa Y, Hernandez-Benitez R, Wu J, Zhu J, Kim EJ, et al. In vivo genome editing via CRISPR/Cas9 mediated homology-independent targeted integration. Nature. 2016;540(7631):144-9.

CHAPTER 5

DIFFERENTIAL TARGETING OF FELINE PHOTORECEPTORS BY RECOMBINANT ADENO-ASSOCIATED VIRAL VECTORS: IMPLICATIONS FOR PRECLINICAL GENE THERAPY TRIALS

Minella AL, Mowat FM, Willett KL, Sledge D, Bartoe JT, Bennett J, Petersen-Jones SM.

Differential targeting of feline photoreceptors by recombinant adeno-associated viral

vectors: implications for preclinical gene therapy trials. *Gene Therapy*. 2014;21(10):

913-20. PMID: 25056608

Author Contributions

Conceived and designed the experiments: ALM, FMM, JTB, JB, SMP-J. Performed the

experiments: ALM, FMM, KLW, DS, JTB, SMP-J. Analyzed the data: ALM, KLW, SMP-J.

Wrote the paper: ALM, KLW, SMP-J. Provided input for the manuscript: FMM, JTB, JB.

5.1 Abstract

The cat is emerging as a promising large animal model for preclinical testing of retinal dystrophy therapies, for example, by gene therapy. However, there is a paucity of studies investigating viral vector gene transfer to the feline retina. We therefore sought to study the tropism of recombinant adeno-associated viral (rAAV) vectors for the feline outer retina. We delivered four rAAV serotypes; rAAV2/2, rAAV2/5, rAAV2/8, and rAAV2/9, each expressing GFP under the control of a cytomegalovirus promoter, to the subretinal space in cats and, for comparison, mice. Cats were monitored for gene expression by *in vivo* imaging and cellular tropism was determined using immunohistochemistry. In cats, rAAV2/2, rAAV2/8, and rAAV2/9 vectors induced faster and stronger GFP expression than rAAV2/5 and all vectors transduced the RPE and photoreceptors. Unlike in mice, cone photoreceptors in the cat retina were more efficiently transduced than rod photoreceptors. In mice, rAAV2/2 only transduced the RPE whereas the other vectors also transduced rods and cones. These results highlight species differences in cellular tropism of rAAV vectors in the outer retina. We conclude that rAAV serotypes are suitable for use in retinal gene therapy trials in feline models, particularly where cone photoreceptors are the target cell.

5.2 Introduction

Leber Congenital Amaurosis (LCA) is a group of hereditary retinal dystrophies with an estimated incidence of 1 in 81,000, that is characterized by early-onset vision loss.(1) With the recent findings that causative mutations for two feline retinal dystrophies are in genes responsible for LCA, the cat has become a promising large animal model for preclinical testing of therapies.(2, 3) The rod-cone dysplasia (*Rdy*) cat has a mutation in the cone rod homeobox gene (*Crx)* resulting in a severe, early-onset, dominant cone-rod dystrophy (the initial description of this as a rod-cone dystrophy was subsequently corrected (3)), mirroring the severe LCA^{CRX}.(4) The retinal degeneration Abyssinian cat (*RdAc*) has a mutation in the centrosomal protein of 290 kDa (*Cep290*) and is a model for recessive non-syndromic *CEP290* retinopathy.(2) Studies to develop gene therapy vectors applicable for LCA^{CRX} and LCA^{CEP290} are underway and these cat models offer the opportunity to test promising approaches in a large animal model.

The feline eye and vision have been extensively studied by retinal physiologists, thus laying the groundwork for the use of this species in therapeutic studies. The similarity in size of the feline and human globe, coupled with the presence of an area centralis and visual streak with similarities to the human macula (namely higher numbers of cones and a greater density of photoreceptors), offers advantages over rodent models for the preclinical testing of therapy. Canine spontaneous retinal dystrophy models, which offer similar advantages, have already proven invaluable for proof-of-concept gene therapy trials.(5, 6) The aforementioned feline models, along with other spontaneous models currently being characterized ((7) L Lyons personal

167

communication 2013, and SM Petersen-Jones, unpublished results), show promise for this purpose.

Recombinant adeno-associated viral (rAAV) constructs have become the vectors of choice for retinal gene therapy.(8) However, there is limited information about the use of rAAV vectors in the feline retina. Successful gene therapy of feline mucopolysaccharidosis VI using an rAAV2 vector delivered subretinally has been reported to transduce feline retinal pigment epithelium.(9) Only one study has been published investigating rAAV transduction of feline photoreceptor cells (the target for both LCA^{CRX} and LCA^{CEP290} therapy), which showed transduction of both rods and cones in two eyes injected subretinally with an rAAV2 construct.(10)

The purpose of the current study was to test a variety of rAAV vector serotypes delivered by subretinal injection for their potential use in preclinical retinal gene therapy trials in feline LCA models.

5.3 Methods

5.3.1 Animals

Ten adult wild-type male domestic shorthair cats (Liberty Research, Inc. Waverly, NY) and eight 3-4 week old female C57Bl6J mice (Harlan Sprague Dawley Inc., Indianapolis, IN) were used. All procedures were conducted according to the ARVO Statement for the Use of Animals in Ophthalmic and Vision Research and were approved by the Michigan State University Institutional Animal Care and Use Committee.

5.3.2 Production of vector

Recombinant adeno-associated virus 2/2, 2/5, 2/8 and 2/9vectors packaged with the green fluorescent protein (GFP) gene driven by the cytomegalovirus promoter were produced by the University of Pennsylvania Viral Vector Core. rAAV vectors were manufactured and purified from cell lysates after triple transfection of HEK293 cells. rAAV particles were purified from cell lysates by two rounds of cesium chloride centrifugation. Vector was concentrated and desalted, using Amicon Ultra-15 centrifugal filtration devices (Millipore, Bedford, MA, USA). Glycerol was added to the concentrate to a final concentration of 5% (v/v), and aliquots stored at -80°C. All vector preparations were evaluated by multiple assays, including whole purity analysis by sodium dodecyl sulfate-polyacrylamide gel electrophoresis, endotoxin determination (with < 20 EUml^{-1} as a lot release criterion), and by TaqMan quantitative PCR for genome copy titration.

For subretinal injection, vectors were diluted to a titer of 5 x 10^{11} viral genomes per milliliter (vgml^{-1}) in sterile balanced salt solution (Alcon Laboratories, Fort Worth, TX).

5.3.3 Subretinal injections

Subretinal injections in cats were performed using the technique previously described in dogs(11) but with the addition of a standard 3-port 23 gauge vitrectomy; 200µL of vector was injected. Six cats received rAAV2/5 in the right eye and rAAV2/8 in the left eye, and four cats received rAAV2/9 in the right eye and rAAV2/2 in the left eye. Post-operatively, 0.2mg dexamethosone (Bimeda LC, Oakbrook, IL) and 4mg methylprednisolone acetate (Depo-medrol. Pfizer Animal Health, Madison, NJ) were injected subconjunctivally. Approximately 2 µl of vector was subretinally injected into mice using a transcleral approach as previously described.(12) Following injection, neomycin,/bacitracin/polymyxin B ointment (Henry Schein, Melville, NY) was applied twice daily for two days. Each vector was injected into 4 mouse eyes.

5.3.4 Monitoring for GFP expression

Fundus photography and GFP expression monitoring was performed in cats daily for 10 days, every-other-day for 1 week, twice weekly for 1 week and once weekly until euthanasia (RetCam II. Clarity Medical Systems, Pleasanton, CA). Mice were maintained for 6-8 weeks, during which time only gross ocular examinations were performed.

5.3.5 Eye processing

Cats were euthanized 21-56 days and mice 55-71 days post- injection. Feline globes were fixed in 4% paraformaldehyde and dissected along the limbus, dividing the anterior and posterior segments. Mouse globes were fixed in 1% paraformaldehyde. Feline anterior and posterior segments and whole mouse eyes were embedded in optimal cutting temperature gel (OCT. Sakura Finetek USA, Inc., Torrance, CA) and flash frozen. Serial 14 µm (cat) and 10µm (mouse) cryosections were prepared for immunohistochemistry (IHC).

5.3.6 Immunohistochemistry

Immunohistochemistry was performed as previously described.(13) Antibodies are listed in Table 5.1. Feline sections were imaged using an Olympus FluoView 1000 Laser Scanning Confocal microscope (Olympus American Inc., Melville, NY). Z-depth series were constructed using Image J software (Adobe Photoshop 3.0 software, Adobe Systems Inc., Mountain View, CA) and examined using Adobe Photoshop 3.0 software (Adobe Systems Inc., Mountain View, CA, USA).   Murine sections were imaged using a Nikon Eclipse 80i microscope (Nikon instruments Inc., Melville, NY) equipped with a CoolSnap ESv camera (Photometrics, Tuscon, AZ).

Antibody	Host	Target	Concentration	Source
Primary antibodies				
Cone Arrestin	Rabbit	Cone photoreceptors	1:10 000	Dr Cheryl Craft, Doheny Eye Institute, University of Southern California, Los Angeles, CA, USA[40]
Glutamine Synthetase	Rabbit	Müller cells	1:1000	Sigma Aldrich Inc., St Louis, MO, USA
Glial Fibrillary Acidic Protein	Rabbit	Activated Müller cells	1:1000	DakoCytomation, Carpinteria, CA, USA
Protein kinase c-alpha	Mouse	Rod bipolar cells	1:3000	BD Biosciences, San Jose, CA, USA
Calbindin	Mouse	Horizontal cells	1:1000	Swant Immunochemicals, Bellinzona, Switzerland
Calretinin	Rabbit	Horizontal cells	1:1000	Swant Immunochemicals
GFP	Rabbit	Green fluorescent protein	1:1000	Invitrogen, Carlsbad, CA, USA
Secondary antibodies				
Alexa Fluor 546 F(ab')2 fragments of goat anti-rabbit IgG (H+L)	Goat	Rabbit primary antibody	1:250	Invitrogen
Alexa Fluor594 rabbit anti-mouse IgG (H+L)	Rabbit	Mouse primary antibody	1:250	Invitrogen

Table 5.1: Antibodies used for immunohistochemistry

171

5.3.7 Cell counting

Rod and cone photoreceptors expressing GFP in cat eyes were counted. Images from three retinal sections from each injected region stained with CAR and DAPI were captured. With the GFP signal masked and cones labeled with hCAR, a masked observer counted and marked 200 rod photoreceptor cell bodies. The GFP signal was then unmasked, and all marked cell bodies positive for GFP expression were counted. All cones (CAR positive) across sections were counted and the number of GFP-labeled cones were recorded.

5.3.8 Immune responses

To detect antibodies against rAAVs, an *in vitro* transduction assay was adapted from previous methods.(14) Briefly, 84-31 cells (293 HEK stably expressing Ad-E4,, University of Pennsylvania Vector Core) were seeded overnight at 6000 cells per well. Half-log serial dilutions of test sera (1:3.16 – 1:10 000) were incubated with appropriate rAAV serotypes containing a GFP reporter at a multiplicity of infection (MOI) optimized such that ~80% of cells were transduced in control wells lacking test sera. Plates were inoculated and incubated at 37° C under 5% CO_2 for 36 hours and then assayed for GFP fluorescence with a Typhoon 9400 Variable Mode Imager (GE Healthcare, Piscataway, NJ). Images were analyzed with Protein Array Analyzer for ImageJ(15) and samples are reported as neutralizing when fluorescence was <50% of un-inhibited controls. An indirect enzyme-linked immunosorbant assay (ELISA) was performed to detect anti-GFP antibodies in serum samples; 0.1 µg of recombinant purified GFP (Clontech, Palo Alto, CA) was incubated overnight at 4° C then blocked and incubated

with feline test sera diluted to 1:400. Samples were then incubated with HRP-conjugated anti-feline IgG secondary antibody (Thermo Fisher Scientific, Waltham, MA) diluted to 1:10000. The plate was developed using SIGMAFAST OPD system (Sigma-Aldrich, St. Louis, MO). Results are presented relative to serum from an un-injected naïve cat. All samples were run in triplicate. For evaluation of inflammatory infiltration three sections of each eye was stained stained with hematoxylin and eosin stain and evaluated based on an objective scoring system (Table 5.2). Four ocular regions were were designated and scored and a total infiltration score was determined for each eye by adding the four individual scores.

Ocular region	Scoring system
Retina	Based on thickness of infiltration around blood vessels 0: no infiltration 1: 1–2 cell layers thick 2: 3–4 cell layers thick 3: 5+ cell layers thick
Subretinal space	0: no infiltration 1: scattered individual cells 2: moderate number of cells with some aggregates 3: large numbers of cells causing expansion of the subretinal space
Choroid and episclera	0: no infiltration 1: scattered individual cells 2: moderate number of cells with some aggregates 3: large numbers of cells causing expansion of the choroid space
Ciliary body	0: no infiltration 1: scattered individual cells 2: moderate number of cells with some aggregates 3: large numbers of cells
Total infiltration score	sum of all scores above (possible range 0–12)

Table 5.2: Inflammatory infiltration scoring rubric

173

5.3.9 Statistical Analysis

All statistical analysis was conducted using SigmaPlot software (SigmaPlot 12. Systat Software Inc. San Jose, CA). Normally distributed cell counting data sets (determined by Shapiro-Wilk normality test) were compared using unpaired t-tests. Non-parametric cell counting data sets were compared by a Mann-Whitney Rank Sum Test. Significance was set at $P < 0.05$. The hematoxylin and eosin data were analyzed using Kruskal-Wallis one way analysis of variance with a significance set at $P < 0.05$.

5.4 Results and Discussion

Subretinal injections of rAAV vectors, all at the same dose (1 X 10^{11}vg) and all expressing green fluorescent protein (GFP) were performed on 20 feline eyes (10 cats) (Table 5.3). During injections the feline retina did not detach as readily as has been our experience in the dog, and the resistance to expanding the detachment resulted in some back-flow of vector into the vitreous. Post-injection inflammation in 17 of 20 eyes was minimal consisting of trace to 1+ aqueous flare (on a scale of 1-4) during the first few days following the procedure, but this was transient and required no treatment. The retinal detachments resolved over this period. However, three eyes were excluded from the study due to the development of procedure-related intraocular inflammation (Table 5.3). The same vector constructs were also injected subretinally in mouse eyes for comparison. There were no adverse complications in these eyes.

Vector	Cat #	Eye #, OS/OD	Concentration	In vivo assessment		Histological assessment		
				Onset of fluorescence (days)	Onset by vector (days; range, mean)	% cones transduced	% rods transduced	Rods versus cones; P, test
rAAV2/2	1	1, OS	10^{11} vgml^{-1}	3	3–4, 3.3 (SD = 0.87)	78% (SD = 19)	6% (SD = 3)	P = 0.0033, two-tailed t-test
	2	2, OS	10^{11} vgml^{-1}	4				
	3	3, OS	10^{11} vgml^{-1}	4, excluded[a]				
	4	4, OS	10^{11} vgml^{-1}	Excluded[b]				
rAAV2/5	5	1, OD	10^{11} vgml^{-1}	7	4–7, 5.1 (SD = 1.86)	74% (SD = 20)	15% (SD = 13)	P = <0.000, two-tailed t-test
	6	2, OD	10^{11} vgml^{-1}	7				
	7	3, OD	10^{11} vgml^{-1}	6				
	8	4, OD	10^{11} vgml^{-1}	UTD[+]				
	9	5, OD	10^{11} vgml^{-1}	4				
	10	6, OD	10^{11} vgml^{-1}	4				
rAAV2/8	5	1, OS	10^{11} vgml^{-1}	3	1–3, 2.4 (SD = 0.77)	85% (SD = 13)	18% (SD = 25)	P = <0.001, Mann–Whitney rank sum test
	6	2, OS	10^{11} vgml^{-1}	2				
	7	3, OS	10^{11} vgml^{-1}	1				
	8	4, OS	10^{11} vgml^{-1}	3				
	9	5, OS	10^{11} vgml^{-1}	3				
	10	6, OS	10^{11} vgml^{-1}	2				
rAAV2/9	1	1, OD	10^{11} vgml^{-1}	3, excluded[a]	2–3, 2.6 (SD = 0.55)	51% (SD = 13)	4% (SD = 0.6)	P = 0.0028, two-tailed t-test
	2	2, OD	10^{11} vgml^{-1}	2				
	3	3, OD	10^{11} vgml^{-1}	Excluded[b]				
	4	4, OD	10^{11} vgml^{-1}	Excluded[b]				

Key: +UTD: unable to determine; Vitreal hemorrhage precluded fundus examination. [a]Excluded from histological analysis only, because of poor section quality. Please refer to methods for histological assessment procedure. [b]Excluded because of inflammation that developed immediately postoperatively.

Table 5.3: Summary of rAAV transduction

5.4.1 *In vivo* GFP expression in cat eyes

Green fluorescence (indicative of GFP expression) was detected by *in vivo* imaging in injected retinal regions of rAAV2/8 injected eyes between 1 and 3 days post-injection. Fluorescence in rAAV2/2, 2/5, and 2/9 injected eyes developed slightly later (Table 1). Fluorescence appeared noticeably brighter in eyes injected with rAAV2/2, 2/8 and 2/9 compared to rAAV2/5 injected eyes, although this difference was not quantified. The stronger GFP expression in rAAV2/8 eyes compared to rAAV2/5 is consistent with previous reports in mice.[21, 22] In two out of three rAAV2/2 injected eyes evidence of posterior segment inflammation was noted (first detectable at 13-18 days post-injection) and was followed by a progressive loss of GFP fluorescence, noted as decreased GFP signal on fluorescent photography (Figure 5.1).
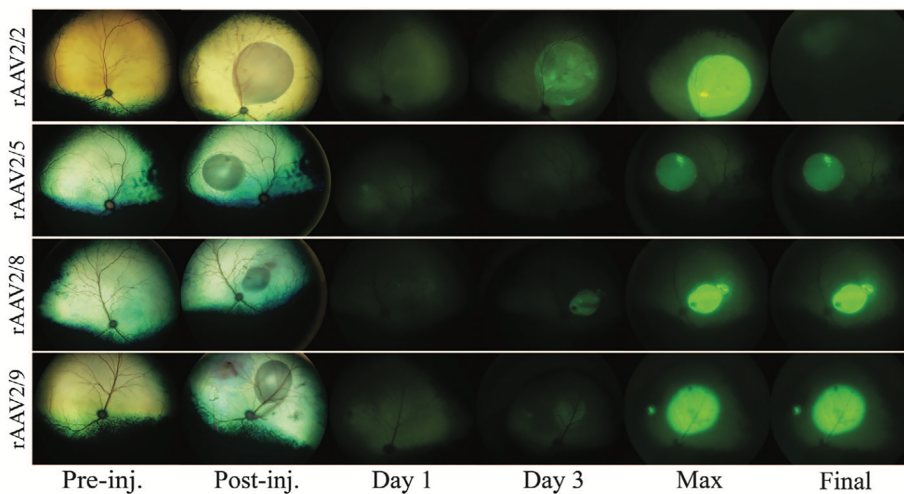
Figure 5.1: *In vivo* transduction of the retina. Representative fundus images of cats from each vector group. Pre-injection (Pre-inj.) column shows the fundus preoperatively and post injection (Post-inj.) images show the 'bleb' created by vector subretinal injection (color images). GFP fluorescence images for the same eyes are shown in subsequent columns at day 1, day 3, maximum GFP expression (Max) and immediately prior to euthanasia (Final). Maximum GFP intensity was reached by day 12 for rAAV2/2, 35 for rAAV2/5, 24 for rAAV2/8 and 28 for rAAV2/9. Note the decrease in GFP expression in the rAAV 2/2 eye.

This decreased signal is similar to the signal decrease noted in the primate retina injected subretinally with the rAAV2-GFP construct, in which fluorescence disappeared over time; however, the kinetics of signal reduction was slower in the primate retina than we note here in the feline retina.(16) Fluorescence was maintained in the remaining eyes for the study duration. The onset of expression in the rAAV2/2 eyes was faster than has been reported in other species, where up to four weeks may be required for expression.(16, 17)

In one rAAV2/8 eye, multiple linear, fluorescent connections between the site of the subretinal injection and the optic nerve head were noted, and most likely represented expression in the nerve fiber layer. The ciliary body in the rAAV2/2 injected eyes showed strong *in vivo* fluorescence (Figure 5.2).
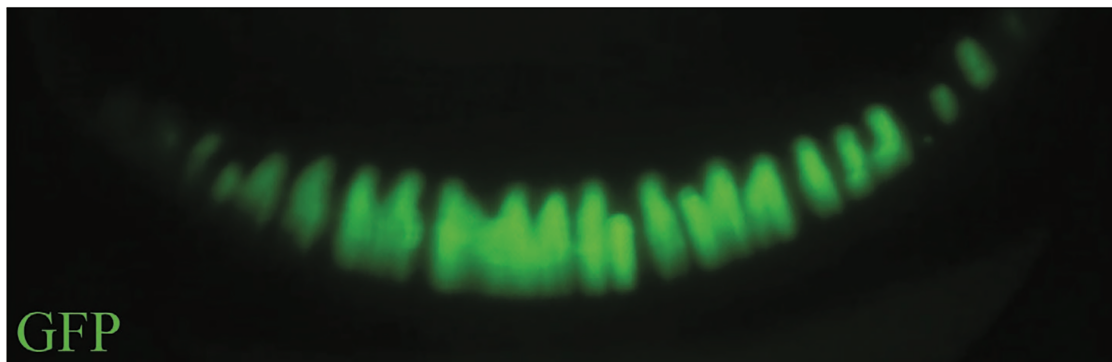
Figure 5.2: *In vivo* expression in the ciliary body. *In vivo* wide-field fundus photograph illustrating rAAV2/2 expression in the ciliary processes. All vectors transduced the ciliary processes, but *in vivo* fluorescence was only noted in rAAV2/2-injected eyes.

### 5.4.2 Histological assessment of GFP expression

Following euthanasia, GFP expressing cells were labeled in feline retinal sections using an anti-GFP antibody. Double labeling with markers specific for different retinal cells was performed to confirm transduced cell type. GFP expression was detected in photoreceptor cells, the retinal pigment epithelium (RPE), and some inner retinal cells for all vectors in the feline eye (Figure 5.2, Table 5.4). In mice, photoreceptors and RPE were transduced by rAAV 2/5, 2/8 and 2/9 whereas rAAV 2/2 transduced only the RPE (Figure 5.3).

Vector	Antibody			
	Pkc-α	GS	Calbindin	Calretinin
rAAV2/2	—	+	—	—
rAAV2/5	—	+	—	—
rAAV2/8	—	+	—	—
rAAV2/9	—	+	—	—

Abbreviations: GS, glutamine synthetase; Pkc-α, protein kinase c-α. Summary of immunohistochemistry results. + sign indicates overlap of the antibody with GFP expression and suggests transduction of the corresponding cell type. All vectors showed Müller cell transduction, as indicated by GS overlap with GFP. No vectors showed bipolar cell transduction or horizontal cell transduction, as indicated by a lack of overlap between GFP and Pkc-α, and calbindin and calretinin.

Table 5.4: Feline inner retinal cell transduction.
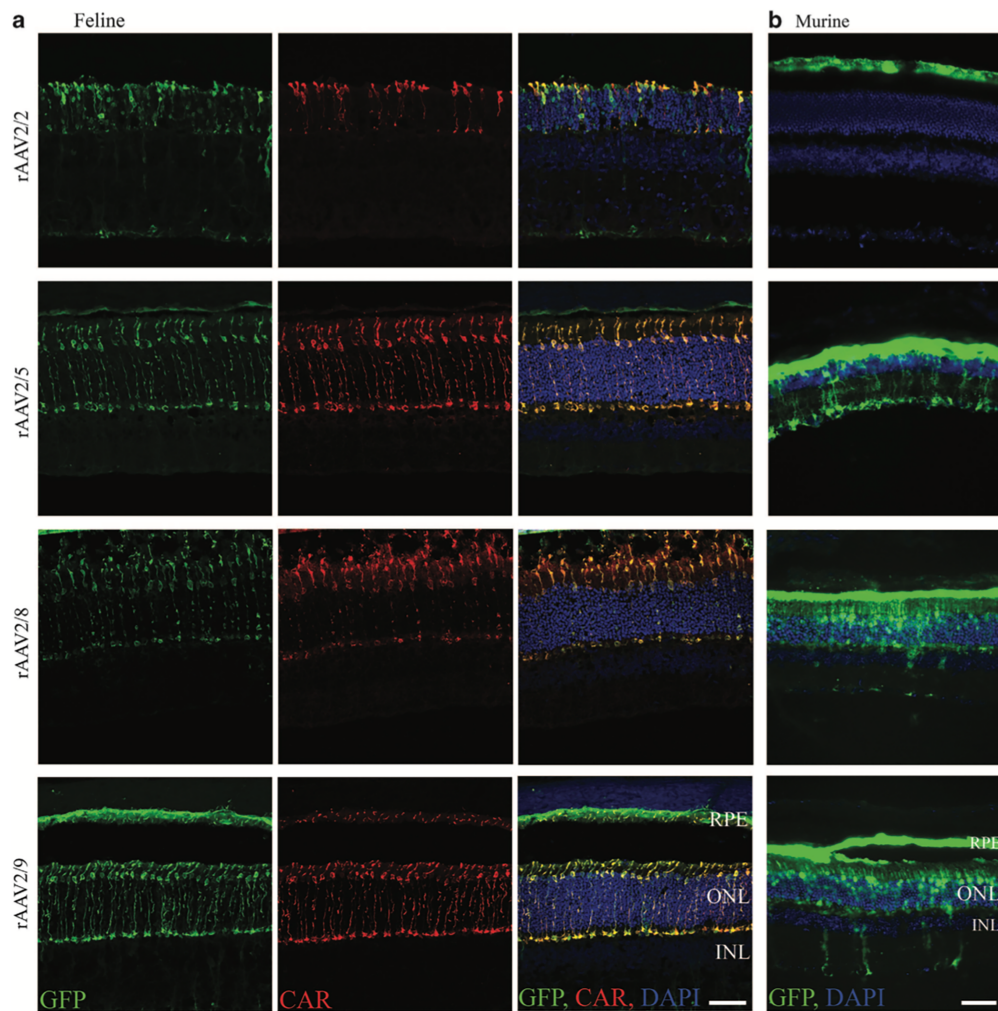
Figure 5.3: Histological transduction of feline and murine outer retinas. (a) Feline retinal sections co-labeled with a GFP antibody and cone arrestin antibody show the predominance of cone transduction for each of the vectors. rAAV2/2 eyes all showed inflammation, thereby affecting section quality, as evidenced in the rAAV2/2 images. (b) In murine retinas, rAAV2/5, 2/8 and 2/9 vectors transduced rods, cones and RPE, whereas rAAV2/2 only transduced the RPE. Scale bar = 50 microns. CAR, cone arrestin labeling; DAPI, nuclear counterstain; INL, inner nuclear layer; ONL, outer nuclear layer.

Photoreceptor transduction was quantified by counting GFP-labeled rods and cones. For all four vectors a significantly higher percentage of cones were transduced than rods (Table 5.3) and the transduced cones had noticeably brighter GFP-labeling (Figure 5.3). rAAV2/8 transduced the highest percentage of photoreceptors, followed by rAAV2/5, rAAV2/2, and lastly, rAAV2/9. The percentage of rods transduced was

significantly higher in rAAV2/8 injected eyes than rAAV2/9 injected eyes (Mann-Whitney

Rank Sum, p =0.019). Although quantification of photoreceptor transduction was not

performed in murine retinas, those vectors that transduced photoreceptor cells

subjectively appeared to have a more efficient transduction of rods than seen in cats
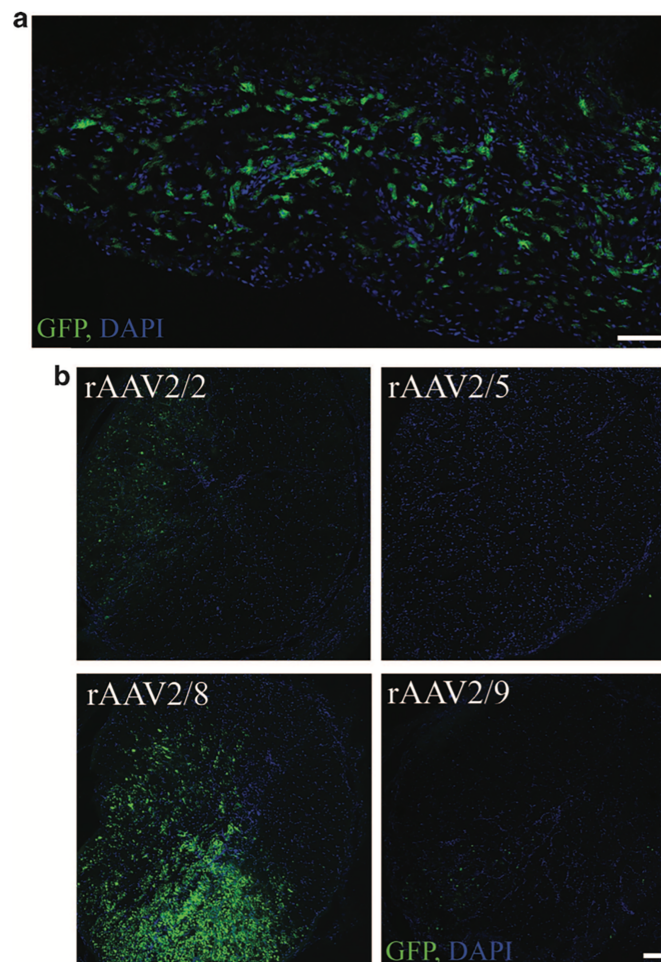
(Figure 5.3).

The greater efficiency of cone transduction compared to rods in the cat retina by

the rAAV serotypes used in this study was unexpected considering the findings in other

species. In mice, rAAV2/2, 2/5, 2/8, and 2/9 vectors have been reported to transduce

photoreceptors but with a rod predominance.(18-20) Similarly, it has been shown that

rAAV2/2, 2/5, and 2/8 transduce canine photoreceptors, also with a rod predominance.

(21-24) Furthermore, a study in nonhuman primates showed strong rod transduction by

rAAV2/2 and 2/8, but with some cone transduction.(25) Similarly, another nonhuman

primate study showed strong rod transduction by rAAV2/2 and 2/8 but, similar to our

findings in the feline, cone and rod transduction with rAAV2/9.(25) Also similar to our

findings, a study investigating rAAV2/5 and 2/8 transduction showed both rod and cone

transduction in the high cone/rod ration porcine retina at comparable doses.(26) Studies

have shown that dosage affects cone transduction with greater cone transduction at

higher doses noted for rAAV2/2, rAAV2/5, and rAAV2/8.(16, 26) The high dose we used

may have contributed to the high cone transduction; however, the relatively poorer rod

transduction cannot be explained by this dosage phenomenon and points to possible

species differences in cone and rod receptor populations. Studies investigating

expression of rAAV serotype-specific receptors on feline photoreceptors may clarify this

species difference. Moreover, our findings that rAAV2/2 transduced only RPE in murine

retinas is in contrast to other studies reporting photoreceptor transduction.(27, 28) This could reflect a slower onset of photoreceptor versus RPE expression from rAAV2/2 in the mouse, or may, conversely, reflect expression "turn-off" as was observed for this vector in some feline retinas. As mice were not euthanized until at least 55 days post injection, it is possible that the murine retina responded to rAAV2/2 similarly to the feline retina and experienced expression turn-off prior to histological evaluation.

In the cat, GFP expression in two out of three rAAV2/2 injected eyes dramatically decreased as early as 21 days post-injection. Histological findings in these eyes showed subjectively thinned retinas with disruption of normal retina architecture, most notable in the outer nuclear layer. These findings are similar to a report of rAAV2/2-injected primate retinas.(16) These findings were most obvious within the region of the subretinal injection; however, retinal histology outside of the subretinally injected region also showed mild retinal thinning and disorganization. Hematoxylin and eosin staining of sections of the posterior eyecup of these eyes showed a plasmacytic and lymphocytic infiltration of the retina, choroid and vitreous.

To evaluate inner retinal transduction, co-labeling for protein kinase c-alpha, calbindin, calretinin, and glutamine synthetase was performed. Protein kinase c-alpha labeled rod bipolar cells were not co-labeled for GFP, and similarly, calretinin and calbindin antibodies, both of which label certain inner retinal cells including horizontal cells, did not colabel with GFP. These results suggest that the vectors evaluated do not transduce bipolar or horizontal cells in the cat from a subretinal injection. Glutamine synthetase was used as a marker for Müller cells and showed substantial colabeling with GFP from all vectors (Figure 5.S1). Glial fibrillary acidic protein (GFAP) was used

as a marker for activated Müller cells and also showed co-labeling with GFP. Glial

fibrillary acidic protein expression is increased in various retinal degenerative and

inflammatory conditions, and positive labeling may therefore indicate glial cell activation

associated with the therapy. Subjectively, glial fibrillary acidic protein labeling was more

extensive in eyes with brighter GFP fluorescence, suggesting that stronger GFP

expression may be associated with greater activation of retinal glia.(29) (Table 5.4,

Figure 5.S1).

Figure 5.4: Histological sections showing GFP expression in other parts of the feline eye. (a). Representative histological image of the ciliary body from an rAAV2/2-injected eye illustrating transduction of cells within the stroma of the ciliary processes. There were similar findings for all vector types. (b) Histological sections of optic nerve from each vector. rAAV 2/8, 2/9 and 2/2 showed transduction of the optic nerve, with 2/8 showing the strongest transduction. rAAV2/5 showed no transduction of the optic nerve. Scale bar = 100 microns.

Transverse sections through the optic nerves showed a well-defined region of GFP labeling in all eyes injected with rAAV2/2, rAAV2/8, and rAAV2/9, but not those injected with rAAV2/5 (Figure 5.4).

Subjectively, the GFP labeling in the optic nerve was brightest in rAAV2/8 eyes, followed by rAAV2/9, and weakest in rAAV2/2. Further investigation is required to determine if transgene expression spreads to the brain as showed in dogs and rats following subretinal injection of rAAV2/8.(30, 31) Stromal cells in the ciliary body and iris leaflet of all eyes labeled positive for GFP (Figure 5.4).

Exposure of these tissues to vector may have resulted from leakage from the subretinal injection site into the vitreous. There was no GFP labeling of the cornea or lens in any eyes.

5.4.3 Immune response

A neutralizing antibody assay was used to detect serum antibodies directed against the vectors in five cats; three cats that received rAAV2/2 in one eye and rAAV2/9 in the contralateral eye, and two cats that received rAAV2/5 in one eye and rAAV2/8 in the contralateral eye. Serum neutralizing antibodies to both injected rAAV serotypes were detected in each cat (Figure 5.5a). The highest titer of neutralizing antibodies was to rAAV2/8, followed by rAAV2/2, rAAV2/5, and rAAV2/9. Development of neutralizing antibodies to rAAV capsids has been reported in other large animal models following injection into the immune-privileged subretinal space.[23, 24] This highlights the importance of considering possible systemic immune reactions to rAAVs when
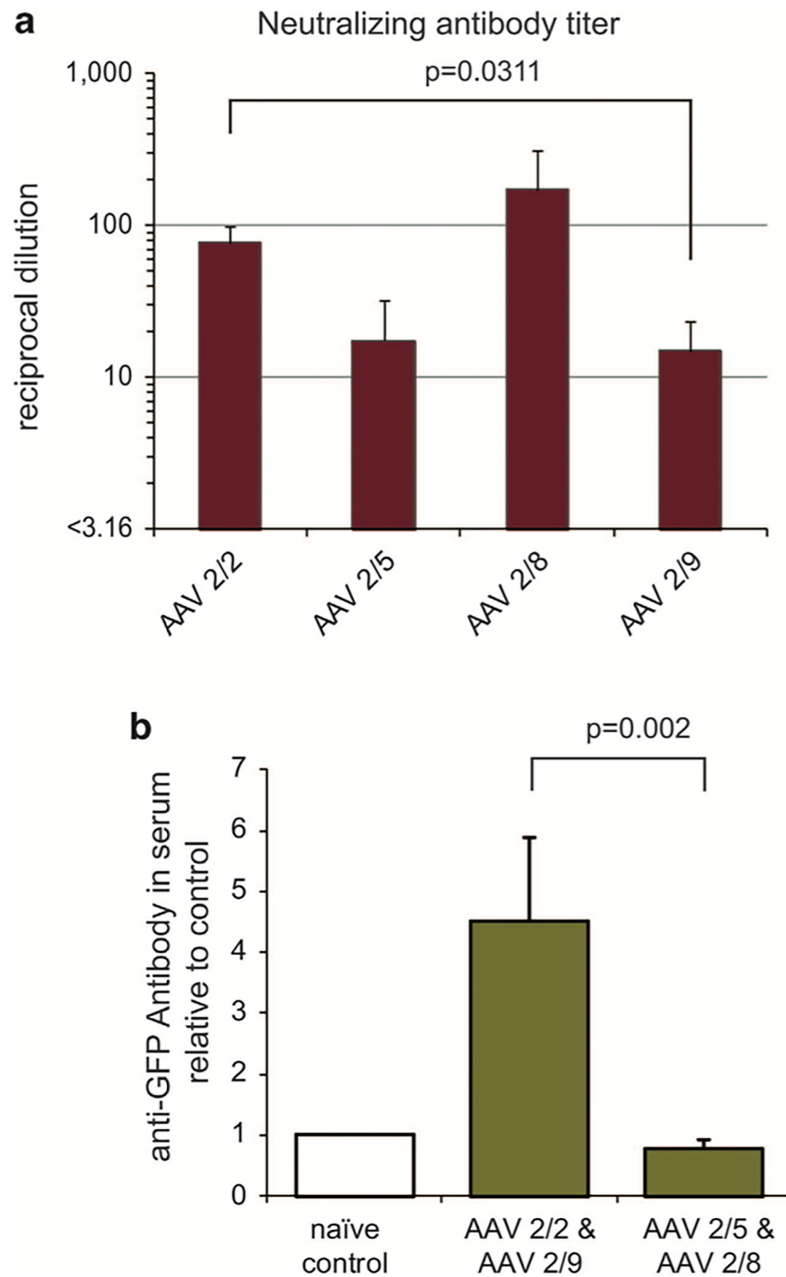
Figure 5.5: Immune responses to the rAAV serotypes and to GFP. (a)
Quantification of Nab assay reported as the reciprocal of the most dilute serum
concentration that blocked infections (+s.e.m.). Note that the antibody response to
rAAV2/2 was significantly greater than that to rAAV2/9, there were no other
significant differences. (b) Indirect ELISA detecting anti-GFP antibodies in the serum,
reported relative to a naïve cat (+s.e.m.). Cats injected with rAAV2/2 and 2/9 showed
a significantly higher response to GFP than those injected with rAAV2/5 and 2/8.
Both assays were performed in triplicate. For animals exposed to rAAV2/2 and
rAAV2/9, n = 3 and for rAAV2/5 and rAAV2/8, n = 2.

conducting gene therapy trials. The immune response to GFP in the five cats was analyzed using an ELISA (Figure 5.5b). Cats injected with rAAV2/2 and rAAV2/9 had a greater titer of anti-GFP antibodies than cats injected with rAAV2/5 and rAAV2/8 (Mann-Whitney Rank Sum Test, p= 0.002). The inflammation and decrease in GFP expression noted in some rAAV2/2 injected eyes may be associated with the initial strong GFP expression either as a direct toxic effect or as a result of immune destruction. It is of note that GFP expression did not decrease in the contralateral rAAV2/9 treated eyes, suggesting either a direct toxic effect rather than a circulating antibody response, or that the blood-retinal barrier remained intact in the contralateral eye. Future studies analyzing the immune response in cats injected with a single vector serotype will be important to clarify these findings. Hematoxylin and eosin staining was performed to analyze inflammatory infiltration. Eighteen of 20 eyes showed at least mild lymphoplasmacytic inflammatory infiltration, with significant variation between individual eyes. Overall, infiltration was most prominent in rAAV2/9 eyes followed by rAAV2/2, then rAAV2/8, and lastly rAAV2/5 with average total infiltration scores of 9.25/12, 6.5/12, 4.7/12, and 1.3/12, respectively. Statistically, infiltration was significantly higher in rAAV2/9 eyes than rAAV2/5 eyes (Kruskal-Wallis one way analysis of variance; $P =$ 0.01). In all cases, the infiltration was evident across the entire retina; however, in 5/20 eyes (1 rAAV2/5, 2 rAAV2/8 and 2 rAAV2/9), the infiltration was subjectively slightly greater in the region of the bleb.

We have demonstrated that a variety of rAAV serotypes transduce feline photoreceptors. More efficient transduction of cones compared to rods differs from other species and highlights that extrapolating vector tropism between species should be

made with caution. Three of the four vectors resulted in GFP presence in ganglion cell axons within the optic nerve. Central nervous system (CNS) transmission of vectors should be considered in future safety studies. The use of tissue-specific promoters may help confine expression to selected target cells, reducing or preventing off-target transgene expression.(32) Immune responses following rAAV gene therapy may be directed at the vector or the expressed transgene. In humans, it is estimated that up to 60% of the population has been exposed to AAV; priming of the immune system to AAVs may predispose clinical patients to even greater immune reactions than seen in pre-clinical animal studies.(33) Injecting vector through a retinotomy, as used here, may allow reflux into the vitreous. As intravitreal administration of rAAVs has been associated with an immune response that can interfere with subsequent transduction events even by the subretinal route,(34, 35) administration route of rAAV retinal gene therapy should be carefully considered. Furthermore, vector titer is known to have a significant effect on the immune response.(29) The titer used here may be higher than needed for adequate therapeutic transgene expression and lower effective titers might reduce the risk of immune-related side effects. Lastly, the only immune modulating therapy used in this study was a single subconjunctival steroid injection immediately post-injection. Additional immunosuppression may be useful to prevent inflammation and subsequent loss of transgene expression.(36-38)

In conclusion, the tested vectors showed preferential cone transduction making them particularly suited for therapy targeted at cone photoreceptors. Further studies testing additional vector and promoter combinations are required to identify the optimal construct for targeting both rods and cones for gene therapy trials in the *Crx* and
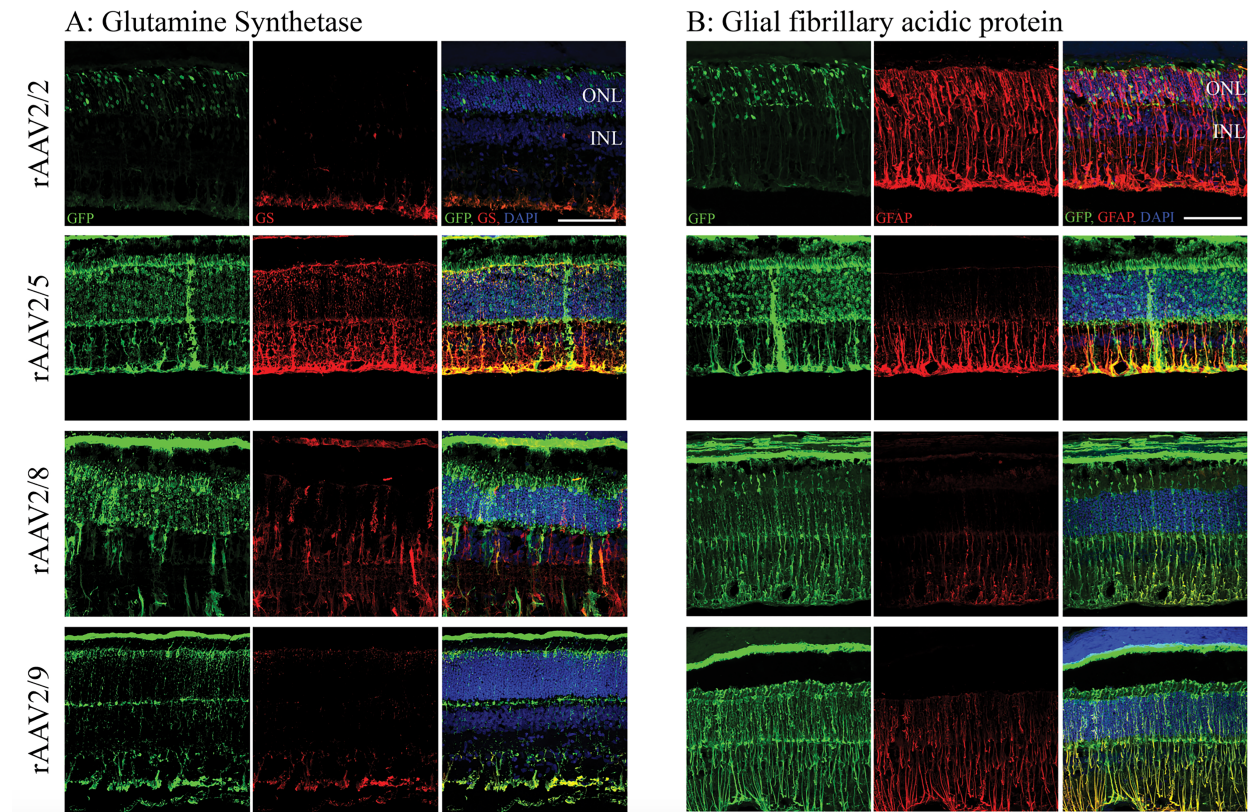
Cep290 mutant cat models. Further studies are also necessary to better characterize

the central nervous system transmission of rAAV vectors and investigate any associated

immune responses.

5.5 Acknowledgments

5.6 Supplemental Information

Figure 5.S1: Müller cell transduction. (**A**) Glutamine synthetase labeling shows overlap with GFP, indicating transduction of Müller cells. (**B**) The degree of GFAP expression varied between the vectors and is indicative of the degree of glial activation. GFAP expression was most prominent in rAAV2/2 injected eyes (top row), which also had outer nuclear layer thinning and disorganization. Scale bar = 100μm.

REFERENCES

REFERENCES

1.   Stone EM. Leber congenital amaurosis - a model for efficient genetic testing of heterogeneous disorders: LXIV Edward Jackson Memorial Lecture. Am J Ophthalmol. 2007;144(6):791-811.

2.   Menotti-Raymond M, David VA, Schaffer AA, Stephens R, Wells D, Kumar-Singh R, et al. Mutation in CEP290 discovered for cat model of human retinal degeneration. Journal of Heredity. 2007;98:211-20.

3.   Menotti-Raymond M, Deckman KH, David V, Myrkalo J, O'Brien SJ, Narfstrom K. Mutation discovered in a feline model of human congenital retinal blinding disease. Invest Ophthalmol Vis Sci. 2010;51(6):2852-9.

4.   Furukawa T, Morrow EM, Cepko CL. Crx, a novel otx-like homeobox gene, shows photoreceptor-specific expression and regulates photoreceptor differentiation. Cell. 1997;91:531-41.

5.   Acland GM, Aguirre GD, Ray J, Zhang Q, Aleman TS, Cideciyan AV, et al. Gene therapy restores vision in a canine model of childhood blindness. Nat genet. 2001;28(1): 92-5.

6.   Beltran WA, Cideciyan AV, Lewin AS, Iwabe S, Khanna H, Sumaroka A, et al. Gene therapy rescues photoreceptor blindness in dogs and paves the way for treating human X-linked retinitis pigmentosa. Proc Natl Acad Sci U S A. 2012;109(6):2132-7.

7.   Rah H, Maggs DJ, Blankenship TN, Narfström K, Lyons LA. Early-onset, autosomal recessive, progressive retinal atrophy in Persian cats. Invest OphthalmolVisSci. 2005;46:1742-7.

8.   Buch PK, Bainbridge JW, Ali RR. AAV-mediated gene therapy for retinal disorders: from mouse to man. Gene Ther. 2008;15:849-57.

9.   Ho TT, Maguire AM, Aguirre GD, Surace EM, Anand V, Zeng Y, et al. Phenotypic rescue after adeno-associated virus-mediated delivery of 4-sulfatase to the retinal pigment epithelium of feline mucopolysaccharidosis VI. J Gene Med. 2002;4(6):613-21.

10.   Bainbridge JW, Mistry A, Schlichtenbrede FC, Smith A, Broderick C, De Alwis M, et al. Stable rAAV-mediated transduction of rod and cone photoreceptors in the canine retina. Gene Ther. 2003;10(16):1336-44.

11.   Petersen-Jones SM, Bartoe JT, Fischer AJ, Scott M, Boye SL, Chiodo V, et al. AAV retinal transduction in a large animal model species: comparison of a self-

complementary AAV2/5 with a single-stranded AAV2/5 vector. Mol Vis. 2009;15:1835-42.

12.   Tan MH, Smith AJ, Pawlyk B, Xu X, Liu X, Bainbridge JB, et al. Gene therapy for retinitis pigmentosa and Leber congenital amaurosis caused by defects in AIPL1: effective rescue of mouse models of partial and complete Aipl1 deficiency using AAV2/2 and AAV2/8 vectors. Hum Mol Genet. 2009;18(12):2099-114.

13.   Mowat FM, Breuwer AR, Bartoe JT, Annear MJ, Zhang Z, Smith AJ, et al. RPE65 gene therapy slows cone loss in Rpe65-deficient dogs. Gene Ther. 2013;20(5):545-55.

14.   Kay MA, Manno CS, Ragni MV, Larson PJ, Couto LB, McClelland A, et al. Evidence for gene transfer and expression of factor IX in haemophilia B patients treated with an AAV vector. Nat Genet. 2000;24(3):257-61.

15.   Carpentier G, Henault E, editors. Protein array analyzer for ImageJ. Proceedings of the ImageJ User and Developer Conference; 2010; Centre de Recherche Public.

16.   Vandenberghe LH, Bell P, Maguire AM, Cearley CN, Xiao R, Calcedo R, et al. Dosage thresholds for AAV2 and AAV8 photoreceptor gene therapy in monkey. Sci Transl Med. 2011;3(88):88ra54.

17.   Rabinowitz JE, Rolling F, Li C, Conrath H, Xiao W, Xiao X, et al. Cross-packaging of a single adeno-associated virus (AAV) type 2 vector genome into multiple AAV serotypes enables transduction with broad specificity. Journal of virology. 2002;76(2): 791-801.

18.   Allocca M, Mussolino C, Garcia-Hoyos M, Sanges D, Iodice C, Petrillo M, et al. Novel adeno-associated virus serotypes efficiently transduce murine photoreceptors. J Virol. 2007;81(20):11372-80.

19.   Natkunarajah M, Trittibach P, McIntosh J, Duran Y, Barker SE, Smith AJ, et al. Assessment of ocular transduction using single-stranded and self-complementary recombinant adeno-associated virus serotype 2/8. Gene Ther. 2008;15:463-7.

20.   Lebherz C, Maguire A, Tang W, Bennett J, Wilson JM. Novel AAV serotypes for improved ocular gene transfer. J Gene Med. 2008;10(4):375-82.

21.   Beltran WA. The use of canine models of inherited retinal degeneration to test novel therapeutic approaches. Vet Ophthalmol. 2009;12(3):192-204.

22.   Bainbridge JWB, Mistry A, Schlichtenbrede FC, Smith A, Broderick C, De Alwis M, et al. Stable rAAV-mediated transduction of rod and cone photoreceptors in the canine retina. Gene Ther. 2003;10(16):1336-44.

23.   Acland GM, Aguirre GD, Bennett J, Aleman TS, Cideciyan AV, Bennicelli J, et al. Long-term restoration of rod and cone vision by single dose rAAV-mediated gene transfer to the retina in a canine model of childhood blindness. Molecular therapy : the journal of the American Society of Gene Therapy. 2005;12(6):1072-82.

24.   Stieger K, Colle MA, Dubreil L, Mendes-Madeira A, Weber M, Le Meur G, et al. Subretinal delivery of recombinant AAV serotype 8 vector in dogs results in gene transfer to neurons in the brain. Molecular Therapy. 2008;16(5):916-23.

25.   Vandenberghe LH, Bell P, Maguire AM, Xiao R, Hopkins TB, Grant R, et al. AAV9 targets cone photoreceptors in the nonhuman primate retina. PLoS One. 2013;8(1):e53463.

26.   Mussolino C, della Corte M, Rossi S, Viola F, Di Vicino U, Marrocco E, et al. AAV-mediated photoreceptor transduction of the pig cone-enriched retina. Gene therapy. 2011;18(7):637-45.

27.   Gao G, Vandenberghe LH, Wilson JM. New recombinant serotypes of AAV vectors. Current gene therapy. 2005;5(3):285-97.

28.   Lei B, Zhang K, Yue Y, Ghosh A, Duan D. Adeno-associated virus serotype-9 mediated retinal outer plexiform layer transduction is mainly through the photoreceptors. Advances in experimental medicine and biology. 2010;664:671-8.

29.   Beltran WA, Boye SL, Boye SE, Chiodo VA, Lewin AS, Hauswirth WW, et al. rAAV2/5 gene-targeting to rods:dose-dependent efficiency and complications associated with different promoters. Gene Ther. 2010;17(9):1162-74.

30.   Stieger K, Colle MA, Dubreil L, Mendes-Madeira A, Weber M, Le MG, et al. Subretinal delivery of recombinant AAV serotype 8 vector in dogs results in gene transfer to neurons in the brain. MolTher. 2008;16:916-23.

31.   Dudus L, Anand V, Acland GM, Chen SJ, Wilson JM, Fisher KJ, et al. Persistent transgene product in retina, optic nerve and brain after intraocular injection of rAAV. Vision research. 1999;39(15):2545-53.

32.   Mancuso K, Hendrickson AE, Connor TB, Jr., Mauck MC, Kinsella JJ, Hauswirth WW, et al. Recombinant adeno-associated virus targets passenger gene expression to cones in primate retina. J Opt Soc Am A Opt Image Sci Vis. 2007;24(5):1411-6.

33.   Boutin S, Monteilhet V, Veron P, Leborgne C, Benveniste O, Montus MF, et al. Prevalence of serum IgG and neutralizing factors against adeno-associated virus (AAV) types 1, 2, 5, 6, 8, and 9 in the healthy population: implications for gene therapy using AAV vectors. Hum Gene Ther. 2010;21(6):704-12.

34.   Anand V, Duffy B, Yang Z, Dejneka NS, Maguire AM, Bennett J. A deviant immune response to viral proteins and transgene product is generated on subretinal administration of adenovirus and adeno-associated virus. MolTher. 2002;5(2):125-32.

35.   Li Q, Miller R, Han PY, Pang J, Dinculescu A, Chiodo V, et al. Intraocular route of AAV2 vector administration defines humoral immune response and therapeutic potential. Mol Vis. 2008;14:1760-9.

36.   Chirmule N, Xiao W, Truneh A, Schnell MA, Hughes JV, Zoltick P, et al. Humoral immunity to adeno-associated virus type 2 vectors following administration to murine and nonhuman primate muscle. J Virol. 2000;74(5):2420-5.

37.   Halbert CL, Standaert TA, Wilson CB, Miller AD. Successful readministration of adeno-associated virus vectors to the mouse lung requires transient immunosuppression during the initial exposure. J Virol. 1998;72(12):9795-805.

38.   Kay MA, Meuse L, Gown AM, Linsley P, Hollenbaugh D, Aruffo A, et al. Transient immunomodulation with anti-CD40 ligand antibody and CTLA4Ig enhances persistence and secondary adenovirus-mediated gene transfer into mouse liver. Proc Natl Acad Sci U S A. 1997;94(9):4686-91.

CHAPTER 6

DISCUSSION AND FUTURE DIRECTIONS

The *CEP290* mutant cat provides a valuable large animal model for studying retinal dystrophies caused by mutations in this gene. With an eye similar in size and proportions to the human eye, a central retina semi-homologous to the human macula, and a spontaneous mutation in this gene, there is great opportunity for investigation. Understanding the phenotype and molecular underpinning of the disease in cats is imperative as we move towards using this model for treatment trials. Furthermore, assessing treatment modalities *in vitro* and identifying optimal delivery vectors are necessary steps before reaching these trials. This dissertation aims to better understand the *CEP290* mutant feline, to determine objective markers for assessing disease progression and treatment planning and assessment, to evaluate delivery vehicles in the feline, and to work towards a genome editing treatment for this model.

We start by showing that the *CEP290* mutant cat produces a low-level of wild-type transcript, showing use of the wild-type splice donor site even in the presence of the mutation-created splice donor site. Additionally, we show that there is also production of truncated mutant transcript, suggesting the possibility that mutant cats could produce both full-length wild-type protein as well as truncated protein. Automated western blot analysis, though proving difficult to differentiate between the full-length and truncated proteins which are close in size, provides evidence that suggests mutant cats do produce both wild-type and truncated protein. Given the predicted mild effect on the protein predicted by the truncation, we suspect the truncated protein has residual function. We therefore hypothesize that the milder phenotype seen in the cat, relative to most human *CEP290* retinopathy patients, is due to CEP290 function resulting from the presence of both wild-type and truncated protein.

196

This interesting finding maybe also hold implications for treatment development against these diseases. These results may suggest that even with truncation the CEP290 protein remains at least partially functional. This finding is significant given the limitations caused by the large size of the *CEP290* gene, which precludes packaging of the full transcript into the retinal gene therapy vector of choice, the adeno-associated viral (AAV) vector. Given findings in a zebrafish model that suggest a partial transcript could be sufficient to improve vision in *CEP290* retinopathy patients, our findings suggesting that truncated protein may be produced and may retain some functionality suggest that this could be true in higher order animals as well. To build on this, future studies should test progressively more truncated transcript to determine what length and segments of the *CEP290* gene are necessary for improvement in vision in higher order animals, such as in the rd16 mouse or the *CEP290* mutant cat. It must be determined if half transcript length, the length that would fit in an AAV vector, would be sufficient for improvement in vision.

The milder phenotype with a later-onset and slowly-progressing retinopathy has been well described in the literature but an element of the disease phenotype warranted further clarification- the regional rate of retinal degeneration. This was another important question as people with *CEP290* retinopathies typically show a characteristic preservation of the central retina. Given the presence of an *area centralis* in the cat and the resultant utility of cat models for studying central retinal disease, it was important to definitively clarify whether the cat also shows slower degeneration in the central retina relative to other retinal regions. To study this we utilized spectral-domain optical coherence tomography (SD-OCT), a tool never used in the *CEP290* cat that can provide

valuable information *in vivo*. Using SD-OCT we were able to study the regional degeneration of the retina over time. Our results show that mutant cats do show slower degeneration in the central retina, similar to the pattern of degeneration seen in people. This strengthens the *CEP290* cat as a model for *CEP290* retinopathies and also means this model has great potential for studying treatments aimed at the central retina. Given the higher density of photoreceptor cells and the higher proportion of cones, treatments aimed at this region may respond differently to components of treatment such as the retinal detachment caused by subretinal injection. As such, testing of central retinal treatments in an animal model is integral before human clinical trials can be pursued.

Additionally, tools for following disease progression, treatment efficacy, and for targeting treatments, are necessary to pursue these pre-clinical trials. Though our studies and the characteristic central retinal sparing seen in LCA[CEP290] patients suggest that treatment should target the central retina, it remains important to have methods to identify regions of a patient's retina that will best respond to therapy. SD-OCT can provide this tool, with *in vivo* monitoring of cell layer thickness and retinal architecture. The finding in people that the ellipsoid zone (EZ), a layer discernible on OCT, can be used to identify retinal regions with more preserved photoreceptor cells is an exciting finding that warranted study in the cat model. We therefore analyzed the EZ in our mutant cats and found that, as seen in people, this layer is discernible in more preserved regions and loses integrity or disappears altogether in more degenerate regions. Assessment of the integrity of this layer therefore provides a valuable tool for quickly and effectively assessing regional photoreceptor health. In the future, this tool should be used to further follow disease progression and for treatment trials. During

planning of treatment testing the EZ could be utilized to determine where treatments should be targeted. Following treatment instigation, the EZ can be assessed along with retinal layer thicknesses to assess retinal rescue. Conversely, retinal regions with poor EZ integrity could also be targeted with treatments, after which the effect of the treatment on the EZ could be studied. This may provide valuable information regarding treatment timing. Since LCA^{CEP290} is a childhood disease and may go undiagnosed in earlier stages of disease, pushing the temporal limits of treatment trials may help us develop treatments that could be used in later stages of disease. If we can develop treatments that could target retinal regions that show loss of EZ integrity, suggesting a more degenerate retina, and can lead to rescue of this EZ, this would suggest the treatment could be used after photoreceptor loss has begun, a useful finding that could lead to better treatments for later-stage patients.

Unfortunately, the slowly progressing nature of this disease is actually a research limitation that we have found makes it difficult to study treatments. Studying treatments in this model, for example, would be difficult as it would take years of post-treatment monitoring to appreciate any rescue of vision. The milder nature of the phenotype also makes it more difficult to identify objective markers for treatment monitoring, as the cats simply do not show as many significant differences from wild-type cats as one would find in a more severe model. This held true when we studied ciliation in fibroblast cells grown from mutant cats. In an effort to identify an objective marker in fibroblast cells that we anticipated using for treatment development, we induced ciliation in these cells and studied cilia length across genotypes. Given the ciliary location and function of the CEP290 protein, it is logical that loss of this protein or its function would lead to stunted

ciliation in mutant cells. However, given the milder phenotype seen in the cats and the hypomorphic situation we confirmed, we were suspicious that the residual CEP290 protein and function would be sufficient for mutant cells to produce normal length cilia. However, recognizing the potential utility of this simple measurement if there was a difference between mutant cells and wild-type or carrier cells, we felt it was important to study to definitively determine if this could be used as a marker. As we suspected however, mutant cats showed no defect in ciliation of fibroblast cells, with cilia that were nearly identical in length to those grown by wild-type and heterozygous cells. Cilia length is therefore not a useful marker and future studies should be aimed at identifying differences between mutant and wild-type/heterozygous cells such that treatment testing in cells can be thoroughly assessed.

The cells we grew and verified still provide a valuable *in vitro* tool that holds great utility. The cells can be used for developing, studying, and fine-tuning treatments before taking these treatments into the cat model. This provides a quicker and easier tool for this treatment development and would allow for the reduction of animal numbers and trial cost as treatments could be optimized in the cells rather than in the cats themselves. One such treatment type that could be effectively tested in the cells are CRISPR/Cas9 nuclease based therapies. CRISPR-Cas9 nuclease therapies have shown great promise against a variety of inherited diseases, with the power to genetically edit the genome for purposes such as removing mutations, inserting new sequences, and knocking out genes. These treatments require considerable fine-tuning however. Our cells provide an ideal tool for this purpose. Using these cells we have been able to show successful RNA transfection of feline cells, as well as appropriate

cutting of the mutant sequence. Future studies should therefore aim to successfully insert the desired sequence. In our initial attempts at CRISPR/Cas9 nuclease treatment development we also attempted to use a "nickase" method to reduce off-target mutagenesis. This method was not successful in feline cells in our trials but would be a valuable and potentially safer treatment. Further studies to troubleshoot this method in the feline is therefore also worthwhile.

Additionally, these steps could potentially be even more quickly studied if the phenotype were modified to increase severity. This is another potential advantage of the *in vitro* tool- the potential to genetically modify these cells to make the phenotype more severe, creating a more useful tool that would show more obvious differences from wild-type cells. Once successful editing is achieved in the cells, these developed and optimized treatments can then be taken into the cat model for *in vivo* treatment testing. Similarly, genome editing could be utilized to make the phenotype more severe in the actual cat by editing blastocysts for example. Though ambitious, this strategy could allow for the creation of a new *CEP290* mutant cat model that would have a more severe disease with faster progression that would be even more useful for treatment trials. It would also conceivably be possible to generate a cat that had the same deep intronic cryptic exon as in patient with LCA^{CEP290}.

For delivering a variety of treatments to the retina, a vector for delivery is necessary. The above discussed partial transcript or CRISPR therapies for example, would require a vehicle for delivery of the transcript, CRISPR components, or CRISPR-corrected induced pluripotent stem cells to the retina. A large body of research has shown that the ideal vector for delivery to the retina is the AAV vector, however, very

201

limited testing of these vectors had been done in the feline retina. This testing was important as significant species differences in vector characteristics such as cellular tropism have been found in previous studies. We therefore tested four of the most commonly used hybrid AAV vectors in the wild-type feline retina. Interestingly, we found that the four vectors show stronger targeting of cone photoreceptor cells than rod cells, a finding that reiterates the species differences in cellular tropism and speaks to the need to use caution when extrapolating between species. However, these findings set the stage for AAV testing in the feline and provide valuable information that can be used as studies move toward any treatment testing in the feline retina that utilizes AAV vectors as the delivery vehicle. Further studies are warranted to study additional vectors and modifications to vectors to determine the ideal vectors for use in the feline retina. This vector can then be utilized for *in vivo* treatment testing, such as testing of those treatments mentioned above.

The *CEP290* mutant feline is a valuable tool for understanding *CEP290* retinopathies and for developing treatments against them. In this dissertation we provide a better understanding of the model and lay the groundwork for treatment development. Further studies are necessary to fine-tune the CRISPR-Cas9 nuclease treatment and to determine objective markers in this slowly-degenerating model. Once these aims are achieved, *in vivo* treatment trials in this model could provide valuable data as the field works towards treatments that could be tested in human clinical trials.